NATIONAL UNIVERSITY OF SCIENCE AND TECHNOLOGY „POLITEHNICA“ OF BUCHAREST

DOCTORAL SCHOOL OF CHEMICAL ENGINEERING AND BIOTECHNOLOGIES

DOCTORAL THESIS

A MODERN APPROACH OF PATHOLOGY AND CLINICAL ANALYSIS

PhD Student: Eng. M.D. Alexandru-Adrian Bratei

Coordinators: Prof. Dr. habil Raluca Ioana van Staden
Prof. Dr. habil Simona Gurzu

BUCHAREST
2024

Contents

ACKNOWLEDGEMENTS

I would like to express my thanks and deep gratitude to the doctoral coordinators Prof. Dr. Habil. Raluca-Ioana van Staden and Prof. Dr. Habil. Simona Gurzu for the outstanding coordination, recommendations and useful advice provided for the doctoral studies as well as for the preparation of the doctoral thesis.

I express my sincere thanks and full gratitude to my family who gave me all the support, understanding and strength to complete my doctoral studies with excellent results.

Introduction

Pathological diagnosis brings together a wide range of medical specialties, both surgical and clinical, being indispensable in the management of patients with neoplastic lesions. This diagnosis is mainly made in two ways:

- Morphological - based on some qualitative aspects, using the optical microscope;
- Molecular - based on molecular expression, using immunohistochemistry techniques.

The analysis of the molecular profile using immunohistochemical techniques is based on the use of special staining on tissue sections to highlight the presence or absence of a marker.

However, these methods are limited to the tumor tissue without taking into account the systemic effect of tumor presence. Also, the tumor diagnosis of certainty is also made by the pathologist based on the analysis of cellular characteristics. All current techniques are expensive and time-consuming, and most use tissular material obtained invasively.

In the context of these deficits, this work was aimed to introduce an alternative method that would come with a complementary role for the evaluation of the clinicopathological characteristics and for the early detection of neoplastic processes. This is the stochastic method that allows the rapid, low-cost assessment with excellent accuracy and reproducibility of tumor biomarker levels in the main biological fluids, namely blood, urine and saliva.

Quantification of the levels of some commonly used biomarkers in the immunohistochemical analysis of neoplastic lesions comes as a complementary minimally invasive method. Their concentrations in blood, urine and saliva are in close correlation with molecular biodynamics, mass transfer processes and kinetics of biochemical processes within the metabolic pathways of each biomarker. In addition to the basal level of biomarkers related to cell turnover, the release of biomolecules into the blood stream is achieved either by the tumor mass or by the adjacent non-tumor tissues as an effect of the presence of the tumor. Thus, it is expected that these levels depend on the clinicopathological characteristics of the tumor as will be presented in detail in this paper.

The exploitation of this method has been achieved holistically, starting from the conceptual development of stochastic sensors, with their calibration and standardization, followed by application to biological samples to evaluate the presence and concentrations of tumor markers within them. The correlation with the clinicopathological characteristics for colorectal adenocarcinoma and gastric adenocarcinoma followed and the obtained results will be presented in detail.

Stochastic analysis of biomolecules

Stochastic analysis is an electrochemical technique of qualitative and quantitative detection of biomolecules in various fluids. This method is based on stochastic sensors that will be detailed in this paper.

Stochastic sensors were inspired by biology, where it was observed that there are channels/pores that react and respond specifically to the existence in the environment of certain ions or biomolecules. Such examples include amiloride-sensitive sodium channels that mediate salty taste and vanilloid receptors that mediate hot taste. Starting from the analysis of the interaction of these channels with a specific substrate, numerous sensors capable of detecting and quantifying from small ions to organic molecules to proteins and DNA have been developed to date.

As the metabolic pathways are intricate and the interaction of the channel as a receptor with the biomolecule as a substrate has the effect of activating certain biochemical pathways in biological systems, the reproduction of these sensors in the laboratory would not be effective. The shortcomings of this mechanism consist in:

- low reproducibility due to the complexity of the system;
- difficulties in the interpretation of the results, because the metabolic pathways are closely interconnected and a certain substrate could simultaneously lead to the activation of several parallel pathways;
- constraints relative to working conditions, as these sensors are structurally proteins and operate optimally within a narrow range of temperature and pH values.

Starting from these observations, the use in the same form as in biological systems is not feasible and a conceptual chemical-mathematical approach was required.

It started from the fact that a channel has 2 states – the active state when the substrate is bound and the inactive state when the substrate is not bound. The substrate binds non-covalently to a site within the protein-pore, and this aspect makes the binding reversible and establishes an equilibrium similar to the binding of an enzyme to the substrate ($S + P \rightleftharpoons S \bullet P$, where S is the substrate, P is the pore protein (inactive state), $S \bullet P$ is the substrate-protein complex corresponding to the active state).

Moreover, the chemical equilibrium is dynamic, being strongly influenced by the concentration of the substrate. As the substrate concentration increases, the equilibrium will be shifted more to the right, with the proportion of the active form of the pore increasing.

The pore switches to the active state by efficient substrate binding following an efficient collision and returns to the inactive (ground) state after unbinding the substrate. Thus, each pore will exist in each state for a certain period of time.

The biochemical principle of the operation of these channels is based on the activation of the channel function. Thus, by binding the substrate, the channel changes its tertiary and quaternary structures, forming an open channel through which, generally, ionic exchanges take place along the electrochemical gradient.

The time interval in which the pore is in an active state depends on a number of factors such as:

- binding strength (a substrate bound weaker to the pore site will unbind more easily and have a shorter active-state period);
- pore geometry (a complex geometry could favor site unbinding);
- the nature and geometry of the substrate (a larger substrate will have a harder time reaching the binding site and will remain bound for a shorter time).

The amount of time the pore is inactive depends on:

- location of the binding site within the pore (a site located deeper is more difficult for the substrate to access and thus it will take longer for an effective collision to occur);
- geometry of the substrate binding site (a complex geometry could make access to the substrate binding site difficult);
- the average diameter of the pore up to the level of the site (the larger the diameter, the easier access the substrate will have);
- substrate concentration (the higher the concentration, the more collisions there will be and the probability of an effective collision will increase, so the duration of the inactive state will decrease).

Among the factors influencing both the active and inactive states are temperature and pH. The influence of temperature is felt both in the possibility of thermal denaturation of the protein components within the pore and the substrate, as well as in the change in the speed related to the Brownian movement of the molecules. The influence of pH consists in changing the electric charge of various amino acid sequences in the structure of the pore and the substrate, with the alteration of the tertiary and quaternary structures.

Being a system with a very large number of molecules, for a more mathematically correct approach, an analysis of the distribution of active and inactive states is required. This can be done most easily according to the temporal criterion, respectively according to the spatial criterion.

The analysis of the distribution according to the temporal criteria is done at the channel level observing the time during which the substrate is bound to the pore – the time while the pore is in active form (ta), respectively the time when the substrate is not bound to the pore – the time while the pore is in form inactive (ti). We can thus define the probability that a channel is in an active state (respectively in an inactive state) as the ratio between ta (respectively ti) and the total time of a cycle (ta + ti). The two states are alternate and successive, but the duration of each state is variable. For these reasons, the average value is taken for each.

As previously analyzed, the value of the duration of the active state depends on the nature of the substrate and the structure of the pore over time, the value of the duration of the inactive state depends on the location of the binding site, the geometry of the pore and is inversely proportional to the concentration of the substrate.

Spatial criterion analysis targets the distribution of channels/pores and also takes into account their number and accessibility. In biological systems, the channels are proteinaceous in nature and are distributed within the lipidic cell membrane. Cell membranes have been intensively studied and valued for their fluid mosaic characteristic. In other words, lipid and protein molecules within it move freely, being able to perform translational (thus the surface distribution of protein structures is uniform), rotational (does not influence the distribution of channels/pores) and flip-flop (more characteristic) movements for lipid molecules, practically insignificant for protein structures.

Translational motions are much slower than the Brownian motion of biomolecules within a fluid, resulting in a similar number of biomolecules adjacent to a channel. However, the degree of deformation of the total surface should also be taken into account, because in the context of a pronounced folding as found in the epithelial structures of the digestive tract, the access will be much easier to the channels on the surface compared to those in the depth. Depending on how deep a channel is found, it may even end up having an insignificant importance. To overcome these impediments, one can work with the average characteristics of channel/pore-type protein structures.

Within a small total area, the only element that would strongly influence the response would be the number of channels. The more channels, the higher the probability of an effective collision.

The temporal and spatial criteria are interconnected, as the higher the number of channels, the longer the value of the average inactivity time for a channel will increase, because the average number of biomolecules adjacent to a channel will be, practically, smaller and thus the probability of an effective collision will be reduced.

In order to capitalize on the principles of this method and to be able to use it in laboratory conditions, a series of modifications should be made in parallel with the tracking of characteristics in

biological systems. In this way the stochastic sensors will be defined and described, making the sensors belong to the field of analytical electrochemistry.

Firstly, a system equivalent to the biological membranes supporting these pores must be sought, therefore it is necessary to preserve the support function of the membrane and to ensure a uniform distribution of the detection structures. Ideally, temperature and pH dependent impediments should be overcome, as these could decisively influence the number of uses of a sensor. Thus, the choice of a biochemical matrix should be avoided. Optimally, a resistant or very little influenced by external factors matrix will be chosen. An example exploited in this work is that of a carbon-based matrix in the allotropic form of graphene. Graphene is a variant of graphite with a two-dimensional planar arrangement in which the carbon atoms are still arranged in a hexagonal lattice, with the mention that it is an excellent conductor of heat and electricity. This is a chemically inert support, therefore the impediment represented by the influence of pH is overcome, and the strength of the bonds is increased so that, in laboratory conditions, the effect of temperature is minimized, becoming practically insignificant. Chemical inertness also contributes to increasing the number of successive uses in various fluids.

The next step would be to identify an equivalent pore structure for which the principle of operation would hold. In biological systems, the electrochemical gradient is given by the electrical charge on either side of the membrane thanks to the ions present in the intracellular and extracellular environment. In the event of using a graphene matrix, the intracellular ion component is no longer an option and the electrochemical gradient could be preserved by externally applying a current source.

The passage of ions through these equivalent pore structures could lead to contamination of the matrix and it is therefore preferable that they can be easily removed between successive uses. In the event of the passage of a large ion, it will become more difficult to eliminate this and therefore the species that would be preferable to pass would be electrons or small ions.

To avoid the impediments represented by the influence of pH and temperature, this membrane equivalent should also associate an increased chemical and thermal inertia. Thus, a protein structure is also to be avoided, but other feasible structures cannot show conformational changes.

By combining the above, it can be concluded that a molecule containing a small-cycle that is chemically and thermally inert under laboratory conditions is required. Since this would change the properties of the graphene matrix, it is called a modifier. Such modifiers could be protoporphyrins, cyclodextrins or cyclic ethers.

Controlling the number of such porous structures for the passage of the electric current is achieved by choosing an optimized mass ratio between the matrix and the modifier.

This mixture should be placed in a support that provides the contact surface with the fluid from which the analytes will be detected and quantified. In this work, the mixture will be introduced into a micropipette tip, and the connection to the external electric current source will be made through a silver wire.

The operating principle of such a sensor is based on the influence the existence of a certain analyte in the fluid to be analyzed has on the electric current passing through the pore equivalent. Thus, when a continuous electric current is passed through the solution at a fixed potential, the passage is uninterrupted through the pore, but if the analyte is fixed to the modifier, it would block the passage of the electric current by decreasing the conductance and there would be an interruption of the flow.

The duration of this blockage is given by the summation of the times of diffusion from the matrix to the pore, the binding to the pore and the diffusion back into the analyte fluid, and is strongly influenced by the nature and size of the analyte. The more complex the geometric features of the biomolecule and the larger the size, the more limited the access and the blockage of the pore will be. As each molecule is structurally unique, it can be concluded that the way it influences the value of these times is also unique. Thus, the blockage time of the passage of the electric current is like a signature for each molecule and is denoted t_{off}. Between two successive blockages, the probability of another effective collision intervenes to make it able to enter the channel from the matrix to the pore. In other words, the higher the concentration of a species, the greater the probability of an effective collision and the shorter the duration between two blockages, effectively being inversely proportional to the concentration. This concentration-dependent period between two successive blockages is called t_{on}.

Based on the above, a biomolecule can be detected in the medium based on the value of t_{off}, and the concentration can be calculated based on the value of t_{on}.

Furthermore, as each molecule is identified and quantified relative to t_{off}, multiple analytes can be determined simultaneously as long as they have t_{off} values far enough apart that they can be experimentally evaluated separately. Furthermore, in the case of simultaneous analysis of several analytes, a longer measurement time is required for each analyte to have a probabilistic opportunity to enter the pore so that its t_{on} value can be determined.

As biological fluids contain a multitude of possible analytes, some with quite similar structural properties, the selection process must be very fine-tuned. This can be done by choosing the right matrix (so that the analyte can fit through its pores), the modifier (so that it can bind to the analyte) and the electric potential (so that it is strong enough to move the protein along the electrochemical gradient).

The electrochemical cell is made up of the actual sensor that was described and detailed above, of a reference electrode – chosen of the second type for stability, consisting of an Ag wire covered with a layer of silver chloride – and a counter electrode (Pt wire). By introducing the sensor, the reference

electrode and the counter electrode into the solution to be analyzed, an amperometric diagram (which is used to measure the intensity of the electric current passing through the pores as a function of time) can be obtained. From this diagram, the values of t_{off} and t_{on} can be obtained, which help identifying the analyte and its concentration [1-22].

Part 1- Sensors for biomarker's detection

In this work, the quantification in biological samples pursued thirteen biomarkers known to be associated with gastric and colorectal adenocarcinomas, namely maspin, MLH1, PMS2, MSH2, MSH6, KRAS, CA 72-4, CA 19-9, CEA, CA125, p53, cathepsin B and cathepsin D. Detailed correlations with the clinicopathological characteristics of the patients in the database were found for the first six biomarkers.

I. Sensors based on IN NB-GR and IQ NB-GR for quantification of MMR proteins and KRAS

1. Experimental part

1.1. *Design of the stochastic microsensors*

The two stochastic microsensors were designed as following: 50µL of IN solution (10^{-3}mol L^{-1}) was added to 50mg graphene paste decorated with N and B (NB-GR) (made by physically mixing NB-GR powder and paraffin oil until a homogenous paste was obtained); 50µL of IQ solution (10^{-3}mol L^{-1}) was added to 50mg graphene paste decorated with N and B (NB-GR) (made by physically mixing NB-GR powder and paraffin oil until a homogenous paste was obtained) (Scheme 1).

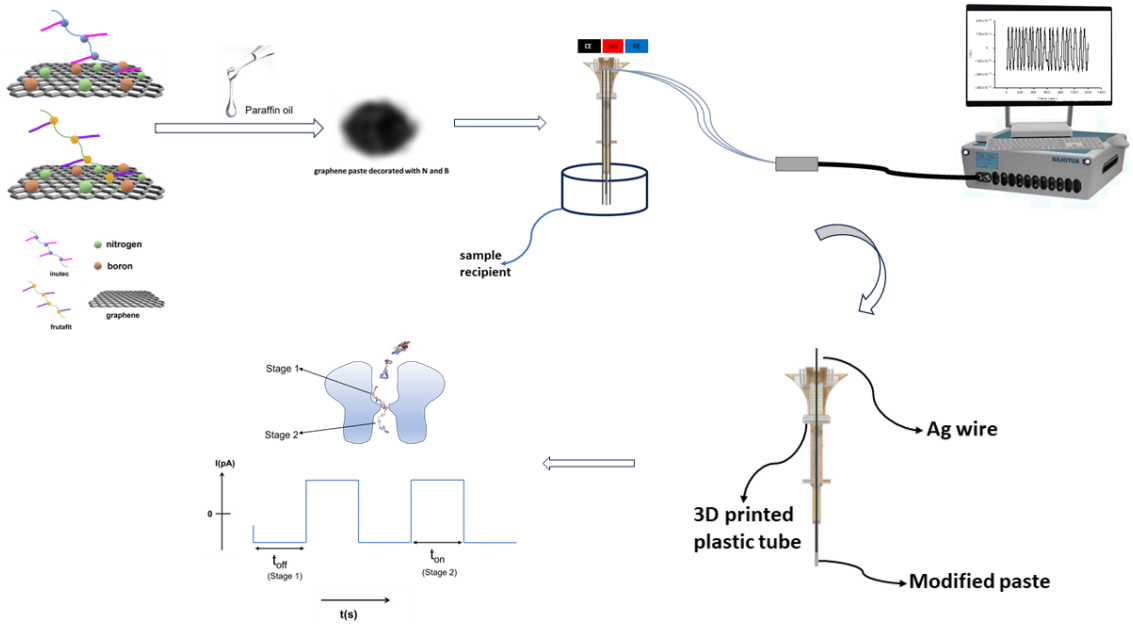

Scheme 1 Design of the stochastic microsensor. Principle of current development.

Each paste was placed in a 3D printed tube with internal diameter of 20µm; an Ag wire made the connection between the paste and the external circuit. Before and after each measurement, the

microsensors were cleaned with deionized water. When not in use, the stochastic microsensors were kept in a dry place, at room temperature.

1.2. Stochastic method

The stochastic method used the chronoamperometric technique performed at 125 mV vs Ag/AgCl. Based on the signatures (t_{off} values) of the MLH1, MSH2, MSH6, PMS2, and of KRAS, these biomarkers were recognized in the biological samples. A series of solutions containing different concentrations of MLH1, MSH2, MSH6, PMS2, and of KRAS were used for the calibration of the two stochastic microsensors. The equations of calibration obtained for the biomarkers using each of the two stochastic microsensors were based on the determination of the t_{on} value (read in between two consecutive t_{off} values); a, and b parameters from the equation of calibration $1/t_{on} = a + b \times Conc._{biomarker}$ were determined using the linear regression method. For the screening of biological samples such as whole blood, urine, saliva, and tumoral tissue, the biomarkers were recognized based on their signature (t_{off} values) (Figures 1 and 2, Scheme 1), the t_{on} values were read and inserted into the equation of calibration for the determination of the concentration of MLH1, MSH2, MSH6, PMS2, and of KRAS in the biological sample.

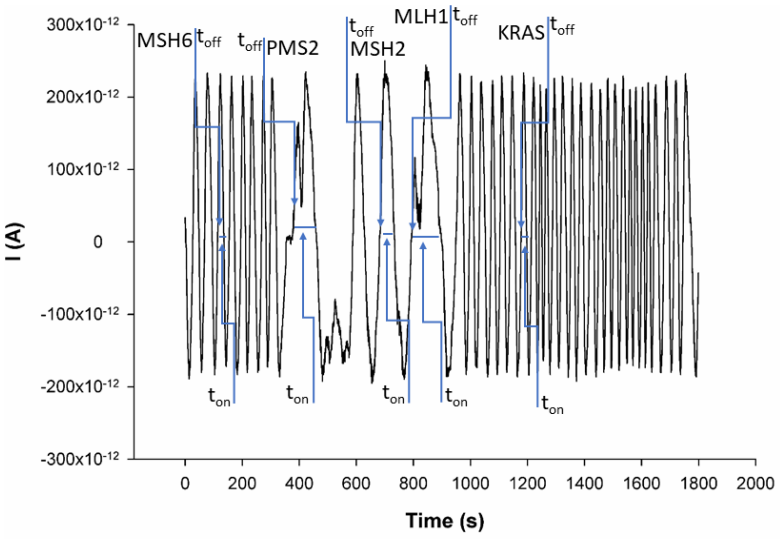

(a)

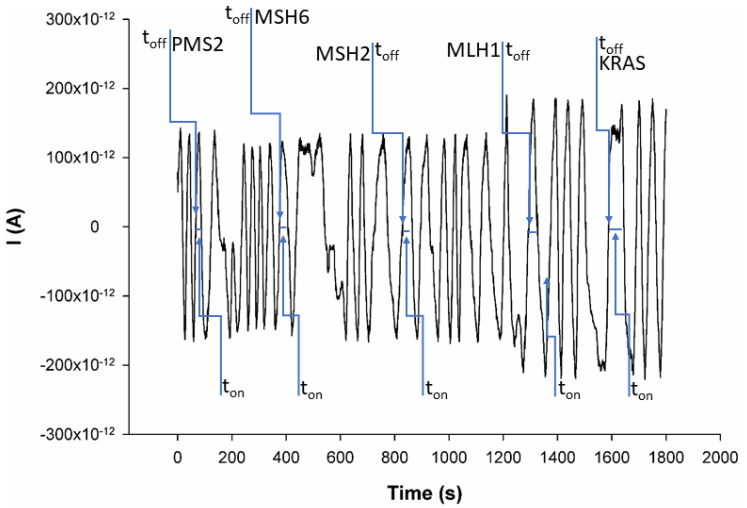
300x10-12
200x10-12
100x10-12
0
-100x10-12
-200x10-12
-300x10-12
I (A)
0 200 400 600 800 1000 1200 1400 1600 1800 2000
Time (s)
toff PMS2
toff MSH6
MSH2 toff
MLH1 toff
toff KRAS
ton

(b)

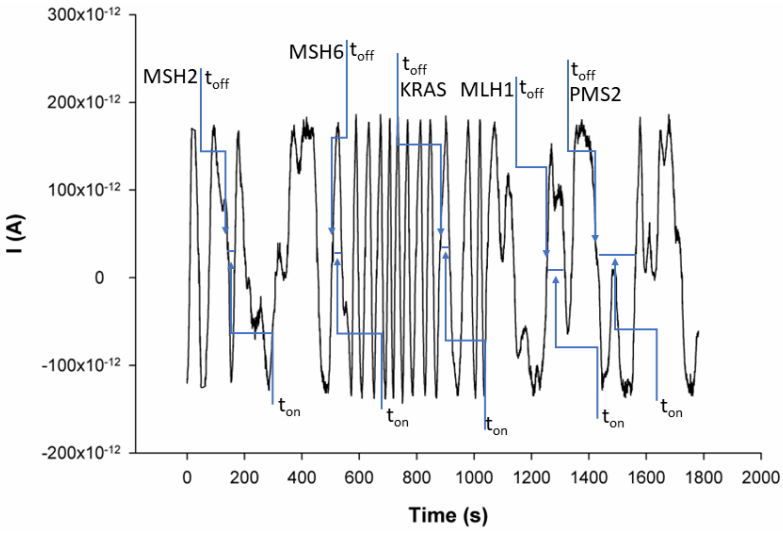
300x10-12
200x10-12
100x10-12
0
-100x10-12
-200x10-12
I (A)
0 200 400 600 800 1000 1200 1400 1600 1800 2000
Time (s)
MSH2 toff
MSH6 toff
toff KRAS
MLH1 toff
toff PMS2
ton

(c)

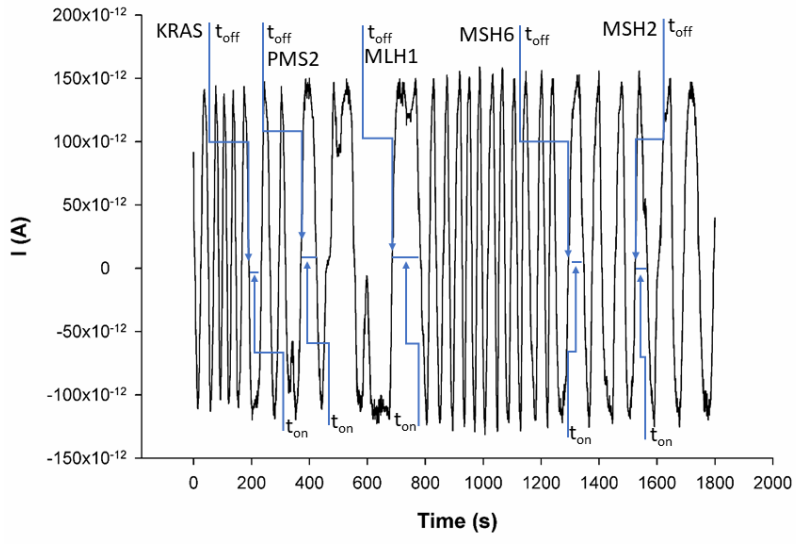

(d)

Figure 1. Typical diagrams obtained by screening (a) whole blood, (b) saliva, (c) urine, and (d) tumoral tissues with the stochastic microsensor based on IN/GR-BN.

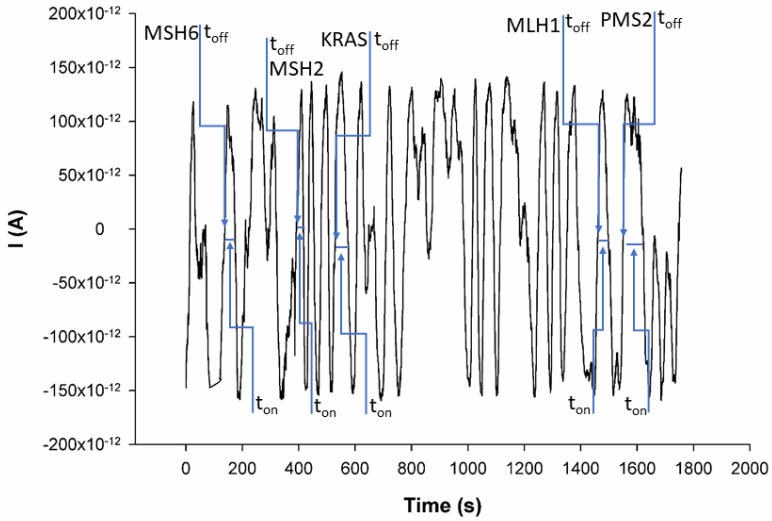

(a)

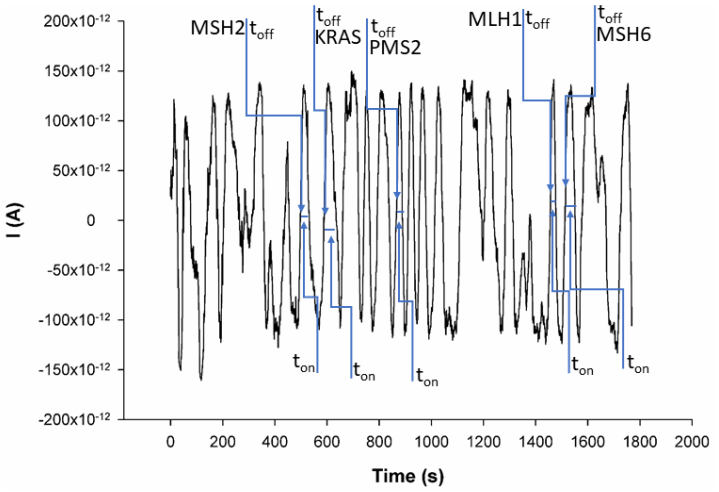
MSH2 t_{off}
t_{off} KRAS
t_{off} PMS2
MLH1 t_{off}
t_{off} MSH6
t_{on}
t_{on}
t_{on}
t_{on}
t_{on}
I (A)
Time (s)

(b)

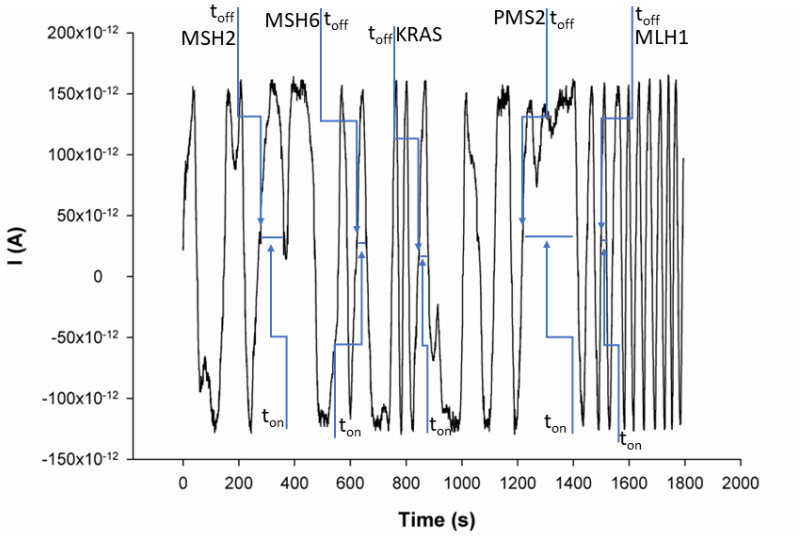
t_{off} MSH2
MSH6 t_{off}
t_{off} KRAS
PMS2 t_{off}
t_{off} MLH1
t_{on}
t_{on}
t_{on}
t_{on}
t_{on}
I (A)
Time (s)

(c)

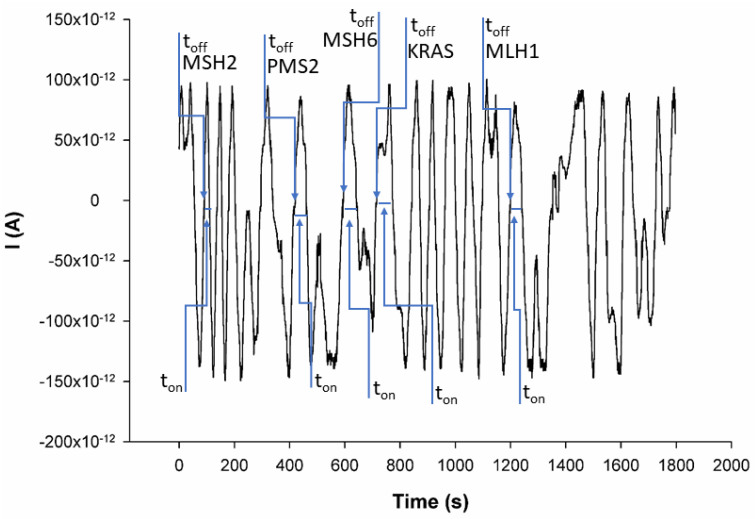

(d)

Figure 2. Typical diagrams obtained by screening (a) whole blood, (b) saliva, (c) urine, and (d) tumoral tissues with the stochastic microsensor based on IQ/GR-BN.

2. Results and discussions

2.1. Response characteristics of stochastic microsensors

The response characteristics for the proposed stochastic microsensors used for the assay of MLH1, MSH2, MSH6, PMS2, and of KRAS are shown in Table 1. The different signatures (t_{off} values) recorded for the MLH1, MSH2, MSH6, PMS2, and of KRAS favorized their simultaneous assay in the biological samples. Calibration graphs are given in Figures S1 and S2.

The widest linear concentration ranges for the assay of MLH1 and MSH6 were obtained when th e stochastic microsensor based on IN was used, while the widest linear concentration ranges for the assay of PMS2 and KRAS were obtained using the stochastic microsensor based on IQ. The modifier of the NB doped graphene paste (IN, IQ) did not influence either the linear concentration range or the limit of determination when used for the assay of MSH2. For the assay of MLH1 and MSH6, the lowest limit of determination was obtained when the IN based stochastic microsensor was used, while for the assay of PMS2, the lowest limit of determination was obtained when the stochastic microsensor based on IQ was used. The modifier (IN, IQ) did not influence the value of the limit of determination for the assay of KRAS.

Table 1. Response characteristics of the stochastic microsensors used for the assay of MLH1, MSH2, MSH6, PMS2, and of KRAS.

Stochastic microsensor based on GR-NB and	Signature, t_{off} (s)	Linear concentration range (g mL^{-1})	Calibration equations; the correlation coefficient, r*	Sensitivity (s^{-1} μg^{-1} mL)	LOQ (fg mL^{-1})
MLH1					
IN	1.6	3.10×10^{-16}-3.00×10^{-6}	$1/t_{on}=0.13+0.13\times C$; r=0.9997	0.13	0.31
IQ	1.2	3.20×10^{-11}-3.20×10^{-6}	$1/t_{on}=0.04+3.73\times10^{-2}\times C$; r=0.9788	3.73×10^{-2}	3.20×10^{4}
MSH2					
IN	1.4	1.00×10^{-15}-1.00×10^{-5}	$1/t_{on}=0.16+3.65\times10^{-2}\times C$; r=0.9985	3.65×10^{-2}	1.00
IQ	1.4	1.00×10^{-15}-1.00×10^{-5}	$1/t_{on}=0.04+8.46\times10^{-3}\times C$; r=0.9478	8.46×10^{-3}	1.00
MSH6					
IN	1.2	2.30×10^{-15}-2.30×10^{-7}	$1/t_{on}=0.03+2.14C$; r=0.9959	2.14	2.30
IQ	2.4	2.70×10^{-9}-2.70×10^{-7}	$1/t_{on}=0.03+1.07\times C$; r=0.9996	1.07	2.70×10^{6}
PMS2					
IN	1.9	2.70×10^{-9}-2.70×10^{-5}	$1/t_{on}=0.03+1.62\times10^{-2}\times C$; r=0.9883	1.62×10^{-2}	2.70×10^{6}
IQ	1.8	2.70×10^{-15}-2.70×10^{-10}	$1/t_{on}=0.03+3.44\times10^{2}\times C$; r=0.9435	3.44×10^{2}	2.70
KRAS					
IN	1.0	2.20×10^{-15}-2.20×10^{-6}	$1/t_{on}=0.32+2.67\times C$; r=0.9987	2.67	2.20
IQ	1.6	2.20×10^{-15}-2.20×10^{-5}	$1/t_{on}=0.04+1.56\times10^{-2}\times C$; r=0.9981	1.56×10^{-2}	2.20

*<C > - concentration = μg mL^{-1}; <t_{on}> = s; LOQ - limit of quantification

All sensors exhibited high sensitivity for the simultaneous assay of MLH1, MSH2, MSH6, PMS2, and KRAS in synthetic solutions, and in whole blood, saliva, urine, and tumoral tissue samples. No changes in response characteristics values were recorded when the stochastic microsensors were characterized in whole blood, saliva, urine, and tumoral tissues. High sensitivities were recorded for both sensors when used for the assay of mismatch repair proteins and KRAS. Compared with the

sensors proposed earlier for the simultaneous assay of MMP and KRAS [23, 24], the proposed stochastic microsensors provided lower limits of determination for the assay of MSH2, MSH6, PMS2, and KRAS, and wider linear concentration ranges for the assay of MLH1, MSH2, and MSH6.

Reproducibility studies were performed for each of the two stochastic microsensors. In this regard, 10 stochastic microsensors of each type were manufactured following the procedure shown in Sensor Design paragraph. Each of the sensors were evaluated in the same way, and the sensitivities were determined and compared when immersed in each of the solutions of the mismatch repair proteins and KRAS. The RSD (%) values recorded for the sensitivities were less than 0.21% when the microsensors based on IQ were tested, and less than 0.10% when the stochastic microsensors based on IN were tested. These values proved the reproducibility of the stochastic microsensors design.

The stability of each stochastic microsensor was checked as following: 30 stochastic microsensors of each type were stored as described in the Design of the stochastic microsensors paragraph. Each day, a new stochastic microsensor was removed from storage and immersed in solutions containing mismatched repair proteins and KRAS at varying concentrations; the sensitivities of each measurement were kept for comparison after the entire lot of stochastic microsensors was consumed in 30 days. The results recorded at the end of the period showed the high stability of the stochastic microsensors in time because the variation of the sensitivities in time was less than 0.08%, despite the modifier (IN, IQ) used for the stochastic microsensors' design.

2.2. Determination of MLH1, MSH2, MSH6, PMS2, and KRAS in biological samples

More than 100 sets of biological samples: whole blood, saliva, urine, and tumoral tissues were screened using the proposed stochastic microsensors. Examples of diagrams obtained are shown in Figures 1 and 2. After the identification of each of the mismatch repair protein and of KRAS, their concentration was determined accordingly with the procedure described in the Stochastic method paragraph.

The results shown in Figure 3 prove the good correlation between the concentration obtained for MLH1, MSH2, MSH6, PMS2, and KRAS in whole blood, saliva, urine, and tumoral tissue samples.

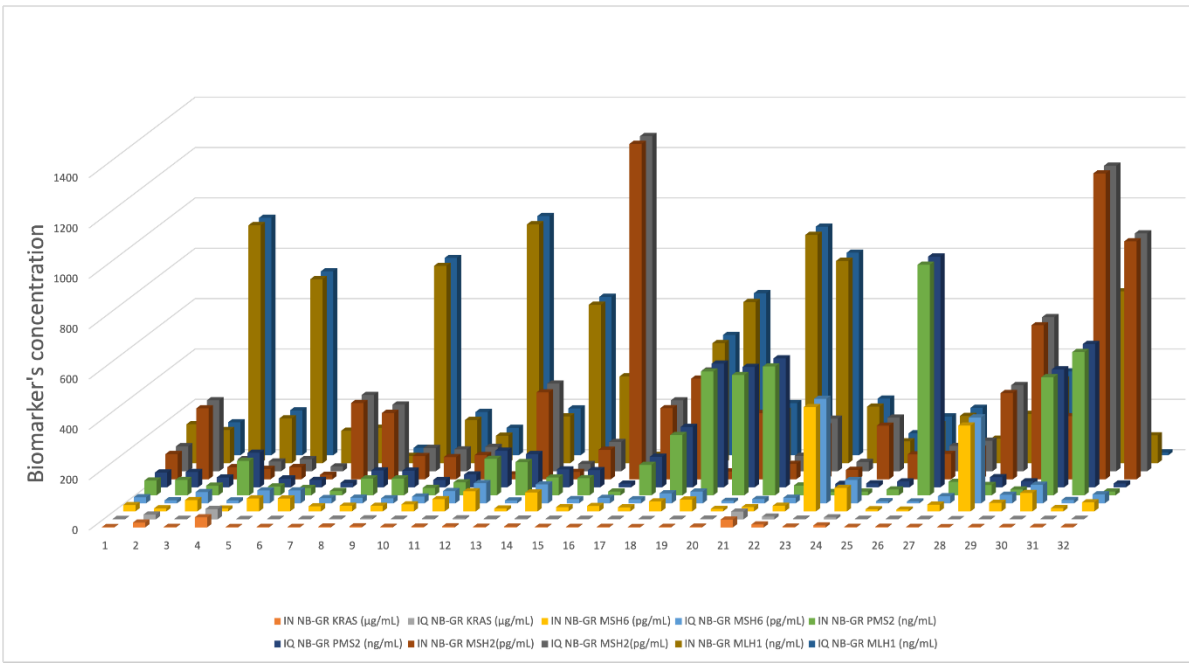
Biomarker's concentration
0
200
400
600
800
1000
1200
1400
1 2 3 4 5 6 7 8 9 10 11 12 13 14 15 16 17 18 19 20 21 22 23 24 25 26 27 28 29 30 31 32
IN NB-GR KRAS (µg/mL)
IQ NB-GR KRAS (µg/mL)
IN NB-GR MSH6 (pg/mL)
IQ NB-GR MSH6 (pg/mL)
IN NB-GR PMS2 (ng/mL)
IQ NB-GR PMS2 (ng/mL)
IN NB-GR MSH2(pg/mL)
IQ NB-GR MSH2(pg/mL)
IN NB-GR MLH1 (ng/mL)
IQ NB-GR MLH1 (ng/mL)

(a)

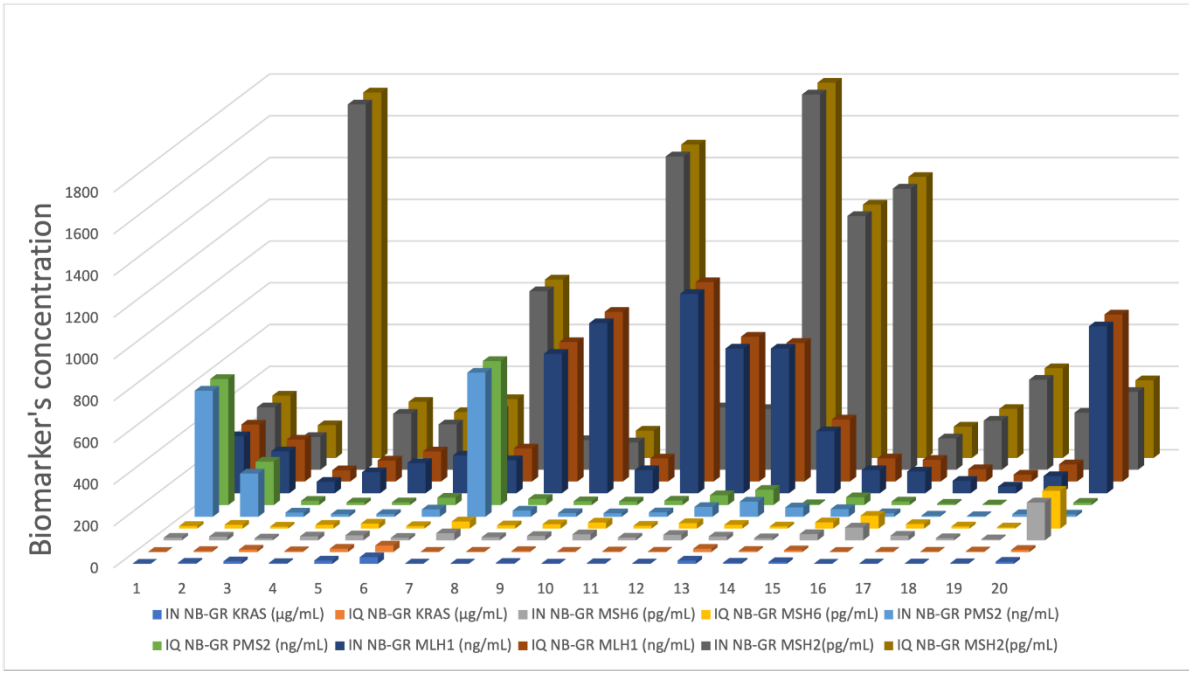
Biomarker's concentration
0
200
400
600
800
1000
1200
1400
1600
1800
1 2 3 4 5 6 7 8 9 10 11 12 13 14 15 16 17 18 19 20
IN NB-GR KRAS (µg/mL)
IQ NB-GR KRAS (µg/mL)
IN NB-GR MSH6 (pg/mL)
IQ NB-GR MSH6 (pg/mL)
IN NB-GR PMS2 (ng/mL)
IQ NB-GR PMS2 (ng/mL)
IN NB-GR MLH1 (ng/mL)
IQ NB-GR MLH1 (ng/mL)
IN NB-GR MSH2(pg/mL)
IQ NB-GR MSH2(pg/mL)

(b)

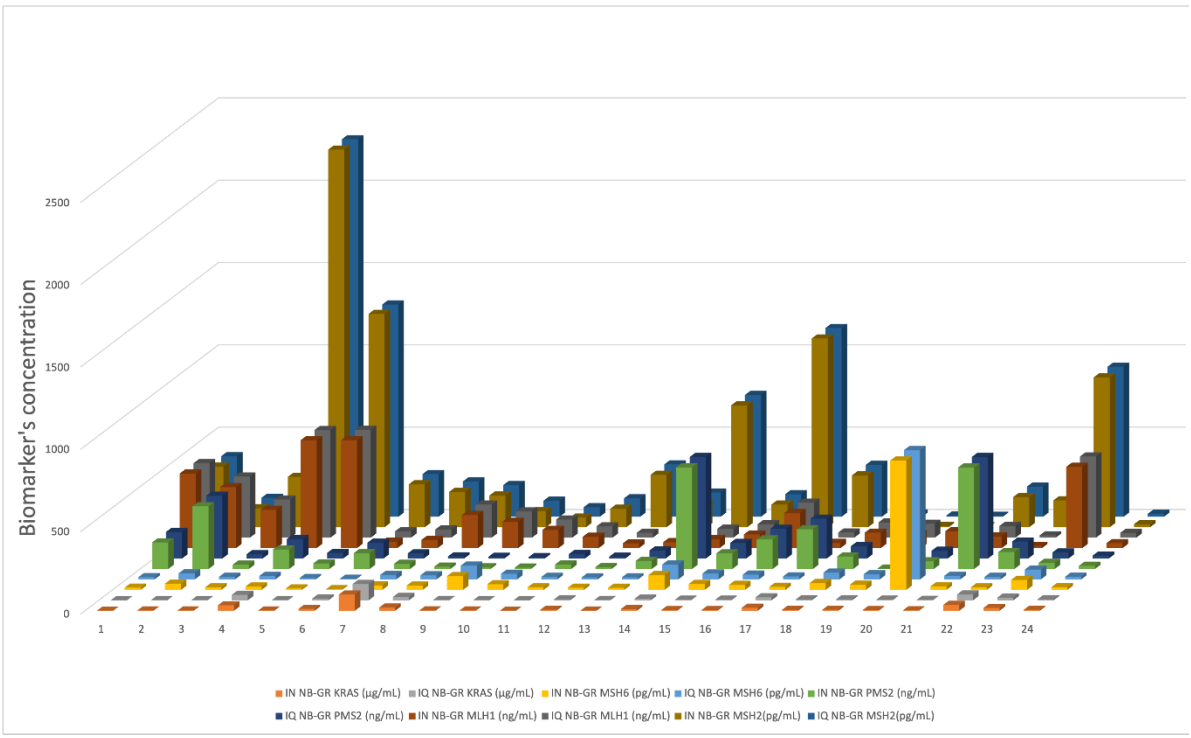

(c)

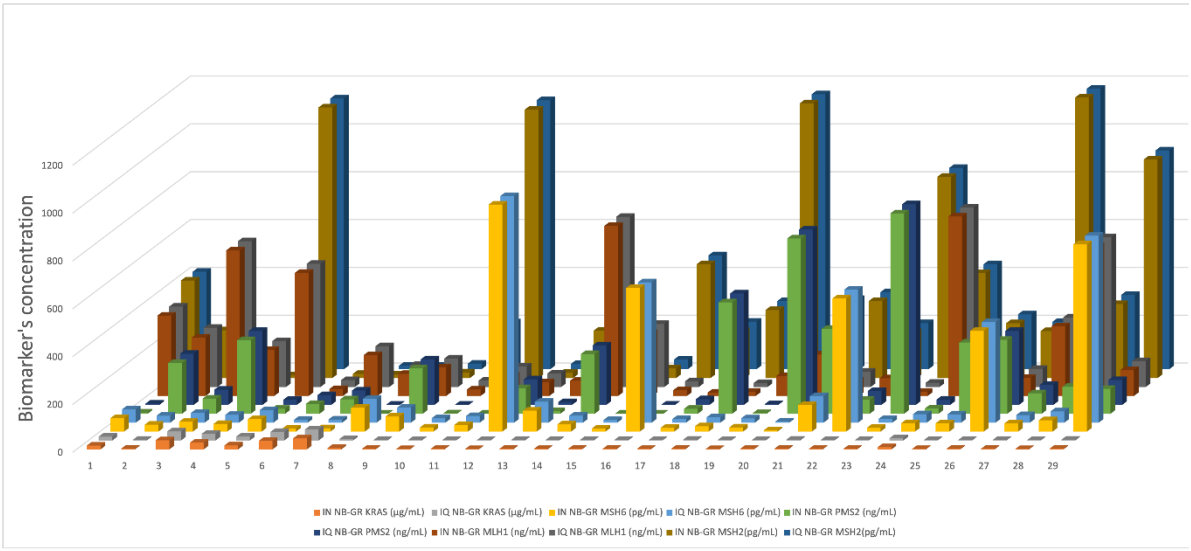

(d)

Figure 3. Determination of MLH1, MSH2, MSH6, PMS2, and KRAS in (a) whole blood, (b) saliva, (c) urine, and (d) tumoral tissue samples using the stochastic microsensors based on GR-NB and IN, respectively, IQ.

A paired Student t-test was also done at the 99.00% confidence level, for which the tabulated value was 4.13. All values obtained – when the results of IN based stochastic microsensor were compared with the IQ based stochastic microsensor, for the t-test were lower than 3.00, proving that there is no significant difference between the results obtained using the two stochastic microsensors.

Further validation was performed by doing recovery tests of the MLH1, MSH2, MSH6, PMS2, and KRAS in whole blood, saliva, urine, and tumoral tissue samples using the two stochastic microsensors based on IN and IQ. The initial amounts of MLH1, MSH2, MSH6, PMS2, and KRAS in whole blood, saliva, urine, and tumoral tissue samples were determined, and after that, in each type of sample, different amounts – from very small to higher amounts (calculated to be fitted within the working concentration range of each of the sensors) were added to the samples, and new measurements were performed. The added amount was compared with the found amount of MLH1, MSH2, MSH6, PMS2, and KRAS in whole blood, saliva, urine, and tumoral tissue samples. The results are given in Table 2.

Table 2. Recovery of MLH1, MSH2, MSH6, PMS2, and KRAS from biological samples (N = 10).

Stochastic microsensors based on GR-NB and	**Recovery %**				
	MLH-1	**MSH-2**	**MSH-6**	**PMS-2**	**KRAS**
			Whole blood		
IN	99.10±0.01	99.18±0.02	99.98±0.01	99.54±0.02	98.95±0.02
IQ	99.17±0.03	99.12±0.02	99.95±0.04	99.00±0.03	99.83±0.05
			Saliva		
IN	99.10±0.01	99.25±0.02	99.97±0.02	99.48±0.02	99.97±0.02
IQ	98.96±0.04	99.15±0.06	99.12±0.05	98.99±0.03	98.90±0.02
			Urine		
IN	98.91±0.02	99.32±0.02	99.15±0.01	98.93±0.02	99.54±0.03
IQ	98.23±0.04	98.95±0.02	99.00±0.05	98.91±0.03	98.93±0.03
			Tumoral tissue		
IN	99.99±0.01	99.97±0.03	99.91±0.02	99.99±0.03	99.96±0.01
IQ	99.35±0.04	99.23±0.02	99.49±0.01	99.53±0.02	99.81±0.05

The recovery tests performed show high values for recoveries (all higher than 98.00%) with very low RSD (%), lower than 0.10%, when 10 measurements were performed. Accordingly, high accuracy and precision were achieved when the proposed stochastic sensors were used for the screening of biological samples.

Tables 3,4,5, and 6 shown the results obtained using the proposed microsensors and ELISA (the standard method used for the assay of MLH1, MSH2, MSH6, PMS2, and KRAS).

Table 3 Comparison of data obtained using the stochastic microsensors and ELISA kits for determination of MLH1, MSH2, MSH6, PMS2, and KRAS in whole blood (N=10).

Sample No.	Method based on	MLH1, ng mL^{-1}	MSH2, pg mL^{-1}	MSH6, pg mL^{-1}	PMS2, ng mL^{-1}	KRAS, μg mL^{-1}
1	GR-NB-IN	157.00±0.01	99.43±0.01	24.24±0.02	58.86±0.01	1.63±0.01
	GR-NB-IQ	155.43±0.03	100.28±0.02	24.96±0.03	58.79±0.01	1.60±0.02
	ELISA	155.12±0.43	99.12±0.23	25.00±0.67	58.00±0.98	1.62±0.22
2	GR-NB-IN	131.00±0.02	282.18±0.04	12.35±0.03	61.00±0.03	19.14±0.02
	GR-NB-IQ	132.00±0.07	282.00±0.03	12.00±0.04	61.20±0.01	19.19±0.01
	ELISA	132.12±0.54	281.97±0.87	11.97±0.65	60.87±0.32	18.97±0.44
3	GR-NB-IN	943.21±0.02	48.32±0.02	44.90±0.03	39.00±0.02	2.02±0.02
	GR-NB-IQ	945.45±0.04	48.15±0.03	44.80±0.01	38.24±0.01	1.97±0.02
	ELISA	945.99±0.43	48.00±0.76	44.12±0.54	38.00±0.65	1.95±0.33
4	GR-NB-IN	178.00±0.02	38.97±0.04	11.61±0.02	137.30±0.01	40.96±0.01
	GR-NB-IQ	178.15±0.02	41.40±0.03	11.21±0.04	136.95±0.03	40.18±0.02
	ELISA	177.00±0.33	38.00±0.27	11.50±0.97	136.00±0.55	39.00±0.65
5	GR-NB-IN	730.63±0.02	48.48±0.02	51.53±0.01	34.97±0.02	1.49±0.02
	GR-NB-IQ	731.28±0.02	48.56±0.08	51.48±0.04	34.15±0.01	1.67±0.01
	ELISA	730.00±0.32	48.00±0.28	52.40±0.75	34.00±0.58	1.50±0.22
6	GR-NB-IN	129.07±0.01	19.02±0.03	51.51±0.02	29.57±0.02	2.02±0.01
	GR-NB-IQ	129.28±0.03	18.18±0.03	51.20±0.01	29.14±0.02	1.97±0.03
	ELISA	129.00±0.54	17.33±0.38	51.00±0.39	29.00±0.27	2.00±0.25
7	GR-NB-IN	140.29±0.01	303.13±0.02	21.00±0.02	17.40±0.01	1.70±0.04
	GR-NB-IQ	141.00±0.02	302.97±0.04	20.20±0.02	17.17±0.04	1.79±0.02
	ELISA	140.00±0.55	302.00±0.48	20.25±0.30	17.90±0.38	1.70±0.22
8	GR-NB-IN	29.75±0.05	265.00±0.02	22.30±0.01	67.02±0.05	3.12±0.01
	GR-NB-IQ	29.00±0.02	263.63±0.04	22.19±0.07	67.00±0.04	3.42±0.02
	ELISA	29.00±0.43	262.90±0.76	22.00±0.55	66.76±0.50	4.00±0.53
9	GR-NB-IN	783.62±0.02	92.57±0.02	20.10±0.03	66.12±0.04	4.10±0.02

	GR-NB-IQ	784.02±0.03	92.20±0.03	22.03±0.02	67.00±0.02	4.20±0.01
	ELISA	784.00±0.25	92.00±0.57	20.00±0.39	67.40±0.70	3.80±0.43
10	GR-NB-IN	172.00±0.03	87.20±0.02	27.05±0.01	29.29±0.04	2.25±0.02
	GR-NB-IQ	172.04±0.04	88.05±0.02	27.93±0.02	29.54±0.03	2.32±0.03
	ELISA	171.60±0.55	87.50±0.54	27.00±0.87	29.00±0.27	2.00±0.32
11	GR-NB-IN	108.78±0.03	96.96±0.04	48.79±0.05	50.97±0.02	2.87±0.04
	GR-NB-IQ	109.32±0.04	96.12±0.02	48.56±0.03	52.51±0.03	2.98±0.01
	ELISA	108.00±0.33	96.00±0.30	48.00±0.44	50.15±0.28	2.68±0.53
12	GR-NB-IN	950.17±0.02	19.60±0.02	80.37±0.03	145.30±0.02	4.11±0.02
	GR-NB-IQ	948.78±0.03	19.32±0.03	79.98±0.02	144.97±0.02	4.12±0.03
	ELISA	948.00±0.55	19.20±0.38	79.00±0.57	144.00±0.48	4.25±0.27
13	GR-NB-IN	629.17±0.02	28.92±0.04	75.51±0.04	71.28±0.03	3.23±0.02
	GR-NB-IQ	629.49±0.02	29.15±0.04	75.15±0.03	71.03±0.04	3.21±0.01
	ELISA	630.00±0.68	28.50±0.50	75.00±0.20	72.00±0.54	3.50±0.30
14	GR-NB-IN	345.02±0.03	116.30±0.04	16.92±0.02	68.28±0.04	2.21±0.02
	GR-NB-IQ	345.15±0.02	117.17±0.03	16.84±0.03	68.30±0.02	2.19±0.03
	ELISA	345.00±0.70	116.00±0.43	16.00±0.28	68.00±0.29	2.10±0.54
15	GR-NB-IN	477.82±0.02	400.15±0.02	39.97±0.01	240.02±0.01	1.53±0.03
	GR-NB-IQ	477.03±0.04	400.11±0.02	39.40±0.02	239.42±0.02	1.50±0.02
	ELISA	477.50±0.60	400.00±0.28	39.00±0.28	239.40±0.38	1.50±0.17
16	GR-NB-IN	643.77±0.03	30.52±0.04	47.00±0.05	491.40±0.02	2.15±0.01
	GR-NB-IQ	640.27±0.05	31.24±0.04	47.15±0.02	491.92±0.02	2.15±0.07
	ELISA	640.00±0.28	30.30±0.53	47.00±0.21	490.90±0.86	2.00±0.26
17	GR-NB-IN	207.12±0.03	263.12±0.08	9.95±0.02	478.20±0.01	3.09±0.03
	GR-NB-IQ	207.93±0.01	263.01±0.06	10.13±0.03	478.00±0.02	3.05±0.04
	ELISA	207.00±0.65	262.80±0.43	10.00±0.28	477.75±0.60	3.00±0.38
18	GR-NB-IN	907.93±0.02	61.15±0.02	17.19±0.02	512.27±0.01	31.21±0.04
	GR-NB-IQ	906.95±0.04	61.20±0.04	17.20±0.01	512.04±0.02	30.94±0.02
	ELISA	906.00±0.49	61.00±0.54	17.00±0.29	512.25±0.37	30.60±0.20
19	GR-NB-IN	804.60±0.01	209.00±0.03	22.14±0.01	38.15±0.02	11.19±0.02
	GR-NB-IQ	803.92±0.03	210.21±0.01	22.09±0.02	38.83±0.03	11.92±0.03
	ELISA	803.00±0.43	208.95±0.21	22.00±0.27	38.20±0.65	11.00±0.27
20	GR-NB-IN	224.97±0.01	37.19±0.04	415.32±0.04	13.50±0.02	2.94±0.01

	GR-NB-IQ	225.07±0.02	37.37±0.02	414.14±0.03	13.13±0.04	2.95±0.03
	ELISA	224.25±0.28	37.00±0.27	413.20±0.54	13.00±0.28	2.55±0.78
Student t-test for GR-NB-IN		1.87	1.19	1.23	2.01	1.98
Student t-test for GR-NB-IQ		1.77	1.09	1.14	2.16	2.03

Table 4 Comparison of data obtained using the stochastic microsensors and ELISA kits for determination of MLH1, MSH2, MSH6, PMS2, and KRAS in urine (N=10).

Sample No.	Method based on	MLH1, ng mL^{-1}	MSH2, pg mL^{-1}	MSH6, pg mL^{-1}	PMS2, ng mL^{-1}	KRAS, μg mL^{-1}
1	GR-NB-IN	452.30±0.02	367.24±0.01	13.57±0.02	161.29±0.03	0.78±0.03
	GR-NB-IQ	453.01±0.03	367.47±0.03	13.14±0.02	161.32±0.02	0.78±0.01
	ELISA	452.00±0.21	366.80±0.38	13.20±0.54	161.37±0.54	0.70±0.15
2	GR-NB-IN	370.95±0.04	114.98±0.04	37.17±0.01	380.96±0.04	1.76±0.01
	GR-NB-IQ	370.14±0.02	115.08±0.01	37.21±0.02	380.65±0.02	1.74±0.03
	ELISA	368.90±0.76	115.45±0.55	36.90±0.85	380.00±0.22	1.69±0.50
3	GR-NB-IN	231.47±0..04	306.01±0.01	15.38±0.02	26.00±0.03	1.61±0.03
	GR-NB-IQ	232.10±0.05	305.87±0.02	15.36±0.03	26.32±0.01	1.64±0.01
	ELISA	230.90±0.80	305.70±0.75	15.30±0.29	27.00±0.40	1.60±0.25
4	GR-NB-IN	653.01±0.04	2293.04±0.01	20.80±0.02	118.00±0.03	32.95±0.03
	GR-NB-IQ	655.01±0.02	2293.00±0.03	20.03±0.03	118.30±0.01	33.00±0.01
	ELISA	655.00±0.50	2290.60±0.50	19.90±0.90	118.00±0.20	32.00±0.75
5	GR-NB-IN	655.03±0.01	1289.04±0.03	8.49±0.02	33.94±0.02	1.62±0.04
	GR-NB-IQ	655.00±0.02	1295.03±0.02	8.48±0.03	33.74±0.02	1.54±0.02
	ELISA	654.80±0.40	1290.00±0.40	8.50±0.21	33.00±0.75	1.50±0.21
6	GR-NB-IN	38.42±0.03	259.14±0.03	3.85±0.03	95.97±0.03	11.12±0.04
	GR-NB-IQ	38.80±0.02	260.32±0.02	3.80±0.01	95.79±0.02	11.48±0.03
	ELISA	37.90±0.26	258.90±0.43	3.80±0.20	95.00±0.24	11.50±0.20
7	GR-NB-IN	49.73±0.03	214.32±0.02	27.03±0.03	31.20±0.07	98.98±0.03
	GR-NB-IQ	50.02±0.04	214.12±0.02	27.14±0.02	31.13±0.03	98.14±0.01
	ELISA	50.00±0.21	213.70±0.05	27.20±0.30	31.78±.70	99.17±0.30

8	GR-NB-IN	200.93±0.01	192.04±0.01	25.00±0.01	13.15±0.02	20.20±0.02
	GR-NB-IQ	201.00±0.02	192.30±0.04	25.84±0.03	13.90±0.03	19.18±0.03
	ELISA	200.26±0.43	192.00±0.23	25.07±0.54	13.00±0.38	18.97±0.21
9	GR-NB-IN	159.16±0.02	97.27±0.01	83.76±0.03	10.15±0.04	1.94±0.02
	GR-NB-IQ	158.95±0.03	96.95±0.02	83.14±0.01	9.97±0.05	1.92±0.01
	ELISA	158.06±0.54	96.89±0.32	82.78±0.76	9.85±0.23	1.90±0.21
10	GR-NB-IN	110.12±0.01	58.03±0.02	34.22±0.02	8.41±0.03	1.72±0.02
	GR-NB-IQ	110.34±0.02	58.40±0.01	34.18±0.01	8.41±0.02	1.81±0.08
	ELISA	110.05±0.23	57.92±0.43	34.98±0.45	7.54±0.21	1.70±0.34
11	GR-NB-IN	68.39±0.02	111.98±0.03	15.00±0.05	27.31±0.02	0.80±0.02
	GR-NB-IQ	68.40±0.03	112.12±0.02	15.15±0.04	27.30±0.01	0.78±0.01
	ELISA	68.00±0.56	112.89±0.45	15.20±0.23	26.90±0.56	0.70±0.13
12	GR-NB-IN	212.03±0.01	1146.12±0.02	29.30±0.02	179.95±0.02	3.71±0.02
	GR-NB-IQ	212.30±0.04	1146.03±0.02	30.92±0.03	179.19±0.02	3.53±0.01
	ELISA	212.67±0.65	1146.47±0.26	28.47±0.65	178.98±0.43	3.80±0.24
13	GR-NB-IN	31.09±0.03	314.99±0.03	18.12±0.02	241.75±0.01	18.03±0.02
	GR-NB-IQ	31.23±0.02	314.92±0.02	18.23±0.03	241.23±0.03	18.01±0.03
	ELISA	31.78±0.30	313.87±0.43	18.50±0.28	240.95±0.54	17.90±0.43
14	GR-NB-IN	92.48±0.03	20.05±0.08	40.99±0.01	75.32±0.02	5.62±0.02
	GR-NB-IQ	93.50±0.01	21.40±0.02	41.07±0.02	75.78±0.01	5.60±0.02
	ELISA	92.77±0.23	20.19±0.23	39.95±0.29	74.90±0.39	4.98±0.23
15	GR-NB-IN	84.03±0.04	7.30±0.02	31.42±0.05	2.32±0.05	6.01±0.02
	GR-NB-IQ	83.80±0.01	7.40±0.02	30.98±0.03	2.20±0.02	5.98±0.01
	ELISA	82.98±0.43	7.60±0.32	29.97±0.54	2.67±0.21	5.45±0.23
16	GR-NB-IN	102.14±0.03	5.60±0.01	785.03±0.05	47.00±0.03	3.94±0.02
	GR-NB-IQ	102.30±0.02	5.48±0.03	785.00±0.03	46.42±0.01	3.53±0.02
	ELISA	101.95±0.32	5.50±0.38	784.97±0.45	45.76±0.67	3.50±0.23
17	GR-NB-IN	70.83±0.03	183.15±0.02	21.52±0.03	616.71±0.02	2.33±0.01
	GR-NB-IQ	70.96±0.01	183.05±0.03	21.05±0.03	616.03±0.03	2.34±0.04
	ELISA	71.90±0.54	182.90±0.32	21.00±0.23	616.23±0.43	2.50±0.21
18	GR-NB-IN	492.95±0.02	911.05±0.01	59.78±0.02	36.80±0.01	16.06±0.02
	GR-NB-IQ	493.19±0.03	910.02±0.02	60.15±0.01	36.75±0.02	17.03±0.02
	ELISA	495.00±0.34	912.78±0.23	58.76±0.36	36.37±0.21	17.00±0.54

19	GR-NB-IN	29.03±0.03	18.30±0.02	16.28±0.02	18.12±0.01	6.01±0.01
	GR-NB-IQ	29.98±0.01	18.43±0.03	16.32±0.03	18.97±0.03	5.94±0.02
	ELISA	29.56±0.21	17.94±0.43	16.00±0.21	19.14±0.43	5.87±0.23
20	GR-NB-IN	81.97±0.03	136.98±0.04	36.02±0.01	94.38±0.03	3.40±0.01
	GR-NB-IQ	82.83±0.01	137.47±0.03	35.64±0.03	94.62±0.02	3.41±0.02
	ELISA	82.70±0.56	137.23±0.56	35.23±0.21	94.12±0.04	3.50±0.43
Student t-test for GR-NB-IN		1.21	2.14	1.79	1.90	2.46
Student t-test for GR-NB-IQ		1.65	2.03	2.05	1.76	2.20

Table 5 Comparison of data obtained using the stochastic microsensors and ELISA kits for determination of MLH1, MSH2, MSH6, PMS2, and KRAS in saliva (N=10).

Sample No.	Method based on	MLH1, ng mL^{-1}	MSH2, pg mL^{-1}	MSH6, pg mL^{-1}	PMS2, ng mL^{-1}	KRAS, μg mL^{-1}
1	GR-NB-IN	273.47±0.02	299.03±0.01	12.58±0.01	604.40±0.04	1.12±0.03
	GR-NB-IQ	272.97±0.03	299.00±0.02	12.47±0.03	604.02±0.03	1.13±0.01
	ELISA	272.76±0.34	298.65±0.46	12.35±0.34	603.98±0.32	1.10±0.32
2	GR-NB-IN	200.84±0.03	157.00±0.01	17.97±0.01	207.47±0.01	5.60±0.01
	GR-NB-IQ	200.94±0.02	157.12±0.03	18.50±0.03	207.93±0.02	5.40±0.02
	ELISA	200.52±0.43	156.21±0.43	18.20±76	207.00±0.21	6.02±0.32
3	GR-NB-IN	55.02±0.01	1750.43±0.03	9.15±0.01	20.47±0.02	12.47±0.03
	GR-NB-IQ	54.12±0.02	1751.23±0.02	9.28±0.03	20.48±0.03	12.31±0.01
	ELISA	54.45±0.21	1748.98±0.32	10.05±0.21	21.06±0.55	12.12±0.44
4	GR-NB-IN	100.87±0.02	268.43±0.03	18.84±0.01	12.94±0.01	4.32±0.02
	GR-NB-IQ	100.49±0.03	269.21±0.01	18.32±0.03	12.70±0.02	4.55±0.01
	ELISA	100.22±0.45	270.00±0.32	18.00±0.21	12.20±0.32	5.00±0.23
5	GR-NB-IN	143.97±0.02	217.32±0.03	23.97±0.03	13.51±0.01	16.23±0.01
	GR-NB-IQ	144.12±0.02	220.23±0.02	24.14±0.02	13.12±0.03	16.59±0.02
	ELISA	142.67±0.33	220.76±0.54	23.34±0.17	12.90±0.23	16.12±0.45
6	GR-NB-IN	181.14±0.03	281.94±0.01	12.13±0.01	35.51±0.01	32.00±0.01
	GR-NB-IQ	180.93±0.02	282.00±0.02	12.10±0.02	35.42±0.03	31.64±0.02

	ELISA	180.23±0.45	281.56±0.45	12.00±0.54	34.98±0.65	30.76±0.65
7	GR-NB-IN	158.43±0.02	855.43±0.02	34.00±0.02	690.57±0.01	1.98±0.02
	GR-NB-IQ	158.50±0.01	855.07±0.03	34.12±0.03	690.03±0.02	1.97±0.02
	ELISA	157.32±0.54	854.65±0.23	34.23±0.27	691.22±0.54	2.25±0.32
8	GR-NB-IN	668.00±0.02	142.03±0.02	15.17±0.04	30.02±0.08	2.03±0.01
	GR-NB-IQ	668.26±0.03	140.95±0.02	15.74±0.02	29.47±0.03	2.02±0.01
	ELISA	668.43±0.52	137.98±0.65	16.04±0.55	29.05±0.43	2.00±0.43
9	GR-NB-IN	814.93±0.02	131.20±0.07	21.04±0.02	18.03±0.02	5.09±0.01
	GR-NB-IQ	813.02±0.03	130.95±0.02	21.03±0.03	18.12±0.03	5.12±0.02
	ELISA	813.00±0.49	129.67±0.35	20.97±0.44	17.96±0.32	5.67±0.13
10	GR-NB-IN	110.93±0.01	1501.03±0.01	29.12±0.02	17.17±0.03	1.93±0.03
	GR-NB-IQ	110.48±0.03	1502.04±0.02	29.09±0.03	17.02±0.01	1.89±0.01
	ELISA	109.98±0.45	1503.03±0.76	28.97±0.34	16.94±0.43	1.70±0.23
11	GR-NB-IN	955.16±0.03	299.03±0.02	13.12±0.04	21.43±0.02	3.43±0.01
	GR-NB-IQ	955.32±0.01	298.96±0.01	13.70±0.02	21.15±0.03	3.50±0.02
	ELISA	954.98±0.44	298.20±0.34	13.56±0.45	20.67±0.56	4.02±0.23
12	GR-NB-IN	693.43±0.03	290.94±0.04	26.29±0.01	47.29±0.05	2.39±0.03
	GR-NB-IQ	694.00±0.02	291.90±0.03	26.17±0.03	47.15±0.03	2.40±0.02
	ELISA	693.96±0.54	290.45±0.55	27.99±0.43	47.20±0.24	2.78±0.43
13	GR-NB-IN	664.00±0.02	1798.02±0.01	18.60±0.01	72.95±0.01	16.16±0.03
	GR-NB-IQ	664.32±0.03	1798.21±0.03	18.18±0.02	73.12±0.03	16.28±0.02
	ELISA	664.87±0.58	1799.65±0.87	19.08±0.23	72.02±0.23	16.00±0.56
14	GR-NB-IN	297.14±0.01	1215.70±0.02	10.29±0.01	45.12±0.01	6.03±0.01
	GR-NB-IQ	297.13±0.02	1214.28±0.03	10.30±0.02	45.45±0.03	6.10±0.01
	ELISA	298.08±0.43	1215.66±0.56	9.89±0.38	45.34±0.65	7.04±0.55
15	GR-NB-IN	110.98±0.03	1346.87±0.01	30.02±0.01	37.00±0.01	8.92±0.03
	GR-NB-IQ	111.12±0.02	134.96±0.02	29.90±0.02	37.51±0.02	8.64±0.02
	ELISA	110.97±0.43	135.00±0.80	30.07±0.06	37.39±0.34	8.50±0.21
16	GR-NB-IN	104.07±0.02	150.13±0.04	61.32±0.02	17.25±0.05	1.30±0.01
	GR-NB-IQ	104.02±0.03	150.27±0.03	61.63±0.02	17.15±0.03	1.27±0.02
	ELISA	103.98±0.45	150.33±0.65	62.09±0.55	18.02±0.23	2.00±0.45
17	GR-NB-IN	59.87±0.01	235.20±0.01	22.35±0.05	5.98±0.08	2.21±0.04
	GR-NB-IQ	59.13±0.02	234.97±0.02	21.94±0.07	6.52±0.02	2.18±0.03

	ELISA	59.21±0.43	235.02±0.34	22.07±0.43	6.33±0.39	2.76±0.43
18	GR-NB-IN	32.14±0.02	431.27±0.01	10.47±0.03	3.31±0.03	2.37±0.01
	GR-NB-IQ	32.97±0.03	430.12±0.03	10.23±0.02	3.25±0.01	2.41±0.02
	ELISA	33.00±0.56	429.98±0.78	11.05±0.04	3.20±0.34	2.50±0.12
19	GR-NB-IN	82.28±0.02	273.40±0.01	5.20±0.01	12.90±0.01	3.43±0.01
	GR-NB-IQ	82.16±0.03	277.32±0.02	5.43±0.02	12.80±0.02	3.57±0.03
	ELISA	81.80±0.55	276.54±0.48	5.10±0.54	13.07±0.32	4.06±0.65
20	GR-NB-IN	800.10±0.03	373.21±0.01	181.02±0.04	11.11±0.02	10.32±0.01
	GR-NB-IQ	799.98±0.02	372.19±0.02	181.13±0.03	11.12±0.02	10.95±0.02
	ELISA	800.20±0.34	371.87±0.45	182.02±0.56	11.98±0.43	11.00±0.54
Student t-test for GR-NB-IN		2.12	2.19	1.96	1.56	1.67
Student t-test for GR-NB-IQ		1.87	2.02	1.98	2.04	1.70

Table 6 Comparison of data obtained using the stochastic microsensors and ELISA kits for determination of MLH1, MSH2, MSH6, PMS2, and KRAS in tumoral tissues (N=10).

Sample No.	Method based on	MLH1, ng mL^{-1}	MSH2, pg mL^{-1}	MSH6, pg mL^{-1}	PMS2, ng mL^{-1}	KRAS, μg mL^{-1}
1	GR-NB-IN	335.98±0.08	408.13±0.02	55.97±0.03	5.40±0.03	16.05±0.03
	GR-NB-IQ	336.48±0.02	407.93±0.02	55.98±0.02	5.47±0.02	16.14±0.02
	ELISA	335.22±0.43	407.20±0.54	56.32±0.54	5.40±0.23	16.00±0.22
2	GR-NB-IN	243.95±0.01	200.19±0.01	29.00±0.03	212.98±0.03	3.28±0.01
	GR-NB-IQ	248.00±0.02	198.35±0.01	29.18±0.01	213.58±0.03	3.25±0.01
	ELISA	247.90±0.65	198.20±0.58	28.85±0.34	212.50±0.56	3.20±0.29
3	GR-NB-IN	608.68±0.03	17.12±0.02	41.00±0.02	63.63±0.01	38.29±0.03
	GR-NB-IQ	609.84±0.02	17.84±0.02	40.58±0.03	63.60±0.01	38.17±0.01
	ELISA	609.25±0.44	17.00±0.58	40.20±0.87	64.00±0.54	38.55±0.32
4	GR-NB-IN	192.92±0.01	11.72±0.05	32.00±0.02	308.02±0.08	28.08±0.01
	GR-NB-IQ	192.37±0.02	11.68±0.04	32.91±0.03	309.10±0.04	28.12±0.03
	ELISA	192.50±0.22	11.00±0.65	32.00±0.78	308.10±0.44	28.00±0.54
5	GR-NB-IN	515.13±0.04	1131.84±0.03	51.94±0.02	20.97±0.05	16.70±0.02

	GR-NB-IQ	515.43±0.03	1131.97±0.01	52.42±0.01	21.20±0.05	16.30±0.04
	ELISA	515.20±0.70	1130.20±0.54	52.00±0.34	20.20±0.44	16.00±0.78
6	GR-NB-IN	28.93±0.04	17.98±0.02	12.49±0.01	41.02±0.04	35.70±0.02
	GR-NB-IQ	29.20±0.01	17.53±0.02	12.23±0.03	40.98±0.03	36.00±0.03
	ELISA	28.00±0.40	17.23±0.67	12.57±0.87	40.10±0.50	35.97±0.23
7	GR-NB-IN	171.04±0.04	14.94±0.03	13.93±0.03	60.34±0.02	46.23±0.02
	GR-NB-IQ	171.00±0.02	14.82±0.01	13.30±0.01	59.98±0.01	46.15±0.04
	ELISA	170.00±0.27	15.00±0.76	14.50±0.24	60.00±0.54	45.90±0.38
8	GR-NB-IN	92.40±0.03	14.87±0.03	99.87±0.03	1.05±0.02	5.69±0.01
	GR-NB-IQ	92.47±0.03	14.14±0.03	100.01±0.04	1.06±0.03	5.63±0.02
	ELISA	91.90±0.37	14.00±0.55	99.00±0.34	1.00±0.13	5.00±0.34
9	GR-NB-IN	119.57±0.02	24.07±0.01	62.95±0.01	190.27±0.02	2.21±0.01
	GR-NB-IQ	119.37±0.03	24.00±0.03	63.14±0.03	190.37±0.08	2.45±0.02
	ELISA	120.00±0.35	23.23±0.76	62.20±0.55	190.00±0.59	2.00±0.32
10	GR-NB-IN	27.00±0.01	194.37±0.08	17.03±0.01	1.71±0.03	1.70±0.02
	GR-NB-IQ	27.27±0.03	196.04±0.03	18.60±0.01	1.13±0.04	1.73±0.01
	ELISA	26.80±0.24	193.90±0.28	16.90±0.28	2.00±0.27	1.60±0.54
11	GR-NB-IN	85.47±0.02	1123.00±0.02	27.73±0.04	1.16±0.02	2.25±0.03
	GR-NB-IQ	86.00±0.04	1124.95±0.04	27.94±0.02	1.15±0.01	2.20±0.03
	ELISA	85.00±0.43	1125.04±0.43	27.00±0.21	1.20±0.20	2.00±0.44
12	GR-NB-IN	57.12±0.02	22.56±0.02	949.30±0.01	107.21±0.01	1.72±0.03
	GR-NB-IQ	57.03±0.03	22.39±0.03	947.93±0.03	106.96±0.02	1.71±0.02
	ELISA	56.32±0.87	22.78±0.43	946.20±0.28	105.99±0.43	1.60±0.43
13	GR-NB-IN	63.70±0.01	198.43±0.02	87.70±0.02	11.61±0.02	2.35±0.01
	GR-NB-IQ	63.43±0.04	199.03±0.01	87.73±0.01	11.58±0.02	2.38±0.01
	ELISA	63.50±0.40	198.21±0.43	86.60±0.43	11.00±0.21	2.00±0.20
14	GR-NB-IN	711.67±0.05	83.92±0.01	30.21±0.01	250.01±0.01	2.12±0.01
	GR-NB-IQ	711.93±0.02	83.50±0.02	29.50±0.03	249.09±0.01	2.11±0.01
	ELISA	711.00±0.32	83.00±0.54	29.40±0.65	248.00±0.20	2.50±0.32
15	GR-NB-IN	263.90±0.02	40.97±0.04	12.75±0.02	244.07±0.01	4.12±0.01
	GR-NB-IQ	264.05±0.01	40.95±0.03	11.19±0.04	244.95±0.03	4.10±0.04
	ELISA	263.00±0.23	39.80±0.25	11.20±0.28	243.55±0.43	4.00±0.26
16	GR-NB-IN	750.62±0.01	439.15±0.03	35.29±0.02	21.87±0.03	9.47±0.03

	GR-NB-IQ	750.94±0.03	439.24±0.01	35.43±0.03	21.92±0.03	9.42±0.03
	ELISA	748.20±0.32	438.20±0.23	34.70±0.21	22.00±0.43	9.20±0.23
17	GR-NB-IN	109.47±0.03	229.84±0.02	34.69±0.02	298.00±0.02	1.91±0.02
	GR-NB-IQ	109.10±0.02	229.61±0.01	34.68±0.03	298.98±0.01	1.89±0.02
	ELISA	109.23±0.43	229.00±0.29	34.21±0.49	297.54±0.28	1.52±0.21
18	GR-NB-IN	76.00±0.03	197.02±0.01	421.21±0.04	309.04±0.03	2.42±0.01
	GR-NB-IQ	76.43±0.03	197.98±0.03	420.98±0.03	309.10±0.02	2.40±0.02
	ELISA	75.07±0.38	196.98±0.42	420.00±0.43	308.75±0.21	2.20±0.15
19	GR-NB-IN	291.47±0.04	1173.29±0.03	34.22±0.03	85.64±0.04	2.34±0.01
	GR-NB-IQ	291.32±0.02	1172.98±0.02	31.86±0.04	83.24±0.02	2.31±0.02
	ELISA	290.98±0.34	1171.00±0.48	32.50±0.54	82.90±0.57	2.00±0.14
20	GR-NB-IN	107.98±0.02	914.37±0.08	782.93±0.02	104.14±0.08	3.39±0.01
	GR-NB-IQ	108.45±0.01	915.05±0.02	781.97±0.02	103.95±0.02	3.43±0.02
	ELISA	106.50±0.36	914.00±0.38	780.80±0.68	103.20±0.58	3.20±0.18
Student t-test for GR-NB-IN		2.12	1.98	2.03	1.05	2.20
Student t-test for GR-NB-IQ		1.13	1.97	2.40	1.70	1.67

The t-test performed for each of the results obtained using each of the microsensors versus ELISA, at 99.00% confidence level, shown that there is no significant difference between the results obtained using the stochastic microsensors and ELISA.

By comparing the results obtained in this paper with results obtained previously [23, 24] using stochastic sensors, the working concentration ranges are wider, and the limits of determination are far lower favorizing the identification and quantification of MLH1, MSH2, MSH6, PMS2, and KRAS in whole blood, saliva, urine, and tumoral tissue samples, at a very early stage, just when they are released in the body.

II. Sensors based on NSB-EGR and FHD/FTEX for quantification of MMR proteins and KRAS

1. Experimental part

1.1. Materials and reagents

Frutafit HD and frutafit TEX were purchased from Sensus (Roosendaal, The Netherlands). MLH1, MSH2, MSH6, PMS2, and KRAS were purchased from Sigma Aldrich (Milwaukee, USA); the paraffin oil was purchased from Fluka (Buchs, Switzerland). Monosodium phosphate and disodium phosphate were used for the preparation of phosphate buffer, pH=7.5. Deionized water obtained from a Millipore Direct-Q 3 System was used for the preparation of all solutions from 10^{-22} to 10^{-2} g mL^{-1} magnitude order. Nitrogen (9.3%) and Boron (2.4%) - dopped graphene (NB-DG) was provided by the National Institute of Research and Development of Isotopic and Molecular Technologies, Cluj-Napoca, Romania within the grant of the Ministry of Research, Innovation and Digitization, CNCS/CCCDI – UEFISCDI, project number PN-III-P4-ID-PCCF-2016-0006.

1.2. *Design of the combined microplatforms*

Design of the stochastic microsensors: 50μL of FHD and FTEX (10^{-3}mol L^{-1}), respectively, were each added to 50mg dopped graphene (NSB-EGR) paste (made by mixing NSB-EGR powder with paraffin oil). Each of the pastes were placed in 3D printed minitubes with internal diameter of 20μm; an Ag wire made the connection between the paste and the external circuit.

The stochastic microsensor was integrated in a microplatform together with the counter electrode (platinum wire), and the reference electrode (Ag/AgCl electrode) (Scheme 1).

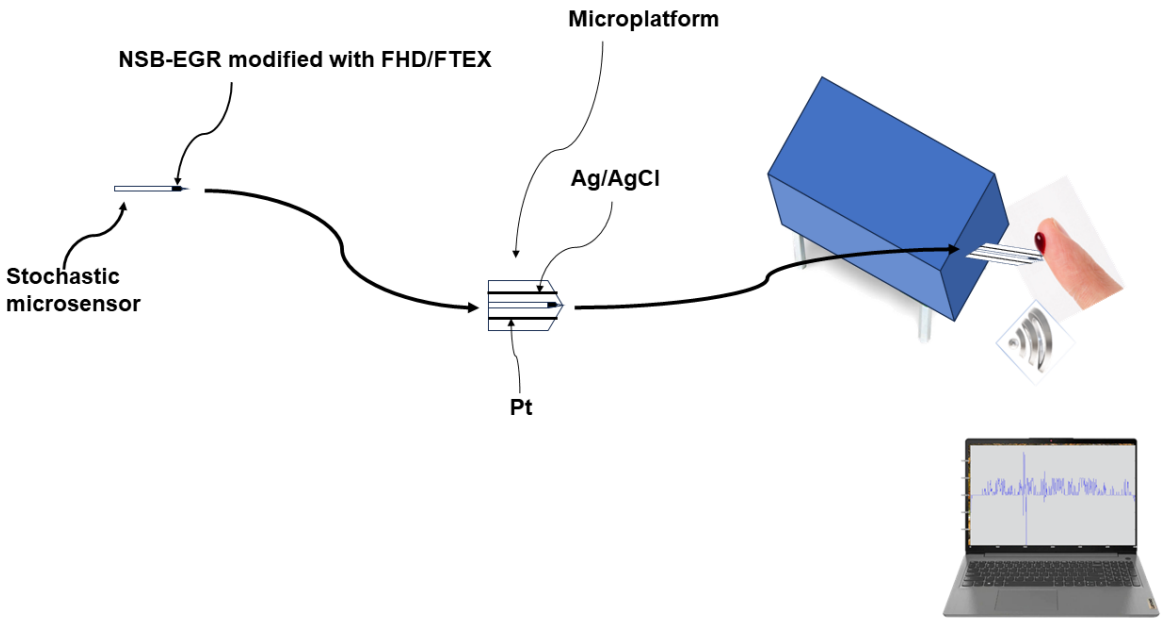

Scheme 1. Design of the stochastic microsensor, and microplatform of measurement used in simultaneous assay of MLH1, MSH2, MSH6, PMS2, and of KRAS in whole blood, urine, saliva, and tumoral tissues.

Before and after each measurement, cleaning with deionized water and soft drying with an adsorbant paper were performed. When not in use, the microplatforms were kept in a dry place, at room temperature.

1.3. Stochastic method

Chronoamperometry was used for all measurements. A potential of 125 mV vs Ag/AgCl was applied, and diagrams were recorded (Figures 1 and 2). The signatures (t_{off} values) of the MLH1, MSH2, MSH6, PMS2, and of KRAS, were identified in the diagrams, and served as recognition elements for the biomarkers. The values of t_{on} served for all quantitative measurements. Series of solutions of MLH1, MSH2, MSH6, PMS2, and of KRAS (with various concentrations) were used for the calibration of the microplatforms. The equations of calibration obtained for the biomarkers using each of the two microplatforms were based on the determination of the t_{on} value (read in between two consecutive t_{off} values); a, and b parameters from the equation of calibration $1/t_{on} = a + b \times Conc._{biomarker}$ were determined using the linear regression method. For the screening of whole blood, urine, saliva, and tumoral tissue, the biomarkers were recognized based on their signature (t_{off} values) (Figures 1 and 2), the t_{on} values were read and inserted into the equation of calibration for the determination of the concentration of MLH1, MSH2, MSH6, PMS2, and of KRAS in whole blood, urine, saliva, and tumoral tissue.

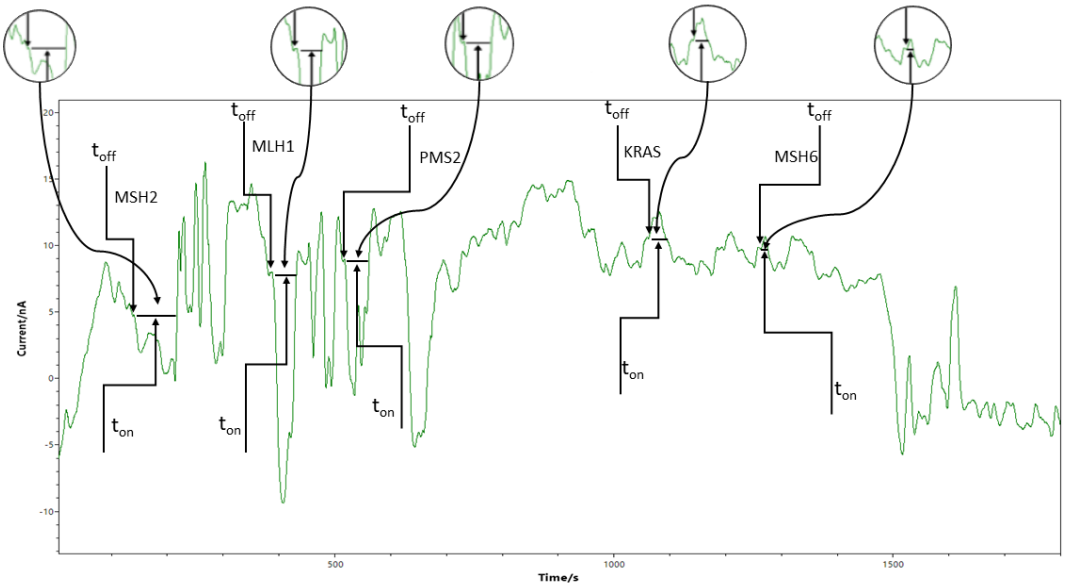
t_off
MSH2
t_on
t_off
MLH1
t_on
t_off
PMS2
t_on
t_off
KRAS
t_on
t_off
MSH6
t_on
Current/nA
Time/s

(a)

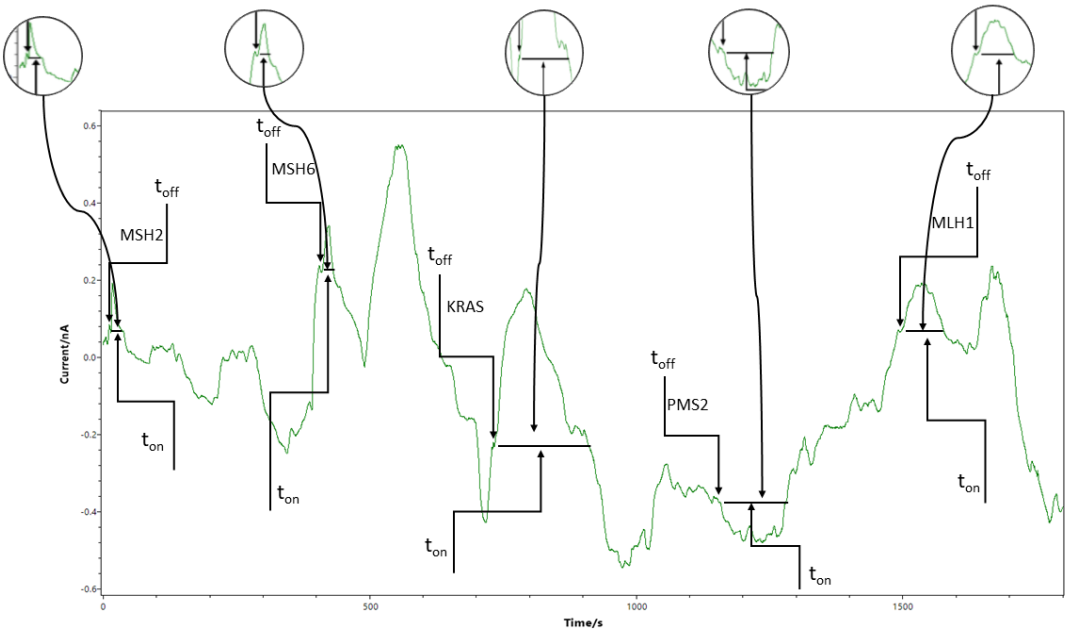
t_off
MSH2
t_on
t_off
MSH6
t_on
t_off
KRAS
t_on
t_off
PMS2
t_on
t_off
MLH1
t_on
Current/nA
Time/s

(b)

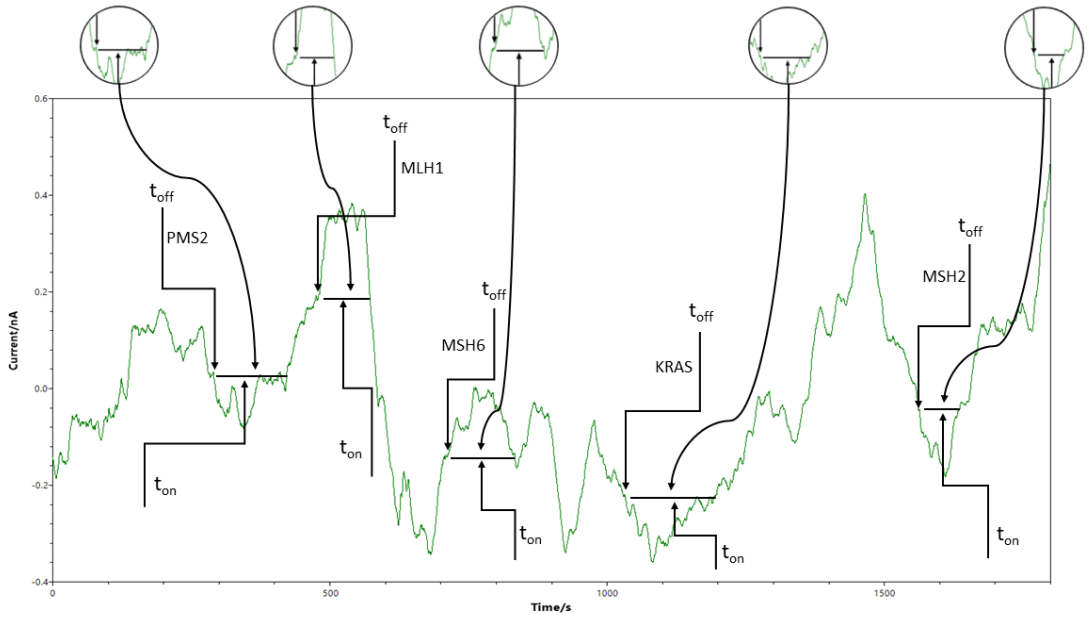

(c)

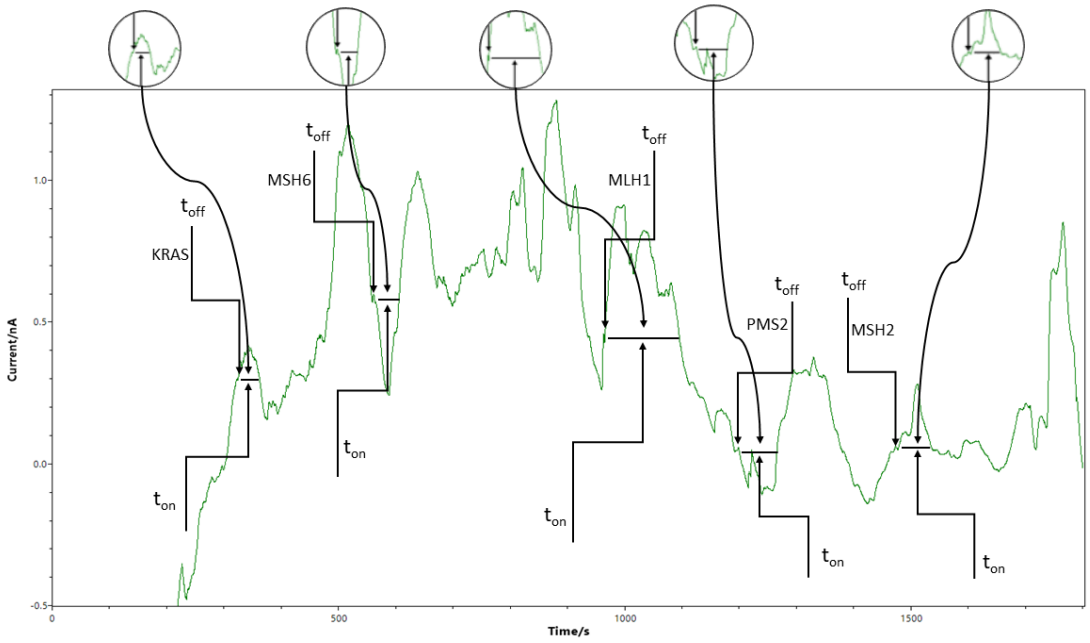

(d)

Figure 1. Typical diagrams obtained by screening (a) whole blood, (b) saliva, (c) urine, and (d) tumoral tissues with the microplatform based on FHD/NSB-EGR.

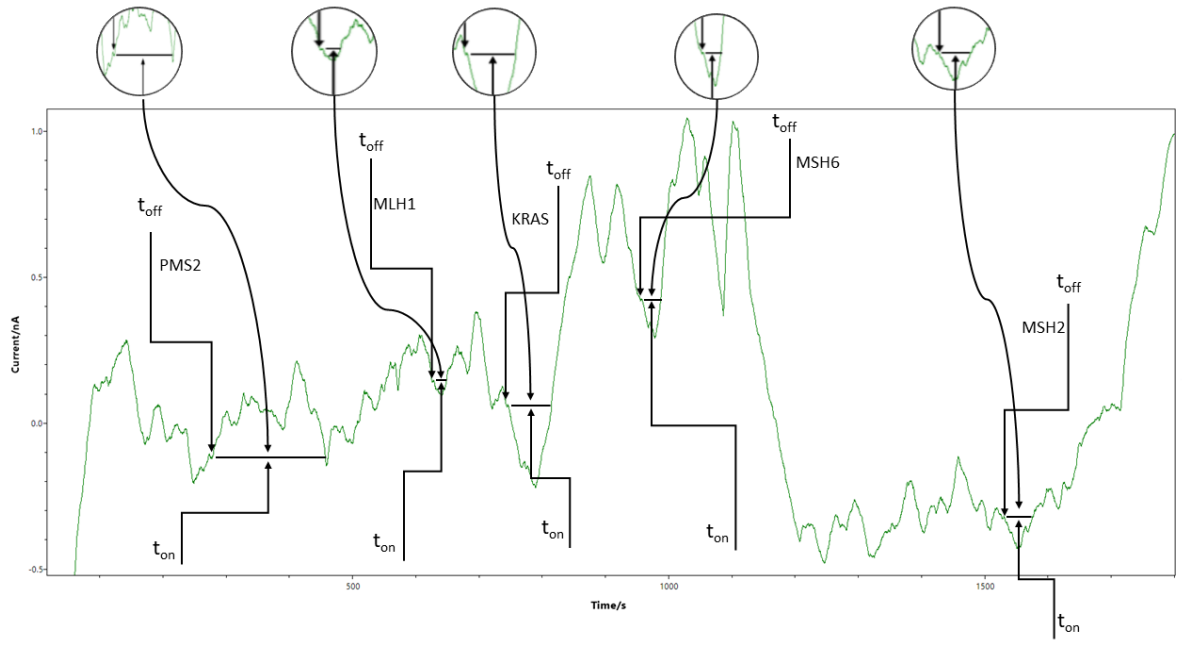
t_off
PMS2
t_on
t_off
MLH1
t_on
t_off
KRAS
t_on
t_off
MSH6
t_on
t_off
MSH2
t_on
Current/nA
Time/s

(a)

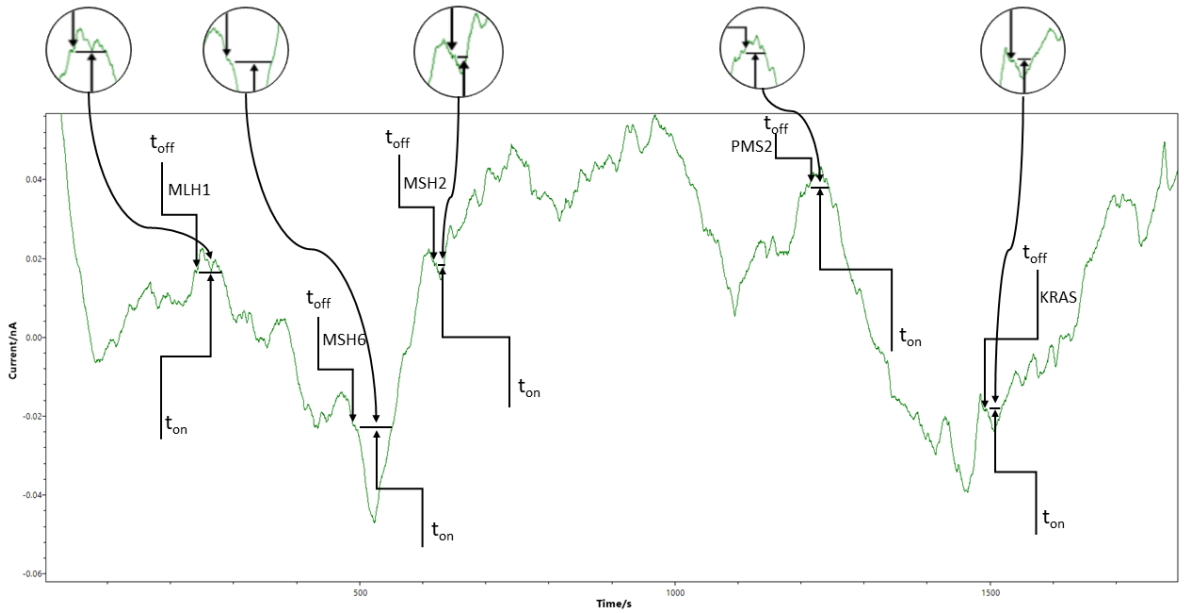
t_off
MLH1
t_on
t_off
MSH6
t_on
t_off
MSH2
t_on
t_off
PMS2
t_on
t_off
KRAS
t_on
Current/nA
Time/s

(b)

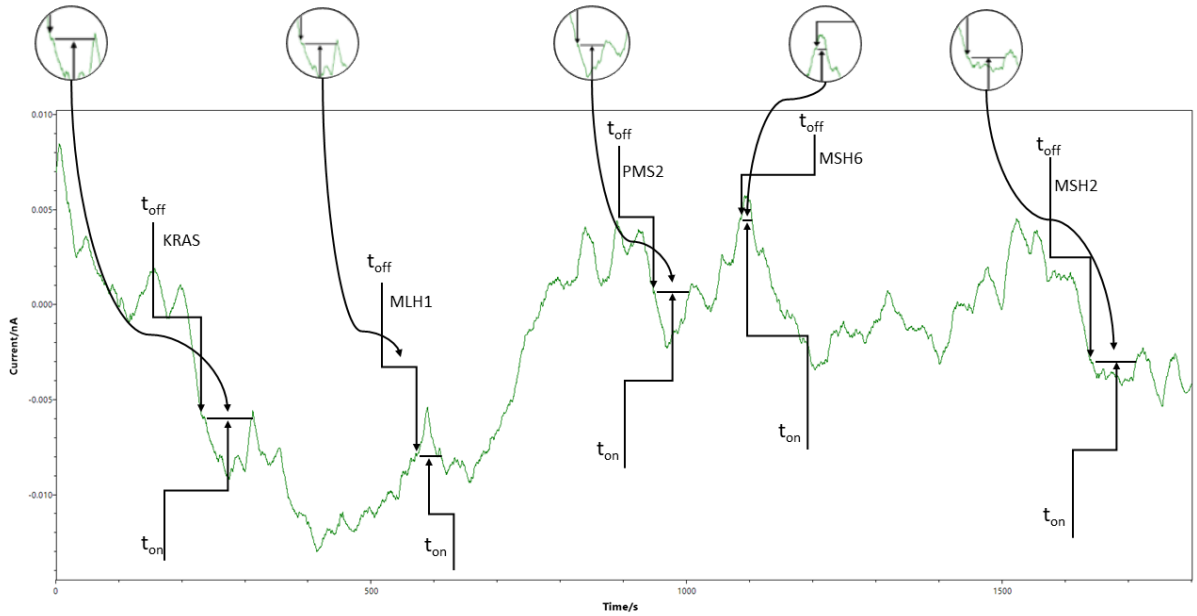

(c)

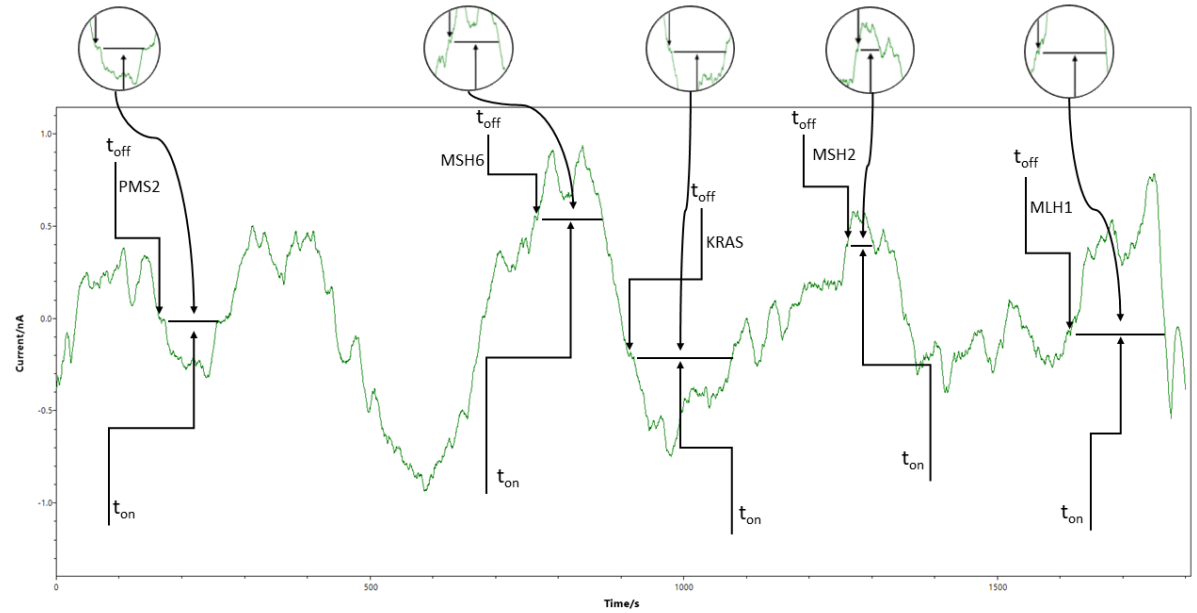

(d)

Figure 2. Typical diagrams obtained by screening (a) whole blood, (b) saliva, (c) urine, and (d) tumoral tissues with the microplatform based on FTEX/NSB-EGR.

Samples

Over 300 samples of whole blood, tumoral tissue, saliva, and urine samples were collected from the patients confirmed with colon cancers, and used for the measurements, without any pretreatment

before the analysis. None of the patients was undergoing any type of treatment for cancer at the collection of the samples. These samples were obtained from the Emergency Clinical Hospital of County Targu-Mures, which was granted permission to conduct the research by the Ethics Committee with the number 32647/14.12.2018, and from the Clinical Hospital County Targu-Mures, which was granted permission to conduct the research by the Ethics Committee with the number 3206/28.02.2019. Informed consent was obtained from all patients.

2. Response characteristics of the combined microplatforms

Stochastic mode was applied to determine all response characteristics of the proposed combined microplatforms. Different signatures were obtained for MLH1, MSH2, MSH6, PMS2, and of KRAS, when the same microplatform was used, proving that a reliable molecular recognition can be performed (Table 1). Response characteristics of the proposed combined microplatforms like, sensitivity, linear concentration range, limit of determination, were determined for both combined microplatforms (Table 1). Lower limits of determination – of fg mL^{-1} were obtained using the combined microplatforms. For the assay of MLH1, the highest sensitivity was recorded when FTEX was used in the design of the combined microplatform, while the widest linear concentration range was recorded when the FHD based combined microplatform was used. For the assay of MSH2, the widest linear concentration range was recorded when the FTEX based combined microplatform was used, while the lowest limit of determination and the highest sensitivity was recorded when the FHD based combined microplatform was utilized for the assay of MSH2. The lowest limit of determination obtained for the assay of MSH6, as well as the widest linear concentration range, and the highest sensitivity were reported for the combined microplatform based on FTEX. The widest linear concentration range and the highest sensitivity for the assay of PMS2 were obtained when the combined microplatform based on FHD was used. For the assay of KRAS, the widest linear concentration range was recorded when the combined microplatform based on FHD was used, and the highest sensitivity was obtained when the combined microplatform based on FTEX was used.

Table 1. Response characteristics of the miniplatforms used for the assay of MLH1, MSH2, MSH6, PMS2, and of KRAS.

Combined microplatform	Signature,	Linear concentration range (g mL^{-1})	Calibration equations; the correlation coefficient, r*	Sensitivity (s^{-1} μg^{-1} mL)	LOQ (fg mL^{-1})

based on NSB-EGR and	t_{off} (s)				
MLH1					
FHD	1.2	3.20×10^{-16}-3.20×10^{-5}	$1/t_{on}=0.11+2.06\times10^{-2}\times C$; r=0.9995	2.06×10^{-2}	0.32
FTEX	2.1	3.20×10^{-15}-3.20×10^{-6}	$1/t_{on}=0.05+1.03\times10^{-1}\times C$; r=0.9902	1.03×10^{-1}	3.20
MSH2					
FHD	2.0	1.00×10^{-15}-1.00×10^{-9}	$1/t_{on}=0.06+2.33\times10^{2}\times C$; r=0.9994	2.33×10^{2}	1.00
FTEX	1.1	1.00×10^{-14}-1.00×10^{-5}	$1/t_{on}=0.10+37.56\times C$; -2r=0.9979	37.56	10.00
MSH6					
FHD	1.8	2.30×10^{-9}-2.30×10^{-5}	$1/t_{on}=0.16+1.02\times10^{-2}\times C$; r=0.9947	1.02×10^{-2}	2.30×10^{6}
FTEX	3.4	2.30×10^{-15}-2.30×10^{-6}	$1/t_{on}=0.11+5.91\times10^{-3}\times C$; r=0.9907	5.91×10^{-3}	2.30
PMS2					
FHD	1.4	2.70×10^{-15}-2.70×10^{-5}	$1/t_{on}=0.15+1.71\times10^{4}\times C$; r=0.9996	1.71×10^{4}	2.70
FTEX	2.5	2.70×10^{-15}-2.70×10^{-6}	$1/t_{on}=0.09+2.00\times10^{-2}\times C$; r=0.9949	2.00×10^{-2}	2.70
KRAS					
FHD	1.6	2.20×10^{-15}-2.20×10^{-5}	$1/t_{on}=0.06+9.50\times10^{-3}\times C$; r=0.9976	9.50×10^{-3}	2.20
FTEX	1.3	2.20×10^{-15}-2.20×10^{-6}	$1/t_{on}=0.13+2.89\times10^{3}\times C$; r=0.9967	2.89×10^{3}	2.20

*<C > - concentration = μg mL^{-1}; <t_{on}> = s; LOQ - limit of quantification

Reproducibility and stability studies were performed for each type of combined microplatform. Ten combined microplatforms based on FHD, and on FTEX, respectively, were designed accordingly with the procedure described above. Measurements of the sensitivities were performed for each combined microplatform, and calculations of %, RSD were performed. Values for the %, RSD of the sensitivities calculated were less than 0.27% for the combined microplatform based on FHD while when FTEX was used %, RSD values less than 0.12% were recorded, proving the design' reproducibility of combined microplatforms. The 20 combined microplatforms' sensitivities were further checked for 30 days in order to establish their stability in time; for all tested combined microplatforms, %, RSD values less than 0.51% were recorded during the 30 days. The variance recorded for measurements performed

using both microplatforms when used for simultaneous assay of MLH1, MSH2, MSH6, PMS2, and of KRAS in whole blood, urine, saliva, and tissue samples, did not exceeded 0.10.

3. Bioanalysis of MMR: MLH1, MSH2, MSH6, PMS2, and of KRAS, using the combined microplatforms

The proposed combined microplatforms were used for the bioanalysis of 300 samples of whole blood, saliva, urine, and tumoral tissues from patients confirmed with colorectal cancer. Diagrams were recorded (Figures 1 and 2) and used for molecular recognition of MMR and KRAS based on their signatures (t_{off} values) as well. After the identification of each of MLH1, MSH2, MSH6, PMS2, and of KRAS, their concentration was determined accordingly with the procedure described in the Stochastic method paragraph.

A very good correlation between the results obtained using the combined microplatform based on FHD and using the combined microplatform based on FTEX (Figure 3) were obtained for all samples: MLH1, MSH2, MSH6, PMS2, and KRAS in whole blood, saliva, urine, and tumoral tissue samples.

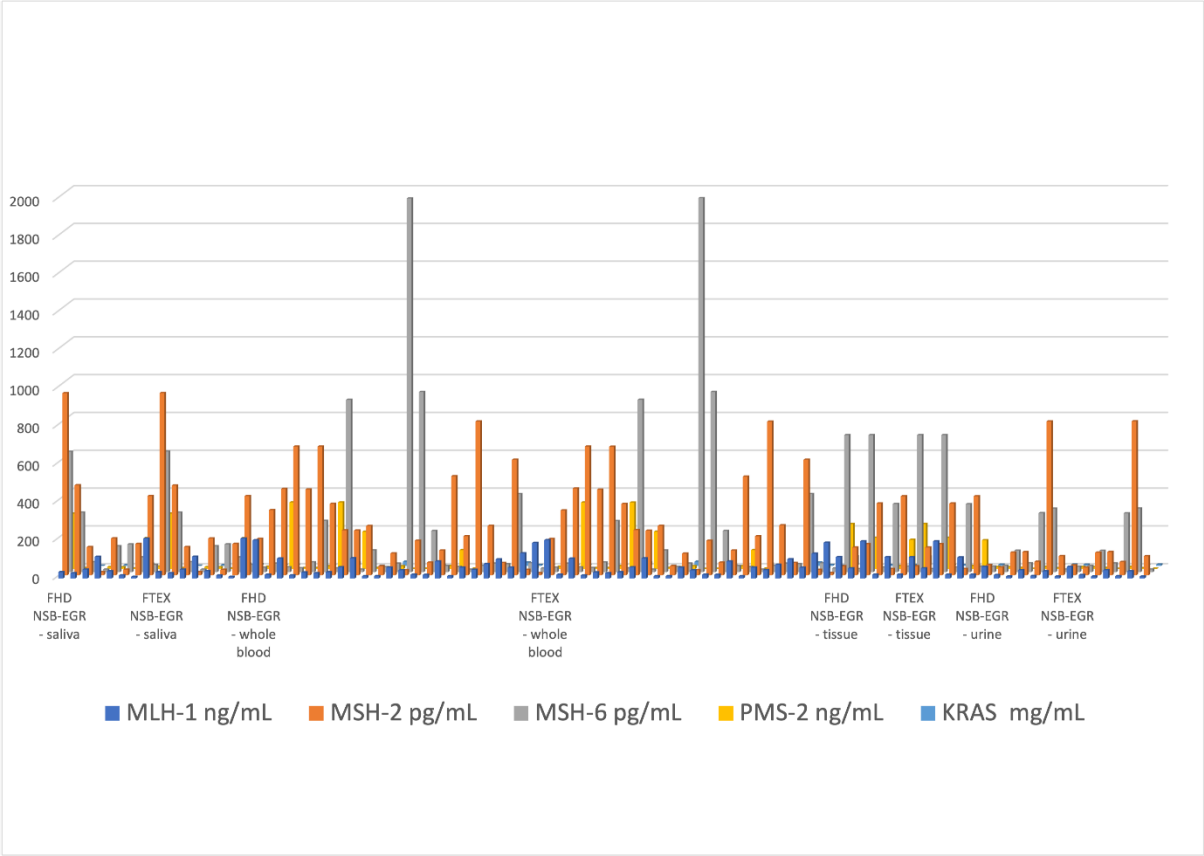

Figure 3. Determination of MLH1, MSH2, MSH6, PMS2, and KRAS in (a) whole blood, (b) saliva, (c) urine, and (d) tumoral tissue samples using the combined microplatforms based on FHD/NSB-EGR, and on FTEX/NSB-EGR.

Table 2 The %, RSD average values recorded for the determination of MLH1, MSH2, MSH6, PMS2, and KRAS in biological samples.

Combined microplatform based on NSB-EGR and		%, RSD									
		FHD NSB-EGR					FTEX NSB-EGR				
Biomarker		MLH-1	MSH-2	MSH-6	PMS-2	KRAS	MLH-1	MSH-2	MSH-6	PMS-2	KRAS
Biological fluid	Saliva	0.02	0.02	0.02	0.02	0.02	0.02	0.02	0.03	0.02	0.03
	Whole blood	0.02	0.03	0.02	0.02	0.02	0.02	0.03	0.02	0.02	0.02
	Tissue	0.02	0.02	0.02	0.03	0.03	0.02	0.02	0.03	0.02	0.02
	Urine	0.02	0.02	0.03	0.02	0.02	0.02	0.02	0.03	0.02	0.02

The %, RSD values associated to Figure 3 are shown in Table 2. The values determined shown a high reproducibility of the measurements performed with the combined microplatform.

The paired Student t-test was performed at 99.00% confidence level for all biomarkers: MLH1, MSH2, MSH6, PMS2, and KRAS. The calculated values for the t-test were lower than 3.21 (tabulated value at 99.00% confidence level is 4.13), proving that there is no significant difference between the results obtained using the two combined microplatforms based on FHD, and on FTEX.

Apart from the t-test, recovery tests of MLH1, MSH2, MSH6, PMS2, and KRAS were performed for whole blood, saliva, urine, and tumoral tissue samples. An initial screening was done to determine the amounts of MLH1, MSH2, MSH6, PMS2, and KRAS in whole blood, saliva, urine, and tumoral tissue samples. Ten different amounts of MLH1, MSH2, MSH6, PMS2, and KRAS were added to the real samples, and the final concentrations were determined. The added amounts of MLH1, MSH2, MSH6, PMS2, and KRAS in whole blood, saliva, urine, and tumoral tissue samples were compared with the found amounts. The results are given in Table 2.

Table 2. Recovery of MLH1, MSH2, MSH6, PMS2, and KRAS from whole blood, saliva, urine, and tumoral tissue samples (N = 10).

Combine microplatform based on NSB-EGR and	**Recovery, %**				
	MLH-1	**MSH-2**	**MSH-6**	**PMS-2**	**KRAS**
Whole blood					
FHD	99.99±0.02	99.96±0.01	99.83±0.02	99.87±0.02	99.95±0.02
FTEX	99.95±0.03	99.47±0.01	99.91±0.01	99.87±0.03	99.96±0.02
Saliva					
FHD	99.21±0.03	99.21±0.02	99.88±0.01	99.12±0.03	99.77±0.04
FTEX	99.77±0.05	99.30±0.01	99.90±0.02	95.43±0.04	99.43±0.02
Urine					
FHD	99.00±0.02	99.20±0.04	99.11±0.02	99.12±0.02	99.18±0.04
FTEX	99.11±0.04	99.22±0.02	99.05±0.01	99.08±0.03	99.21±0.02
Tumoral tissue					
FHD	98.90±0.03	98.60±0.03	98.77±0.02	98.90±0.03	98.73±0.01
FTEX	99.00±0.02	98.75±0.04	98.97±0.01	99.00±0.02	98.78±0.02

The performed recovery tests show high values for recoveries (all higher than 98.50%) with very low RSD (%), lower than 0.06%, when 10 measurements were performed. Accordingly, high accuracy and precision were achieved when the proposed combined microplatforms were used for the bioanalysis of the samples.

Compared to the results obtained for the assay of KRAS and MLH1, MSH2, MSH6, PMS2, [25, 26] using stochastic sensors, the working concentration ranges are wider, and the limits of determination are far lower, favorizing the identification and quantification of MLH1, MSH2, MSH6, PMS2, and KRAS in whole blood, saliva, urine, and tumoral tissue samples, at a very early stage of colon cancer.

III. Stochastics sensors for quantification of cathepsin B, cathepsin D and p53 protein

1. Experimental part

1.1. Reagents and materials

Cathepsins B, D, protein p53, Mn(OAP)Cl, diamond nanopowder and the buffer solution (pH=7.50) were bought from Sigma-Aldrich, while the paraffin oil was bought from Fluka. Nanopowder of graphene was purchased from SkySpring Nanomaterials, Inc., Houston, USA. Deionised water was used for all solutions preparations. Solutions of cathepsin B, cathepsin D, and p53 having different concentrations were obtained using the serial dilution method.

1.2. Construction of the stochastic microsensors

To form a homogeneous paste, the paraffin oil was added to the nanopowder of diamond. To the homogeneous diamond paste was added a solution of 1×10^{-3} mol L^{-1} Mn(OAP)Cl in a ratio of 1:1 (w:V; mg:μL) to give the modified paste for the construction of the Mn(OAP)Cl/nDP stochastic microsensor. For the construction of the Mn(OAP)Cl/nGR stochastic microsensor, paraffin oil was added to the nanopowder of graphene to form a graphene homogeneous paste. To the homogeneous graphene paste a solution of Mn(OAP)Cl (1×10^{-3} mol L^{-1}) was added to the homogeneous paste in a ratio of 1:1 (w:V; mg:μL) to obtain the active side of the Mn(OAP)Cl/nGR stochastic microsensor.

A 3D printer was used to obtain 3D plastic microtubes. These pastes were placed in the printed microtubes. An Ag wire was used as contact between the modified paste and the external circuit. The sensors were stored in dark places, at room temperature.

1.3. Stochastic method

When the potential of 125mV vs Ag/AgCl is applied (chronoamperometric technique), the variation of current will give values of t_{off} known as signatures of the analyte – because they occur when the biomarkers are getting into the channel (current drops to zero), blocking it until the molecule is

getting inside, and they are specific to each biomarker; t_{on} values are measured during the second phase, when the biomarker undergoes inside the channel binding and redox processes (its value is measured in between two t_{off} values) (Figures 1 and 2). Accordingly, the signature (t_{off} value) is a qualitative parameter used in the molecular recognition and differentiation of biomarkers, while the t_{on} value is a quantification parameter, used for the determination of the concentrations of the biomarkers, accordingly with the equation: $1/t_{on} = a + b \times C_{biomarker}$, where $C_{biomarker}$ is the concentration of the biomarker. The parameters of the equations of calibrations for each biomarker, using the two stochastic microsensors based on Mn(OAP)Cl/nDP and on Mn(OAP)Cl/nGr were obtained using the linear regression method. The unknown concentrations of biomarkers were obtained by inserting the t_{on} values obtained from the diagrams (Figures 1, and 2) into the equations of calibrations of each microsensors, for each of the biomarkers.

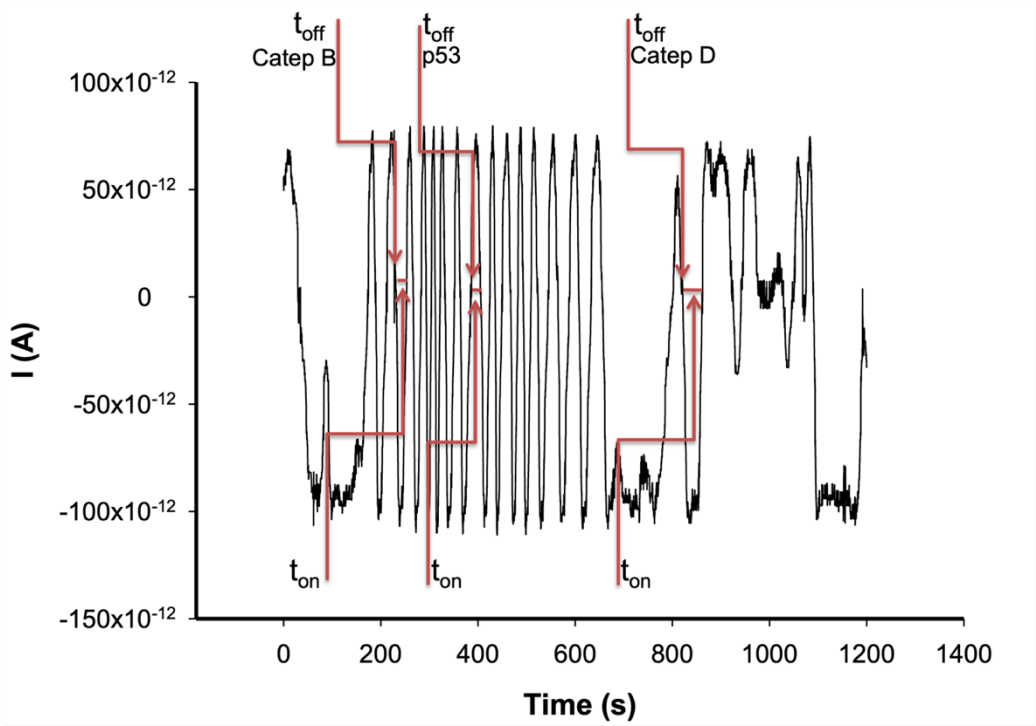

a)

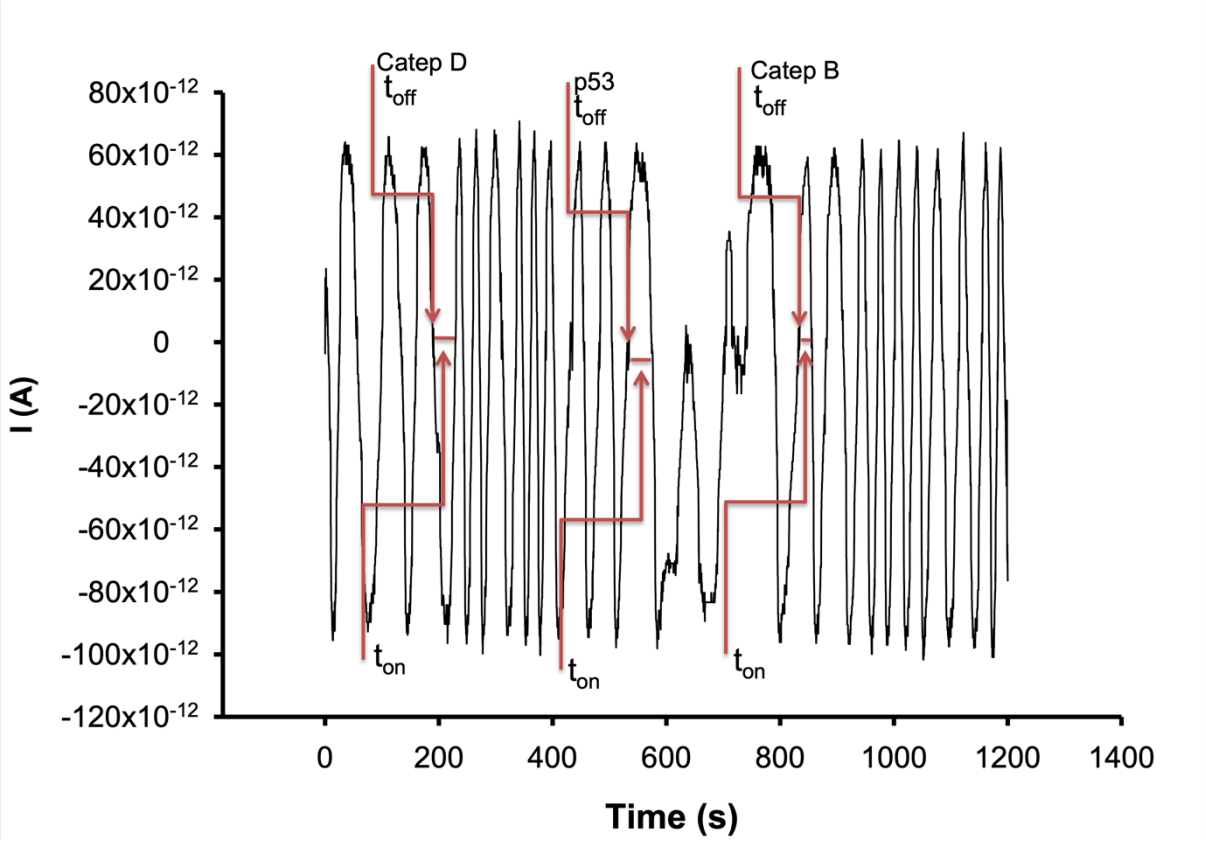
Catep D
t_{off}
p53
t_{off}
Catep B
t_{off}
t_{on}
t_{on}
t_{on}
80x10-12
60x10-12
40x10-12
20x10-12
0
-20x10-12
-40x10-12
-60x10-12
-80x10-12
-100x10-12
-120x10-12
I (A)
0
200
400
600
800
1000
1200
1400
Time (s)

b)

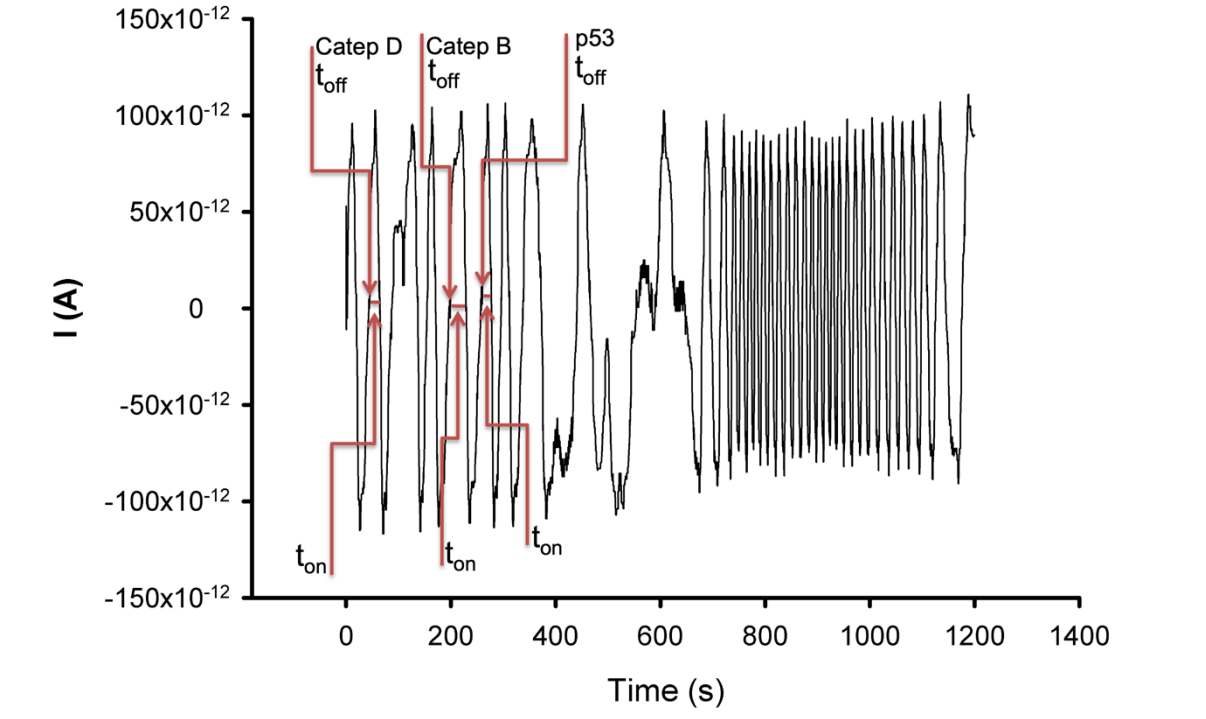
Catep D
t_{off}
Catep B
t_{off}
p53
t_{off}
t_{on}
t_{on}
t_{on}
150x10-12
100x10-12
50x10-12
0
-50x10-12
-100x10-12
-150x10-12
I (A)
0
200
400
600
800
1000
1200
1400
Time (s)

c)

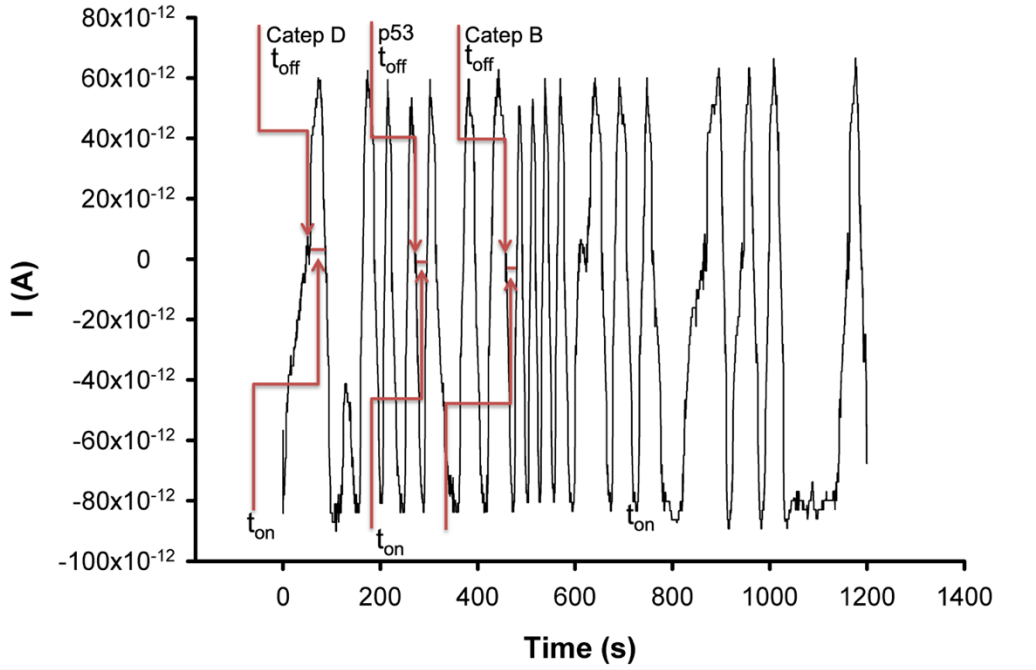

d)

Figure 1 Diagrams obtained for the screening, using the Mn(OAP)Cl/nDP based stochastic microsensors, of (a) saliva, (b) whole blood, (c) tumoral tissue, and (d) urine.

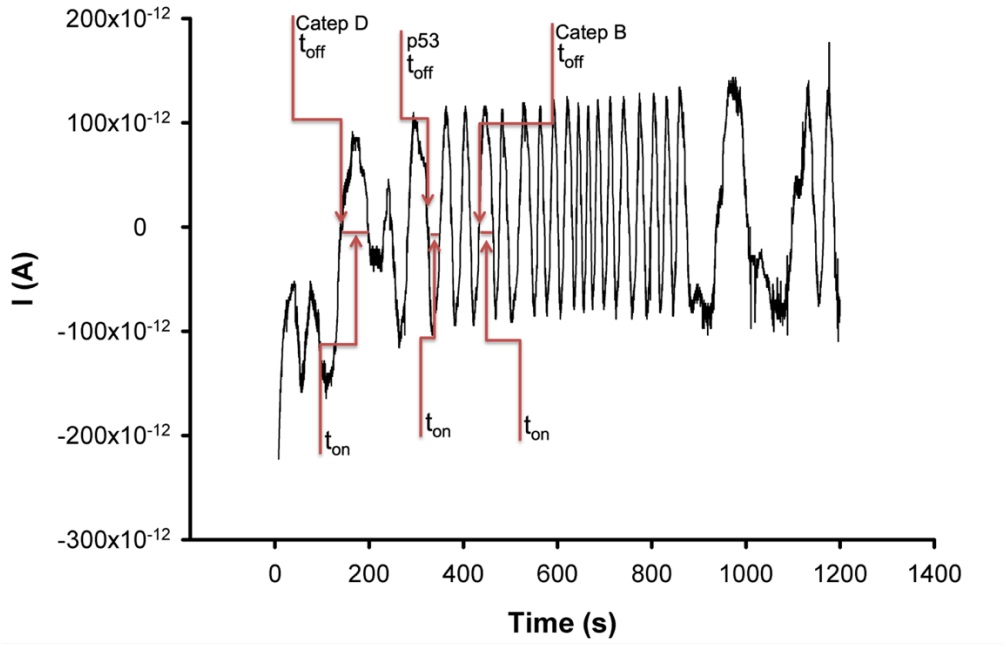

a)

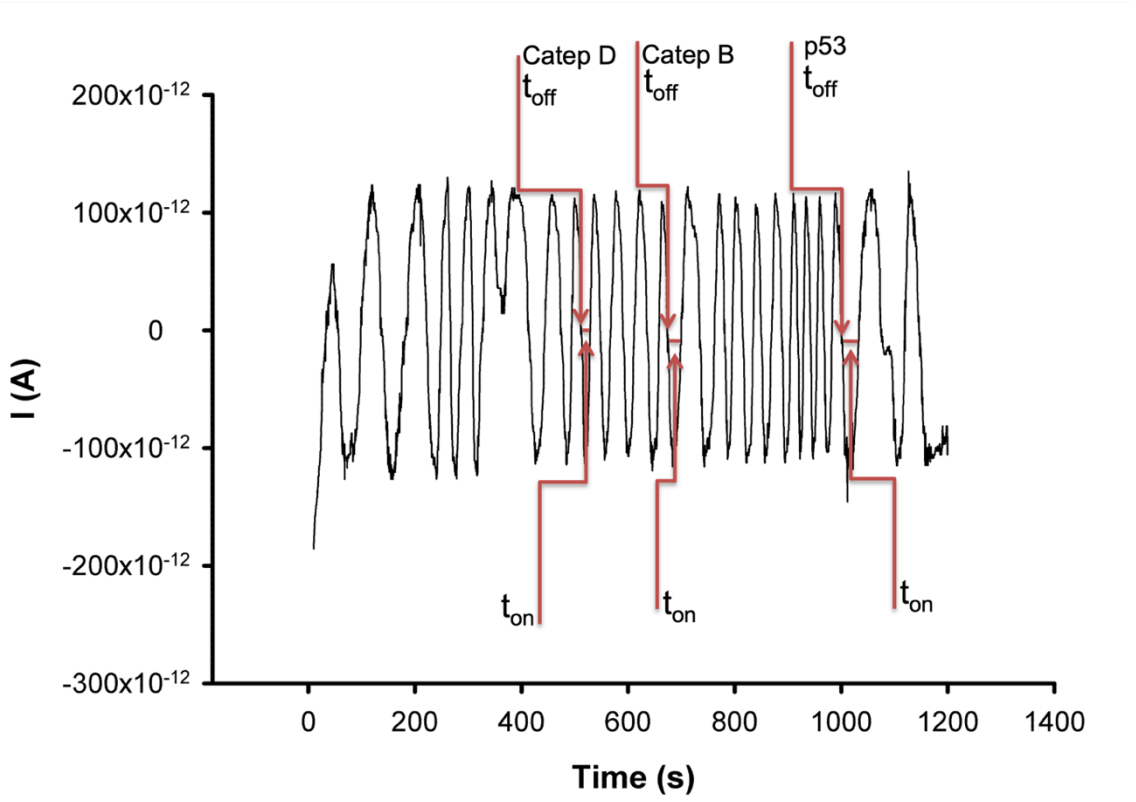
Catep D
t_{off}
Catep B
t_{off}
p53
t_{off}
t_{on}
t_{on}
t_{on}
200x10^{-12}
100x10^{-12}
0
-100x10^{-12}
-200x10^{-12}
-300x10^{-12}
I (A)
0
200
400
600
800
1000
1200
1400
Time (s)

b)

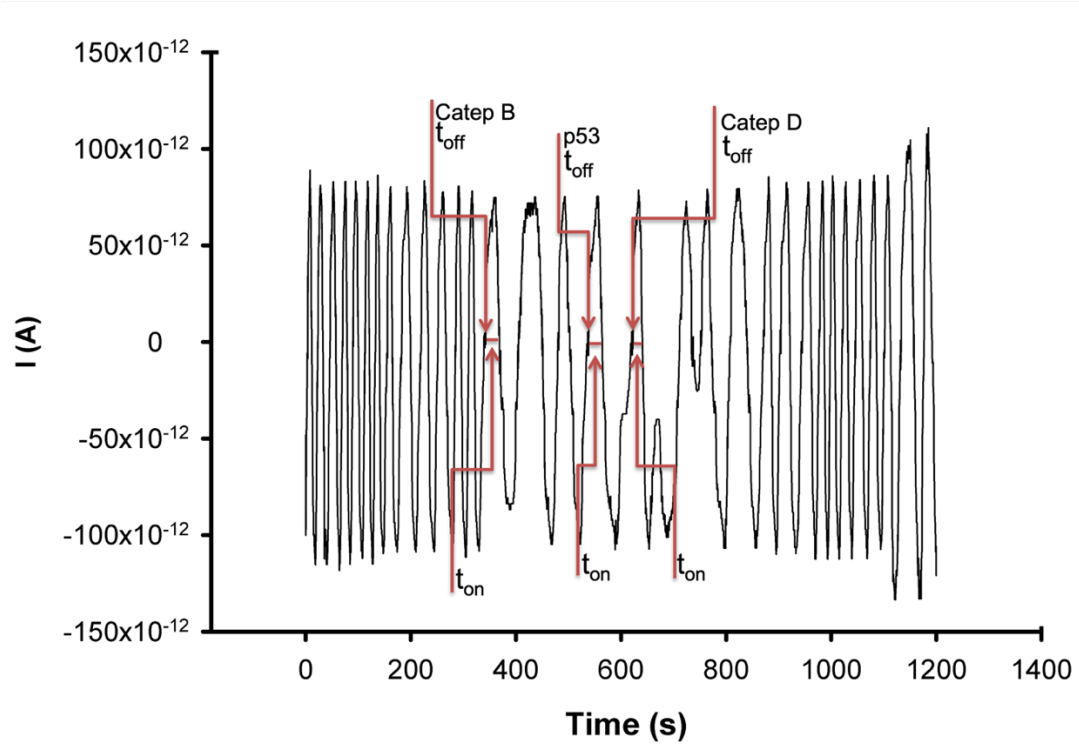
Catep B
t_{off}
p53
t_{off}
Catep D
t_{off}
t_{on}
t_{on}
t_{on}
150x10^{-12}
100x10^{-12}
50x10^{-12}
0
-50x10^{-12}
-100x10^{-12}
-150x10^{-12}
I (A)
0
200
400
600
800
1000
1200
1400
Time (s)

c)

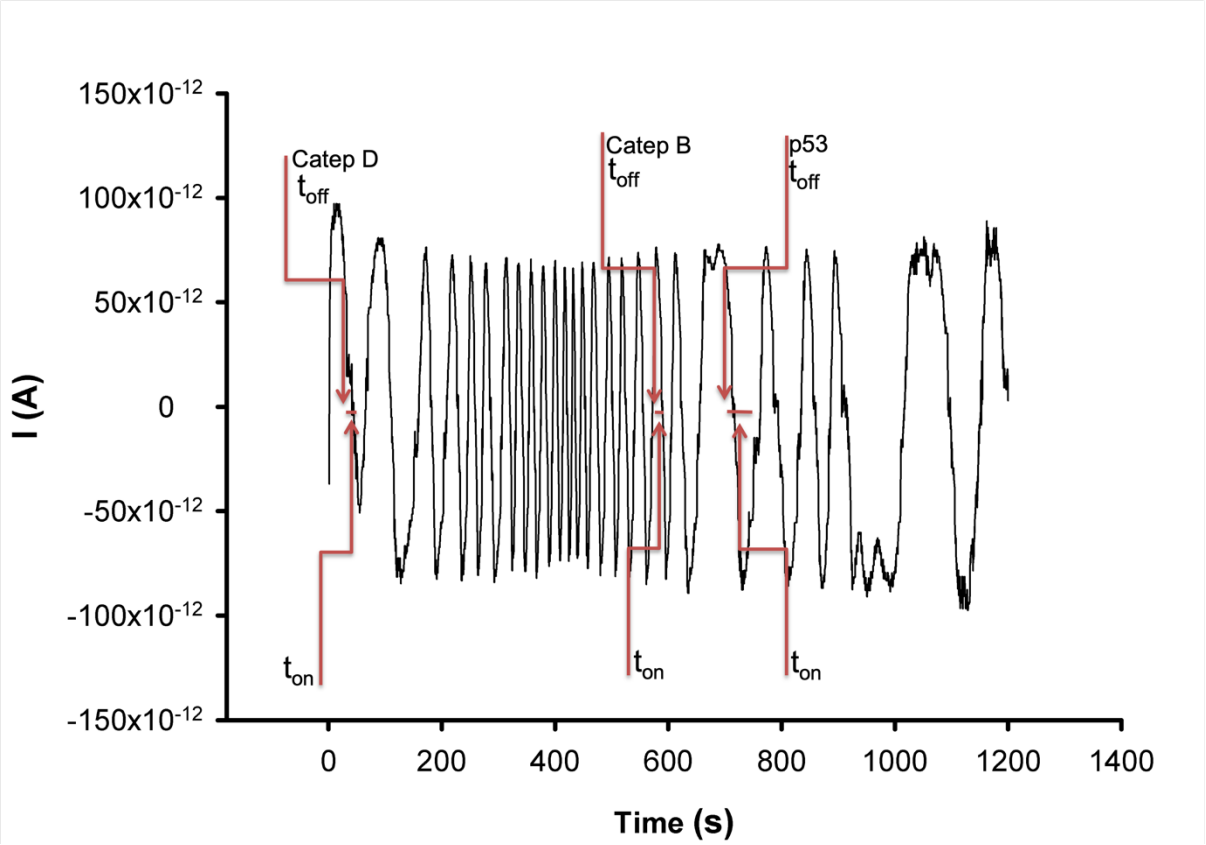

d)

Figure 2 Diagrams obtained for the screening, using the Mn(OAP)Cl/nGr based stochastic microsensors, of (a) saliva, (b) whole blood, (c) tumoral tissue, and (d) urine with the stochastic microsensor based on Mn(OAP)Cl/nGr.

2. Results and discussions

2.1. Morphology of the active surfaces of the stochastic microsensors

Figure 3 shows the qualitative analysis obtained by scanning electron microscopy. As can be seen from Figure 3 (a), the morphological analysis shows that the material is homogeneous in case of paste based on nanodiamond powder (nDP). In the case of using the paste based on nanographene powder (nGr), it can be observed that it contains expanded gaps between the graphene sheets.

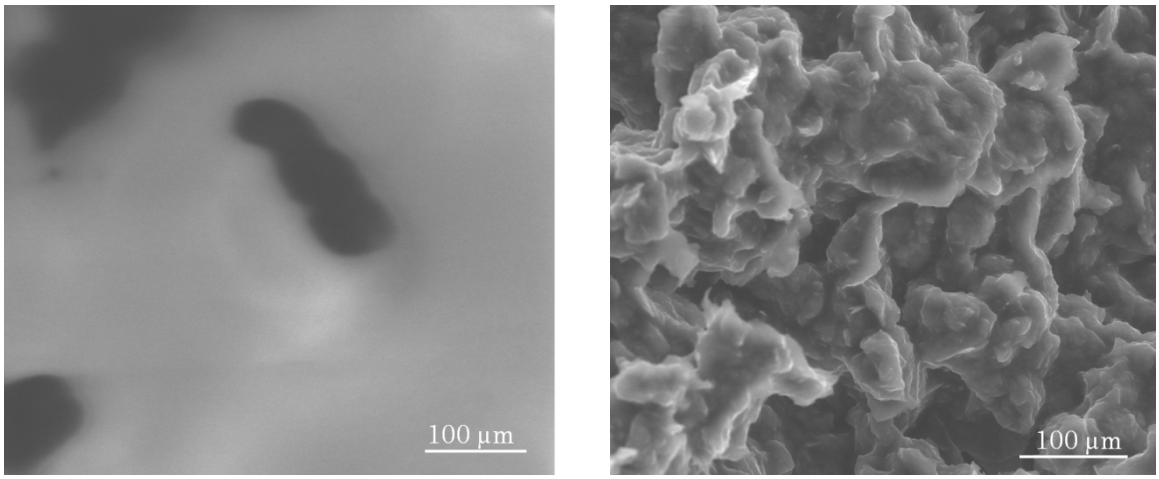

a) ***b)***

Figure 3 SEM images for the active surface of (a) Mn(OAP)Cl/nDP and of Mn(OAP)Cl/nGr.

Also, there are observed in both images the channels – needed to obtain the stochastic signal.

2.2. Response characteristics of the two stochastic microsensors used for the assay of p53, cathepsin B and cathepsin D

The response characteristics of the stochastic microsensors are shown in Table 1.

Table 1 Response characteristics of the stochastic microsensors used for the simultaneous determination of cathepsin B, cathepsin D, and p53.

Stochastic microsensor	Biomarker	Signature t_{off} (s)	Equation of calibration*, r	Sensitivity s^{-1} g^{-1} mL	Limit of quantification (g mL^{-1})	Linear concentration range (g mL^{-1})
Mn(OAP)Cl/nDP	Cathepsin B	1.0	$1/t_{on}=0.04+2.50\times10^{4}C$ r=0.9999	2.50×10^{4}	7.00×10^{-15}	7.00×10^{-15}-7.00×10^{-6}
	Cathepsin D	1.8	$1/t_{on}=0.03+5.99\times10^{3}C$ r=0.9943	5.99×10^{3}	2.50×10^{-15}	2.50×10^{-15}-2.50×10^{-6}
	p53	1.6	$1/t_{on}=0.05+1.95\times10^{4}C$ r=0.9971	1.95×10^{4}	2.56×10^{-12}	2.56×10^{-12}-5.00×10^{-6}
Mn(OAP)Cl/nGr	Cathepsin B	1.4	$1/t_{on}=0.07+2.35\times10^{4}C$ r=0.9898	2.35×10^{4}	7.00×10^{-15}	7.00×10^{-15}-7.00×10^{-15}
	Cathepsin D	1.0	$1/t_{on}=0.07+2.76\times10^{6}C$ r=0.9936	2.76×10^{6}	2.50×10^{-13}	2.50×10^{-13}-2.50×10^{-8}
	p53	1.8	$1/t_{on}=0.03+7.94\times10^{4}C$ r=0.9955	7.94×10^{4}	1.28×10^{-11}	1.28×10^{-11}-1.00×10^{-6}

$\langle C\rangle$ = g mL^{-1} $\langle t_{on}\rangle$ = s

Different values for the signatures were recorded for the three biomarkers when the same microsensor was used, proving that molecular recognition and differentiation of cathepsin D, cathepsin B, and p53 can be performed using the two stochastic microsensors. Very low limits of determination (the lowest concentration from the linear concentration range) were obtained: for the assay of cathepsin B a magnitude order of fg mL^{-1} was obtained, for the assay of cathepsin D, the lowest magnitude order (fg mL^{-1}) was obtained when the microsensor based on Mn(OAP)Cl/nDP was used, while the lowest limit of determination for the assay of p53 was of pg mL^{-1}, when the microsensor based on Mn(OAP)Cl/nDP was used. While for the assay of cathepsin D and p53 no difference in magnitude order was determined for the sensitivity of the two microsensors, for the assay of cathepsin D, the highest sensitivity was achieved using the sensor based on Mn(OAP)Cl/nGr.

Reproducibility and stability studies were performed for each stochastic microsensor. In this regards, ten stochastic microsensors from each type were designed accordingly with the method described above, and the sensitivities' values were recorded and compared for 30 days. For the reproducibility of the design, when compared for each type of the microsensors, the sensitivities, the following were the %, RSD obtained: 0.06% for the stochastic microsensor based on Mn(OAP)Cl/nDP, and 0.10% for the microsensor based on Mn(OAP)Cl/nGr, the sensitivities being measured for each of the microsensors immediately after the modified paste was prepared. The values obtained confirmed the reproducibility of the design of the two types of stochastic microsensors.

For the assay of their stability in time, the determination of the sensitivity for all microsensors was performed every day. For the stochastic microsensors based on Mn(OAP)Cl/nDP, the %, RSD values obtained were 0.13%, while for the stochastic microsensors based on Mn(OAP)Cl/nGr, a value of 0.11% was determined. These results proved a good stability of the modified pastes, and of the stochastic microsensors in time.

The values of the signatures of biomarkers/substances from biological samples are given the selectivity of the stochastic microsensors; differences between the signatures proved their selectivity. Selectivity versus CEA, CA72-4, leucine, serine, glutamine, were checked; all signatures obtained for these

substances were different each from the other and higher than 2.0, proving the selectivity of the proposed stochastic microsensors.

3. Molecular recognition, differentiation and quantification of cathepsin B, cathepsin D, and p53 in biological samples

The stochastic mode described above was used for molecular recognition and quantification of the three biomarkers. The whole blood, saliva, urine, and tumoral tissues from patients confirmed with colorectal/gastric cancers were screened without any processing and diagrams were analysed (Figures 1 and 2). Standard addition method – when known quantities of cathepsin B, cathepsin D, and p53 were added to the four types of biological samples, and comparison method followed by a student-t-test analysis when the results obtained using the two stochastic microsensors were compared, were used for the validation of the proposed stochastic microsensors.

For the standard addition method, determination of cathepsin B, cathepsin D, and p53 were performed before and after addition of known quantities of each of the biomarker in whole blood, urine, saliva, and tumoral tissue; the determined amounts of the biomarkers obtained after the addition of known amounts of biomarkers was compared with the initial amount found in the biological samples (Table 2).

Table 2. Recovery of cathepsin B, cathepsin D, and p53 from whole blood, saliva, urine, and tumoral tissue samples (N = 10).

Stochastic microsensors	Recovery, %		
	Cathepsin B	Cathepsin D	P53
Whole blood			
Mn(OAP)Cl/nDP	99.14±0.01	99.97±0.01	99.95±0.02
Mn(OAP)Cl/nGr	99.23±0.02	99.96±0.03	99.99±0.01
Saliva			
Mn(OAP)Cl/nDP	99.54±0.04	99.88±0.02	99.47±0.02
Mn(OAP)Cl/nGr	99.11±0.08	99.76±0.03	99.97±0.05
Urine			
Mn(OAP)Cl/nDP	98.95±0.03	99.15±0.04	99.23±0.04
Mn(OAP)Cl/nGr	99.06±0.05	98.99±0.03	99.14±0.07
Tumoral tissue			
Mn(OAP)Cl/nDP	98.47±0.06	98.12±0.02	99.00±0.04
Mn(OAP)Cl/nGr	98.98±0.08	98.21±0.03	98.99±0.03

The recovery tests performed show that the biomarkers: cathepsin D, and B, as well as p53, can accurately be determined in the biological samples: whole blood, saliva, urine, and tumoral tissues.

The levels of the three biomarkers have been evaluated in the biological samples using both stochastic microsensors (Figure 4).

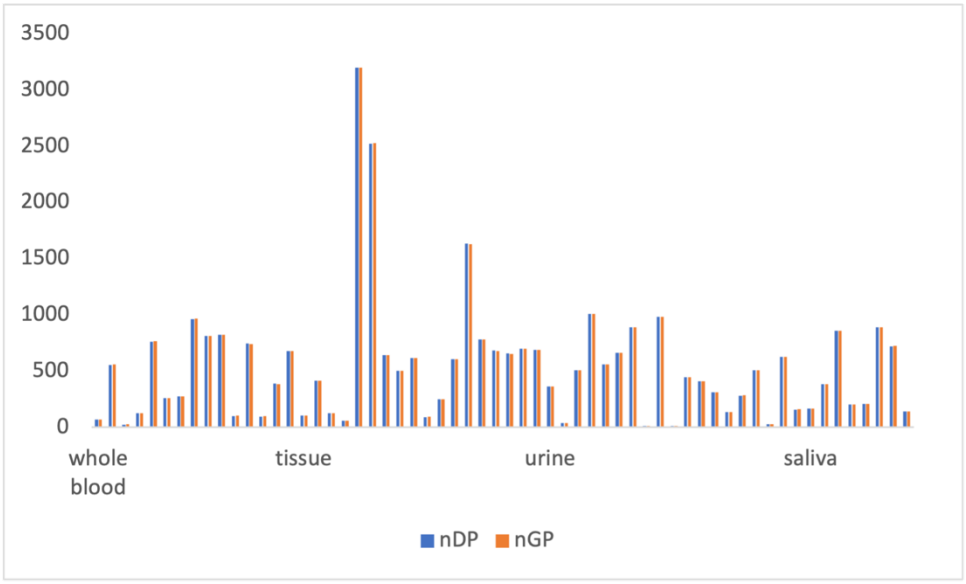

a)

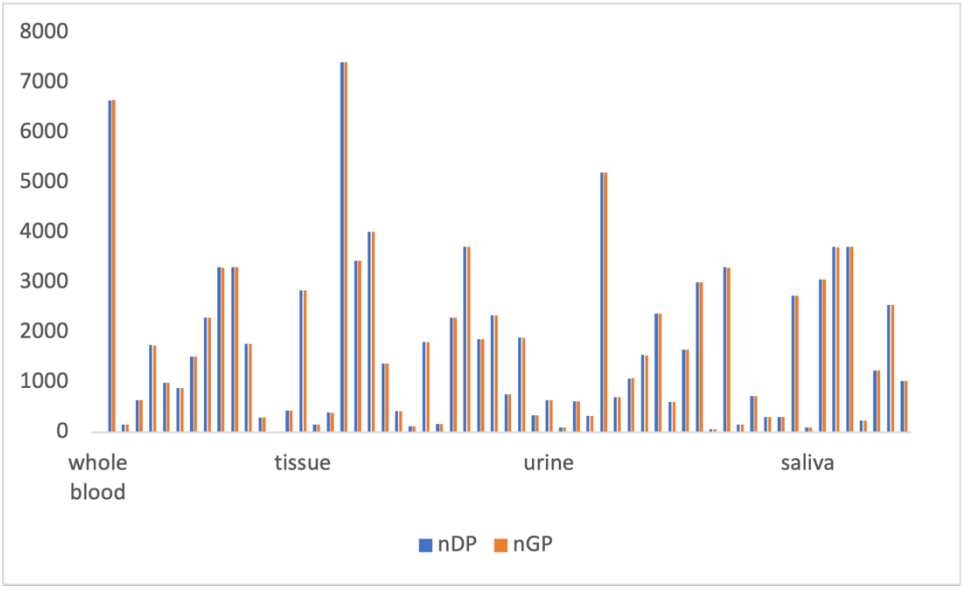

b)

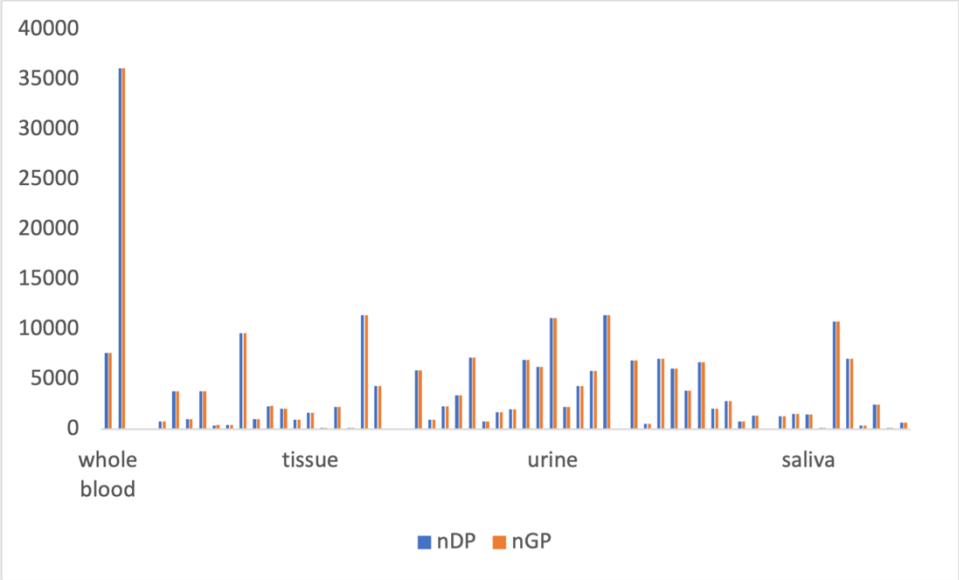

c)

Figure 4. Comparison between the results obtained with the two stochastic microsensors based on Mn(OAP)Cl/nDP and Mn(OAP)Cl/nGr for the assay of a)p53, b)Cathepsin B, and c)Cathepsin D, in whole blood, tissue, urine and saliva.

Figure 4 showed a very good correlation between the results obtained using the stochastic microsensors based on Mn(OAP)Cl/nDP and Mn(OAP)Cl/nGr. A student t-test was performed at 99.00% confidence level (tabulated value is 4.13). The values obtained for the paired – student-t-test were 2.19 for cathepsin D, 1.12 for cathepsin B, and 1.93 for p53. The values obtained for the student-t-test were lower than 4.13, proving that there is no significant difference between the results obtained using the two stochastic microsensors based on Mn(OAP)Cl/nDP and Mn(OAP)Cl/nGr for the assay of cathepsin B, cathepsin D, and p53. Accordingly, the proposed stochastic microsensors can be validated for molecular recognition, differentiation and assay of cathepsin B, cathepsin D, and p53 in whole blood, saliva, urine, and tumoral tissue samples.

IV. Stochastics sensors for quantification of CA 19-9, CA 72-4, CA125 and CEA

1. Experimental part

1.1. Reagents and materials

The four biomarkers (CA 19-9, CA 72-4, CA 125 and CEA) and the phosphate buffer solution (pH=7.50) were purchased from Sigma-Aldrich, while the paraffin oil was purchased from Fluka. The serial dilution method was used for the biomarkers' solutions preparation.

1.2. Synthesis of Boron and Nitrogen decorated Graphenes

The graphene samples were obtained by electrochemically exfoliating the graphite rods, immersed in the appropriate electrolyte (100 mL). For the first sample (NBGr-1), the electrolyte contained 0.1 mol L^{-1} ammonium sulfate, 0.1 mol L^{-1} boric acid and 0.05 mol L^{-1} NaCl. For the second sample (NBGr-2) the electrolyte was made of 0.05 mol L^{-1} ammonium sulfate, 0.1 mol L^{-1} boric acid and 0.05 mol L^{-1} NaCl. The graphite rods were connected to the exfoliation system (home-made system) and a constant voltage of 12 V was applied for about 4 h between the anode and cathode. The black powder resulting from the anode exfoliation and deposited at the bottom of the cell was collected by decantation and thoroughly washed with double-distilled water (10 L). Next, the powder was dispersed by ultrasound for 30 min in 125 mL water and filtered on white-ribbon paper to remove the large particles. The last step was the drying by lyophilization. Both graphene powders: NBGr-1 and NBGr-2 were used in the construction of the stochastic microsensors for the simultaneous assay of CA 19-9, CA 72-4, CA 125 and CEA in biological samples.

1.3. Design of the stochastic microsensors

The two-needle 3D stochastic microsensors were designed as following: each of the powders: NBGr-1 and NBGr-2 were mixed with paraffin oil until a homogeneous paste was obtained. Each of the pastes was mixed with a 10^{-3} mol L^{-1} solution of the oleamide N-(2-mercapto-1H-benzo[d]imidazole-5-yl). 3D microcones with an internal diameter of 10 μm were printed in our laboratory using a 3D Stratasys Objet 24 printer which employs the PolyJet technology for the incremental construction of three-dimensional models through a layer-by-layer process. The material employed in this study is Vero White Plus, which is a firm white opaque polymer. The support material known as FullCure 705 is an acrylic-based photopolymer with a gel-like consistency. It possesses the properties of being easily washable and non-toxic. The precision of the printer was measured to be 0.1 mm. The temperature range during operation was recorded as 18–25 °C, while the relative humidity range was measured as

30–70%. The duration required for the printing of the 3D microcones was 2 hours. The glossy polymer model was fabricated and positioned in a vertical orientation on the printing table in order to minimize the utilization of support material. The diameter of the working electrode's surface was measured to be 10 μm. The modified pastes were placed in 3D microcones (internal diameter 10 μm) specifically designed for the needle 3D stochastic microsensors (Scheme 1).

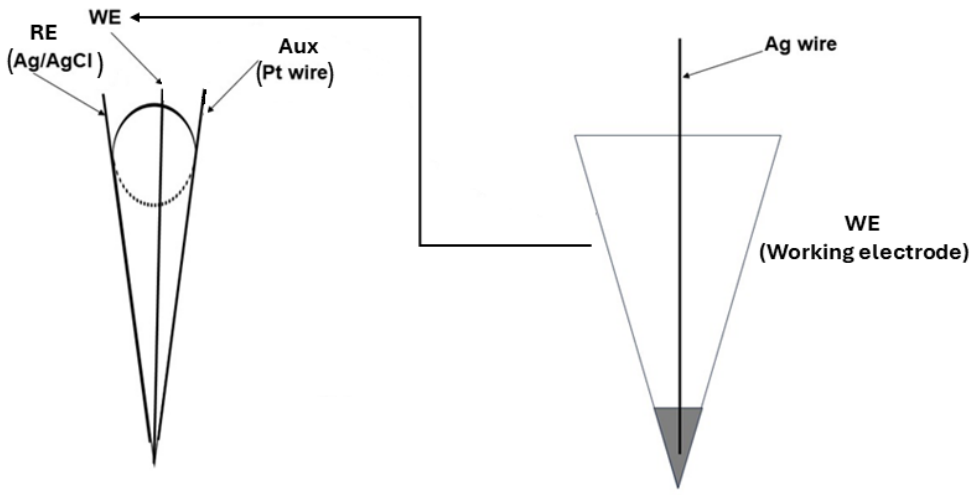

Scheme 1. The design of the needle 3D stochastic microsensor. (WE is the working electrode).

Further, the working electrode (WE) was placed in a cone containing also the reference electrode (Ag/AgCl wire), and the auxiliary electrode (Pt wire) (Scheme 1). When not in use, the needle microsensors were kept in dry places, at room temperature.

1.5. Stochastic method

The stochastic method involves conducting measurements of t_{on} and t_{off} at a consistent voltage (125 mV against Ag/AgCl) through the utilization of a chronoamperometric method. After conducting a thorough analysis of potentials ranging from 0 to 500 mV, a potential of 125 mV was chosen. This specific value was determined to yield readable signatures (t_{off} values) that could be consistently and accurately interpreted. The values of t_{off} – named also as the signatures of the biomarkers (as based on their values the biomarkers are recognized in the diagrams) were used for identification of the four biomarkers (CA 72-4, CA 19-9, CEA and CA 125) and the values of t_{on} (which are read in between two signatures) were used for the determination of the concentration of each of the biomarkers by using calibration equation $1/t_{on} = a + b \times C_{biomarker}$, where $C_{biomarker}$ is the concentration of the biomarkers determined using the proposed 3D needle stochastic microsensors: CA 72-4, CA 19-9, CEA and CA 125, as seen in Figures 1 and 2. The parameter known as "t_{off}" denotes the duration required for the

biomarker to enter the channel. It is commonly referred to as the biomarker's signature and is visually indicated on diagrams using the label "t_{off}." The signature holds significant importance in qualitative analysis as it is closely associated with the molecular identification of biomarkers. Every analyte generates a distinct signature (t_{off}) that is affected by factors such as its size, shape, stereogeometry, unfolding capacity, and velocity when traversing the channel or pore. Consequently, it is rare for two analytes to exhibit identical signatures.

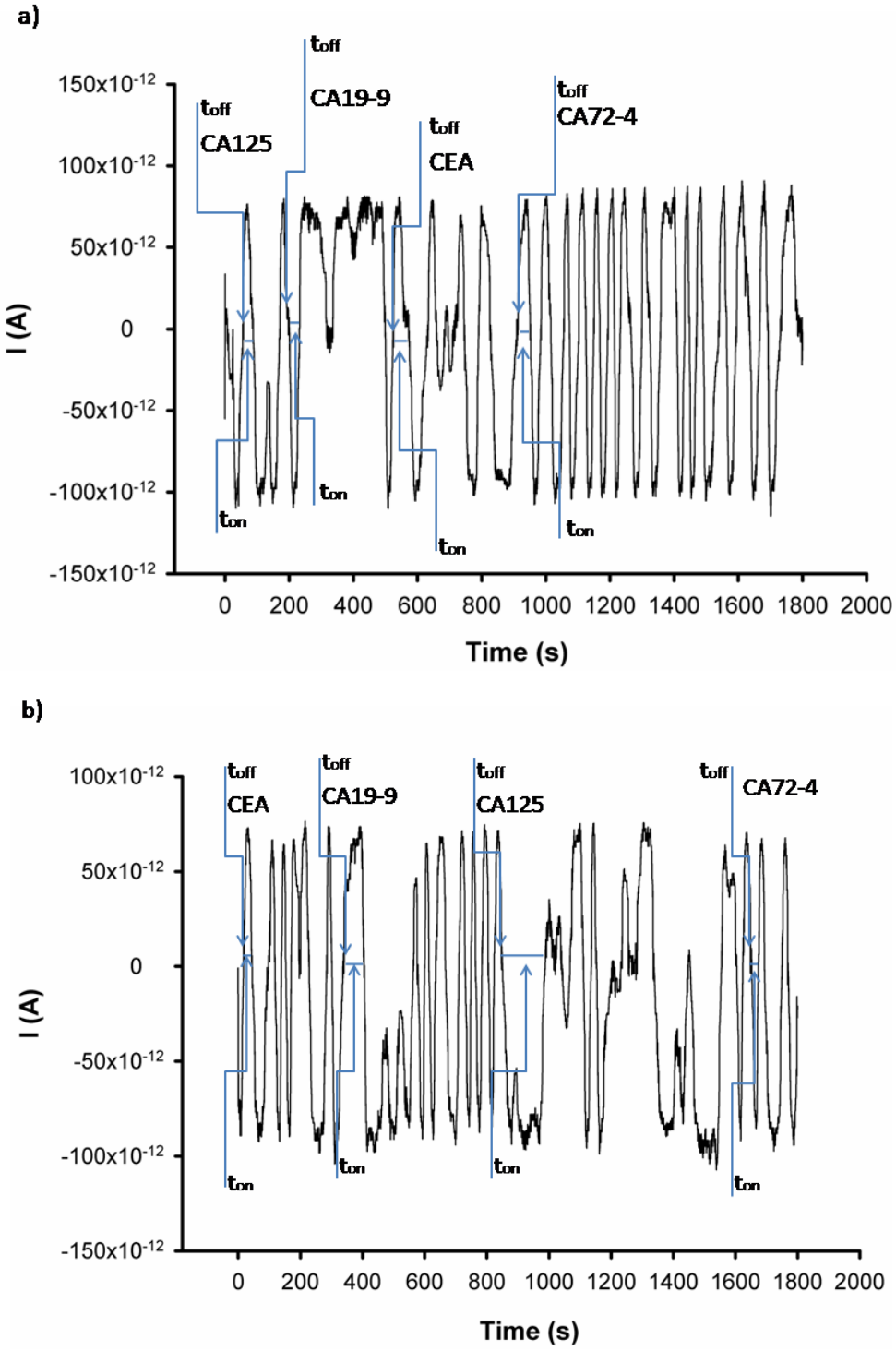

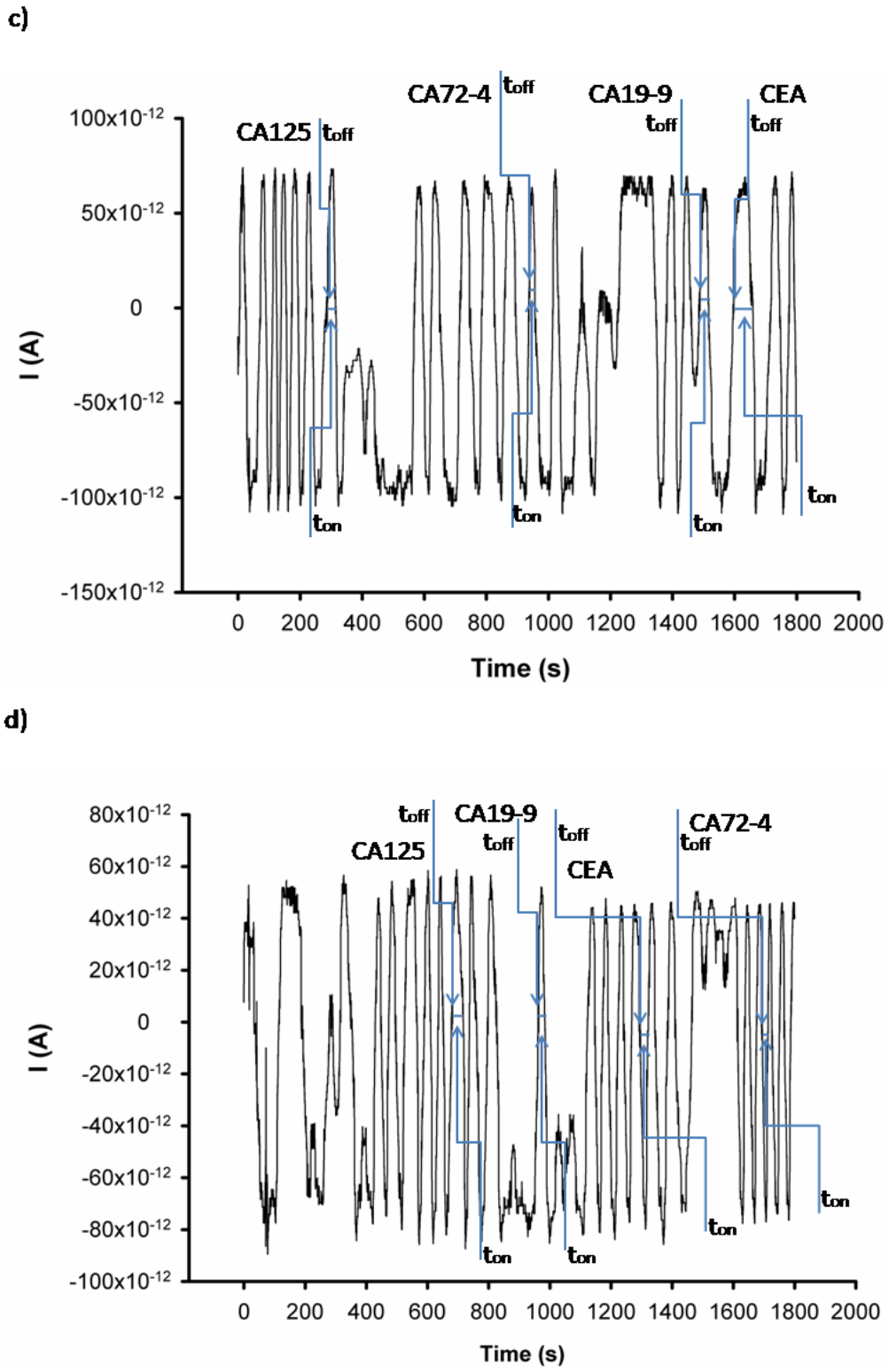

Figure 1. Examples of diagrams obtained when the needle 3D stochastic microsensor based on NBGr-1 was used for the screening of a) saliva, b) whole blood, c) gastric tumor tissue, and d) urine.

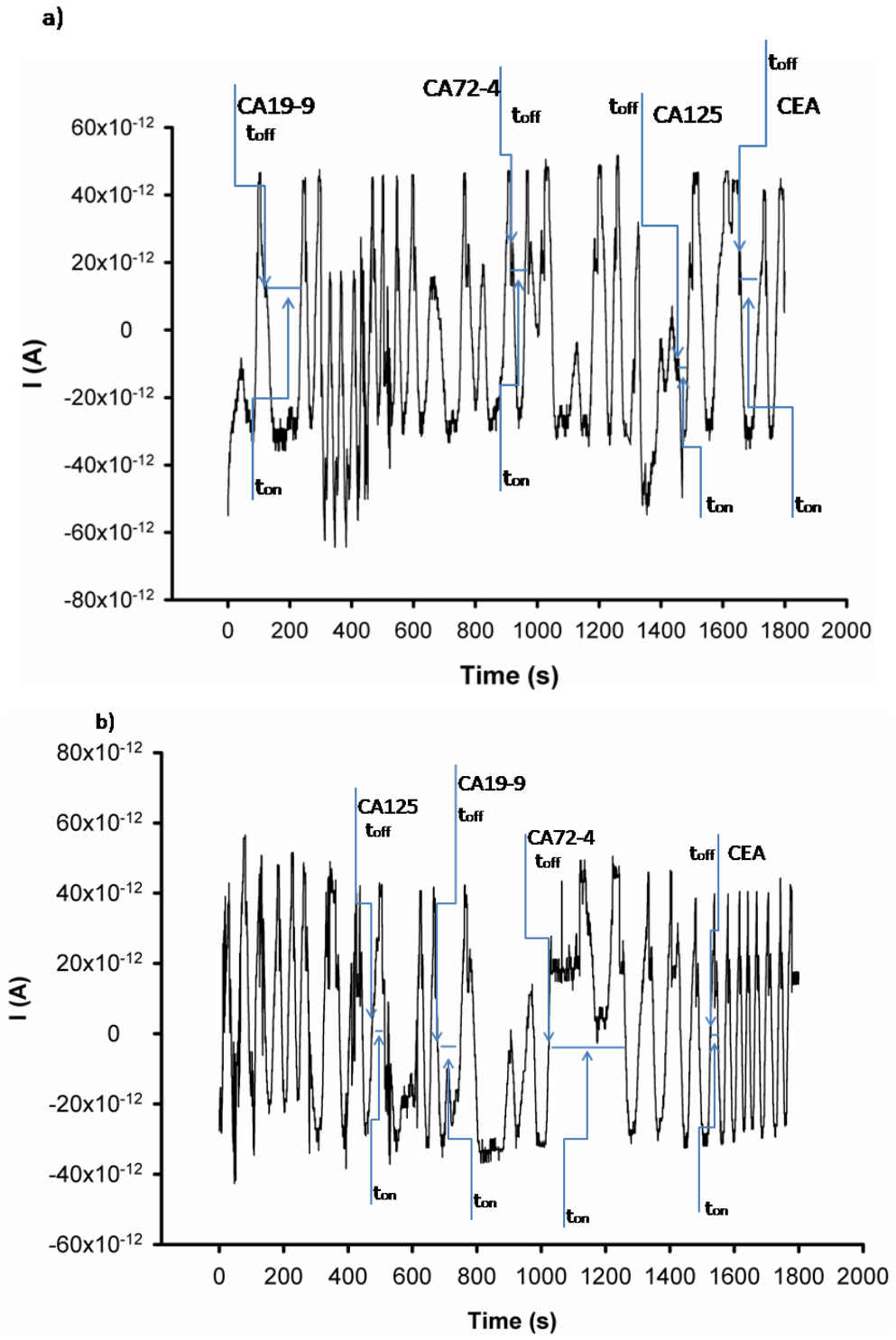
a)
CA19-9
toff
CA72-4
toff
toff
CA125
toff
CEA
ton
ton
ton
ton
60x10-12
40x10-12
20x10-12
0
-20x10-12
-40x10-12
-60x10-12
-80x10-12
I (A)
0 200 400 600 800 1000 1200 1400 1600 1800 2000
Time (s)
b)
CA125
toff
CA19-9
toff
CA72-4
toff
toff
CEA
ton
ton
ton
ton
80x10-12
60x10-12
40x10-12
20x10-12
0
-20x10-12
-40x10-12
-60x10-12
I (A)
0 200 400 600 800 1000 1200 1400 1600 1800 2000
Time (s)

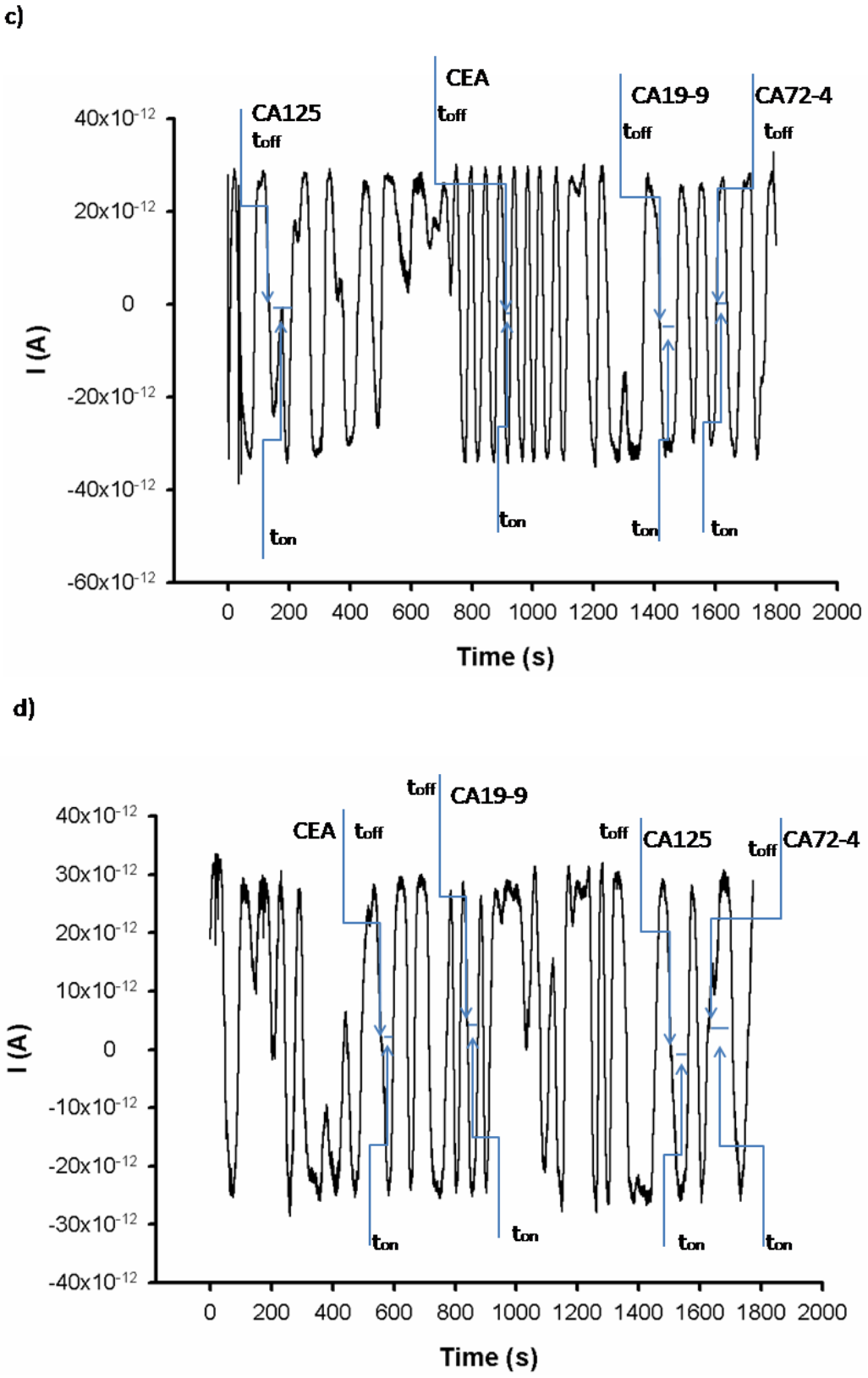

Figure 2. Examples of diagrams obtained when the needle 3D stochastic microsensor based on NBGr-2 was used for the screening of a) saliva, b) whole blood, c) gastric tumor tissue, and d) urine.

2. Results and discussions

2.1. Morphology of the active surface of the needle 3D stochastic microsensors

Electron microscopy images for the pastes based on NBGr-1 and NBGr-2 are presented in Figure 3. The SEM images proved that there are channels on the active side of the 3D needle stochastic microsensors.

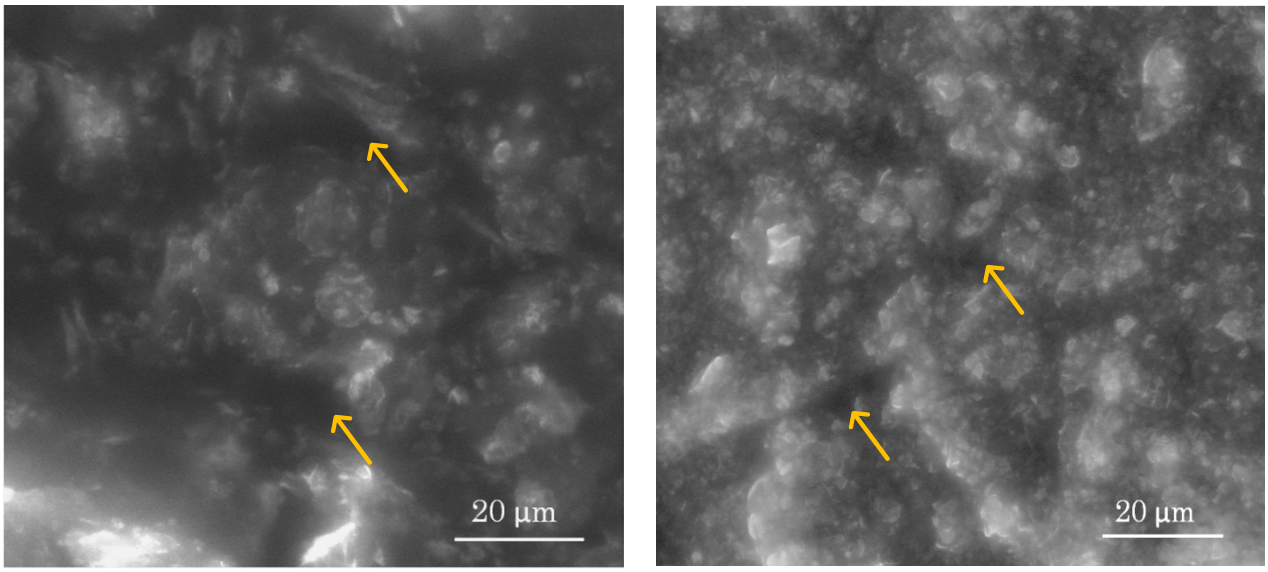

a) *b)*

Figure 3. SEM images for the active side of the needle stochastic microsensor based on a) NBGr-1 and b) NBGr-2.

These channels are needed for the stochastic sensing, and therefore one can say that specific stochastic signals are able to be produced if the sensors are used in chronoamperometry mode. Many surface analysis studies confirmed that the surface of the graphene surface is smoother and stable [41] facilitating the high stability of the modifiers' channels. These channels are needed for the stochastic sensing, and therefore one can say that specific stochastic signals are able to be produced if the sensors are used in chronoamperometry mode.

2.2. Response characteristics of the two stochastic microsensors used for the assay of the four biomarkers (CA 19-9, CA 72-4, CA125 and CEA)

The current development in stochastic sensors is a two phase process: in the first phase, also known as the recognition phase, the biomarker is entering the channel – while entering the channel, the biomarker is blocking it, making the intensity of the current to decrease to zero value – as long as the entering the channel process is taking place (this time needed for the biomarker to enter the channel is

called the signature of the biomarker, and it is marked on the diagrams with t_{off}); the second phase is the one where the quantity of the biomarker is determined, and the t_{on} parameter is connected to the concentration accordingly with the equation shown in the stochastic mode paragraph (see above). While the signature is very important for the qualitative analysis (being the parameter related to the molecular recognition of the biomarkers), the t_{on} parameter gives the response characteristics of the needle 3D stochastic microsensors. The response characteristics of the two-needle 3D stochastic microsensors are shown in Table 1.

Table 1. Response characteristics of the stochastic microsensors used for the simultaneous assay of CA 72-4, CA 19-9, CA 125, CEA.

Needle 3D stochastic microsensor based on	Biomarker	Signature t_{off} (s)	Equation of calibration, r	Sensitivity	Limit of quantification	Linear concentration range
NBGr-2	CA 72-4[1]	1.6	$1/t_{on}=0.04+1.06\times10^{-5}C$ r=0.9923	1.06×10^{-5} s^{-1} U^{-1} mL	4.00×10^{-11} s^{-1} U^{-1} mL	4.00×10^{-11}-4.00×10^{3} s^{-1} U^{-1} mL
	CA 19-9[1]	1.8	$1/t_{on}=0.03+1.82\times10^{-4}C$ r=0.9973	1.82×10^{-4} s^{-1} U^{-1} mL	3.28×10^{-9} s^{-1} U^{-1} mL	3.28×10^{-9}-5.00×10^{2} s^{-1} U^{-1} mL
	CA 125[1]	1.4	$1/t_{on}=0.03+9.92\times10^{-5}C$ r=0.9994	9.92×10^{-5} s^{-1} U^{-1} mL	8.36×10^{-6} s^{-1} U^{-1} mL	8.36×10^{-6}-837.43 s^{-1} U^{-1} mL
	CEA[2]	1.1	$1/t_{on}=0.03+8.13\times10^{5}C$ r=0.9861	8.13×10^{5} s^{-1} g^{-1} mL	4.10×10^{-15} s^{-1} g^{-1} mL	4.10×10^{-15}-2.00×10^{-7} s^{-1} g^{-1} mL
NBGr-1	CA 72-4[1]	1.0	$1/t_{on}=0.04+1.43\times10^{-5}C$ r=0.9977	1.43×10^{-5} s^{-1} U^{-1} mL	4.00×10^{-3} s^{-1} U^{-1} mL	4.00×10^{-3}-4.00×10^{3} s^{-1} U^{-1} mL
	CA 19-9[1]	1.4	$1/t_{on}=0.04+5.88\times10^{-3}C$ r=0.9997	5.88×10^{-3} s^{-1} U^{-1} mL	2.09×10^{-13} s^{-1} U^{-1} mL	2.09×10^{-13}-20.00 s^{-1} U^{-1} mL
	CA 125[1]	1.2	$1/t_{on}=0.04+1.98\times10^{-5}C$ r=0.9955	1.98×10^{-5} s^{-1} U^{-1} mL	8.37×10^{-14} s^{-1} U^{-1} mL	8.37×10^{-14}-8.37×10^{3} s^{-1} U^{-1} mL
	CEA[2]	1.6	$1/t_{on}=0.06+9.24\times10^{4}C$ r=0.9946	9.24×10^{4} s^{-1} g^{-1} mL	1.28×10^{-11} s^{-1} g^{-1} mL	1.28×10^{-11}-1.00×10^{-6} s^{-1} g^{-1} mL

[1] <C> = U mL^{-1} <t_{on}> = s; [2] <C> = g mL^{-1} <t_{on}> = s.

Different signatures were recorded for the four biomarkers, when the same microsensor was used, proving that the two microsensors can be reliably used for the simultaneous assay of the four biomarkers. High sensitivities and low limits of determination were obtained for all needle 3D stochastic microsensors. The limits of determination were deter mined as the lowest concentration found in the linear concentration range accordingly with the new IUPAC recommendation (paragraph 3.36, Note 3) [42]. While the type of graphene did not significatively influence the sensitivity of the assay of the biomarkers (with the exception of CA 19-9 when better sensitivity was recorded when NBGr-2 was used, and CEA when better sensitivity was recorded when NBGr-1 was used), it was influencing more the limits of determination of the biomarkers: lower limits of determination were obtained for CA 72-4 and CEA when the microsensor based on NBGr-2 was used, and for CA 19-9 and CA 125 when the microsensor based on NBGr-1 was used. The electrochemical reaction is induced by the applied voltage on the working electrode, and the quantity of electrons moved (referred to as electrical current) offers insights into the surface condition [43-46]. The rate of change in electric current is directly proportional to the quantity of molecules that have undergone adsorption on the surface, hence imparting valuable sensing data. The linear concentration ranges recorded were wide making possible the assay of the four biomarkers in healthy people, and in patients with gastric cancer from early to late stages.

Reproducibility and stability studies were performed for each of the needle 3D stochastic microsensors. Ten needle 3D stochastic microsensors from each category were designed accordingly with the method described above, and the sensitivities' values were recorded and compared for 60 days. For the reproducibility of the design, the sensitivities recorded for the microsensors of the same type were compared for each biomarker; the %, RSD recorded for the sensitivities of the needle 3D stochastic microsensors were as following: for the microsensor based on NBGr-1 0.03% for CA 72-4, 0.02% for CA 19-9, 0.03% for CA 125, and 0.01% for CEA, while for the microsensor based on NBGr-2, the values recorded were 0.02% for CA 72-4, 0.01% for CA 19-9, 0.04% for CA 125, and 0.01% for CEA. These values obtained for % RSD confirmed the reproducibility of the design of the two types of the needle 3D stochastic microsensors.

The stability in time, was determined by measuring sensitivities of the designed sensors during 60 days. By comparing the sensitivities obtained during this period of time for each type of needle 3D stochastic microsensors, the following statements can be made: for the microsensor based on NBGr-1 the RSD values were: 0.05% for CA 72-4, 0.06% for CA 19-9, 0.08% for CA125, and 0.03% for CEA, while for the microsensor based on NBGr-2, the values recorded were 0.08% for CA72-4, 0.04% for CA19-9,

0.03% for CA125, and 0.03% for CEA. These results proved a good stability of the modified pastes in time, and also of the stochastic microsensors in time.

The selectivity of stochastic microsensors is determined by the recorded values of the signatures associated with biomarkers and other compounds present in biological samples. The presence of discernible differences between these signatures serves as evidence of the microsensors' selectivity. The recorded toff values for various potential interferences serve as indicators of the selectivity of the two stochastic sensors under consideration. The following substances were investigated as possible interferents: p53, cathepsin D, cathepsin B, leucine, serine, and glutamine. The signature of the four biomarkers was determined to be less than 2 s when utilizing both sensors. The other compounds present in the biological samples that were examined as potential interference had distinct characteristics distinct from the hypothesized biomarkers, hence confirming the sensors' selectivity. When the needle 3D stochastic microsensors based on NBGr-1 was used, the following signatures were recorded: 2.4s for p53, 2.7s for cathepsin D, 2.9s for cathepsin B, 3.1s for leucine, 3.9s for serine, and 3.7s for glutamine. When the needle 3D stochastic microsensors based on NBGr-2 was used, the following signatures were recorded: 3.8s for p53, 3.0s for cathepsin D, 2.8s for cathepsin B, 3.5s for leucine, 2.4s for serine, and 2.6s for glutamine.

All signatures obtained for these substances were different each from the other and higher than 2.3, proving the selectivity of the proposed needle 3D stochastic microsensors when used for the assay of CA 19-9, CA 72-4, CA 125 and CEA in biological samples. Accordingly, the needle 3D stochastic microsensors can be selectively used for the assay of CA 19-9, CA 72-4, CA125 and CEA in biological samples.

In comparison to other tools and methods proposed to date, including: an ultrasensitive electrochemical immune sensor proposed for the assay of CA 72-4 by Yan et al. [47], an electrochemical sensor proposed for the simultaneous assay of CA19-9 and CA 72-4, which was based on tumor markers dual recognition via glycosyl imprinting and lectin-specific binding, proposed by Luo et al. [48], an ultrasensitive split-type electrochemical immunosensor based on control – released strategy proposed by Li et al for the assay of CA 19-9 [49], a photoelectrochemical immunosensor proposed by Gholamin et al. for the assay of CA 19-9 [50], a flower – shaped chemiluminescence based – sensor for the assay of CEA [51], a magnetic copper silicate and boronic acid - conjugate AuNCs@keratin – based electrochemical /fluorescent dual – sensing was proposed by Jin et al for the de-termination of CEA [52], and for the assay of CA 125 – a hydrogel based immunosensor proposed by Er et al. [53], and a label – free dual immunosensor proposed by Kamac et al [54], the needle 3D stochastic microsensors proposed in this paper had the following ad-vantages: the developed sensors exhibit reliable molecular recognition capabilities for CA 72-4, CA 19-9, CEA, and CA 125, they demonstrate wider working

concentration ranges compared to those documented in the referenced papers, additionally, the sensors achieve lower limits of determination and higher sensitivities, their design, which does not involve the use of biomolecules, contributes to their enhanced stability over time. Notably, the needle 3D stochastic sensors can be stored at room temperature for a minimum of two months without compromising their functionality. Moreover, they can be utilized on a daily basis for the quantitative analysis of CA 72-4, CA 19-9, CEA, and CA 125 in various biological samples, including whole blood, urine, saliva, and tumor tissues. The aforementioned sensors have a higher degree of selectivity as compared to biomarkers found in whole blood, saliva, urine, and tumoral tissues.

2.3. Ultrasensitive determination of the four biomarkers in all the four biological fluids

The wide working concentration ranges, low limits of determination, possibility of simultaneous determination of CA 72-4, CA 19-9, CEA, and CA 125, made possible the utilization of needle 3D stochastic microsensors for screening tests of whole blood, saliva, urine, and tumoral tissues.

The samples were analysed as soon as possible after they were taken from the patients. The diagrams were recorded, and the first step was to identify, based on their signatures, the biomarkers: CA 72-4, CA 19-9, CEA, and CA 125 in the diagram. In between two signatures, the t_{on} was read. The values of t_{on} were used for the quantitative determination of CA 72-4, CA 19-9, CEA, and CA 125 in whole blood, saliva, urine, and tumoral tissue, accordingly with the stochastic mode procedure described above. The levels of the four biomarkers have been evaluated in all four types of biological fluids (whole blood, saliva, urine and tissue samples) with both sensor and the results are given in Figure 4.

a)


Saliva - NBGr-1
CA72-4 CA19-9 CA125 CEA
Concentration*
Patients' number
* For CA 72-4, CA 19-9 and CA125 – U/mL and for CEA – g/mL


Saliva - NBGr-2
CA72-4 CA19-9 CA125 CEA
Concentration*
Patients' number
* For CA 72-4, CA 19-9 and CA125 – U/mL and for CEA – g/mL

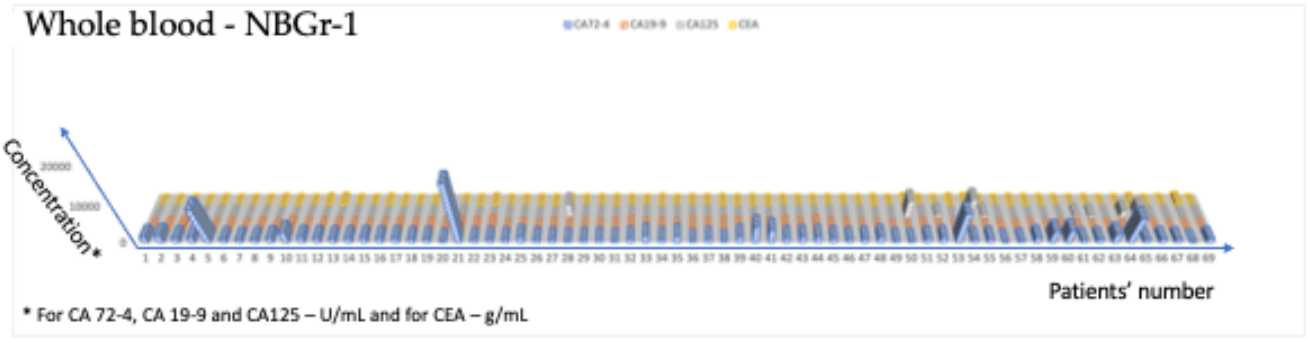
Whole blood - NBGr-1
CA72-4 CA19-9 CA125 CEA
Concentration*
Patients' number
* For CA 72-4, CA 19-9 and CA125 – U/mL and for CEA – g/mL

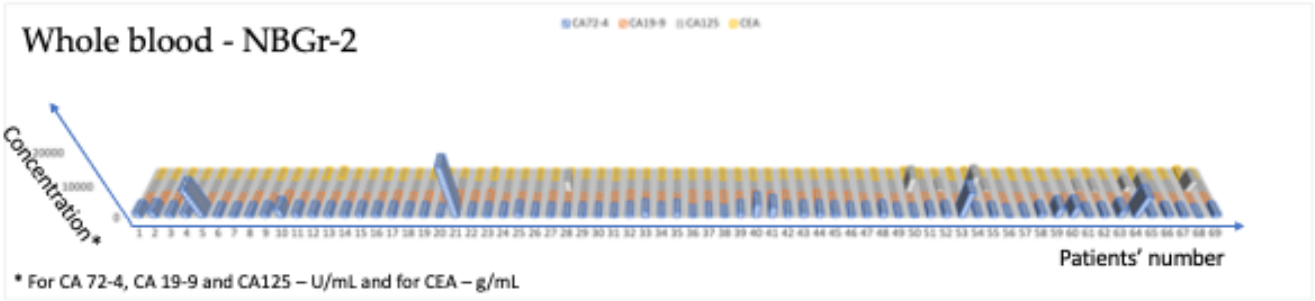
Whole blood - NBGr-2
CA72-4 CA19-9 CA125 CEA
Concentration*
Patients' number
* For CA 72-4, CA 19-9 and CA125 – U/mL and for CEA – g/mL

b)

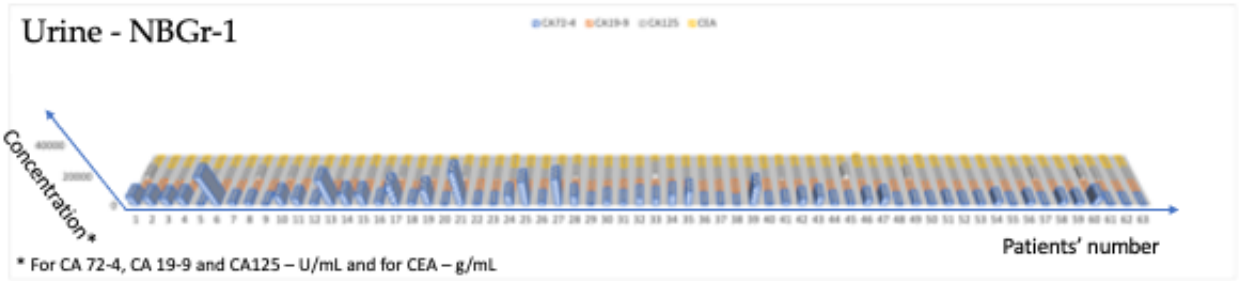

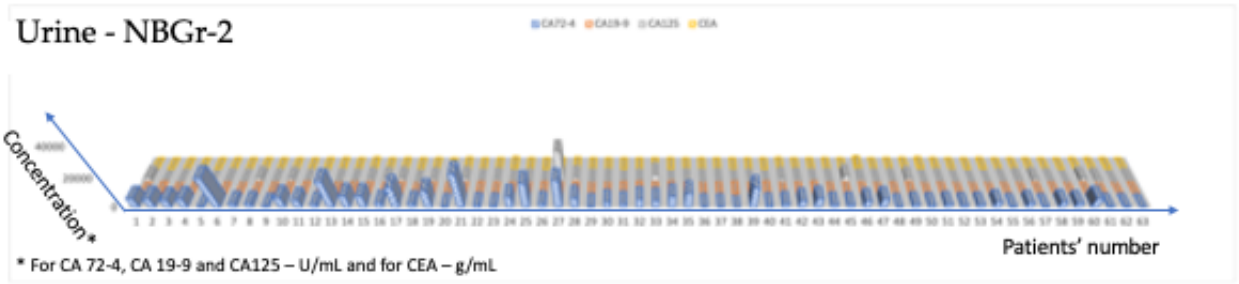

c)

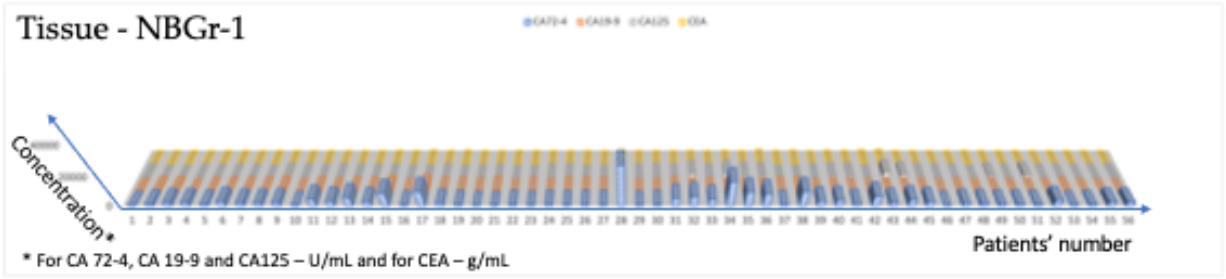

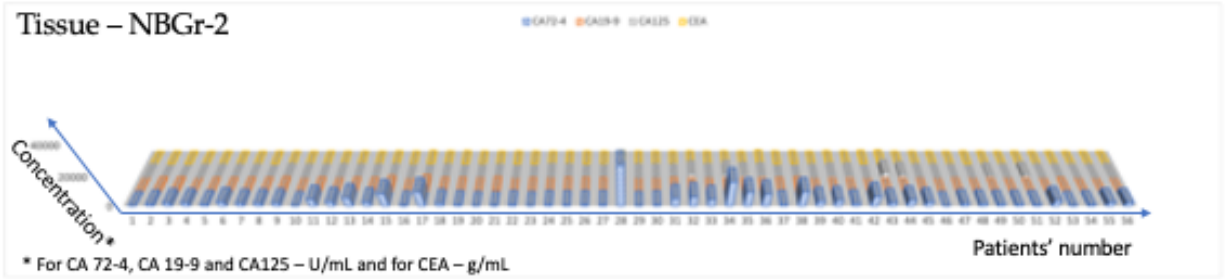

d)

Figure 4. Comparison between the results obtained with the two-needle 3D stochastic microsensors based on NBGr-1 and NBGr-2 for the assay of the four biomarkers in a) saliva b) whole blood c) urine and d) gastric tumor tissue samples.

The student paired t-test was performed at 99.00% confidence level (tabulated theoretical t-value: 4.032), for each biomarker. All calculated t-values were less than 3.500, which is less than the tabulated value, proving that there is no statistically significant difference between the results obtained using the two-needle 3D stochastic microsensors. The F-test was also performed, at 95% confidence level, for ten samples of each kind. The tabulated F value was 3.18. The results obtained when compared the standard deviations obtained for the two-needle 3D stochastic microsensors were lower than 1.00, which is a lower value than the tabulated value, 3.18. This indicates that there is no significant difference in the precision recorded for the two-needle 3D stochastic sensors, and that the standard deviations are not depending on the analysed samples. Accordingly, the proposed microsensors can be used for the screening of whole blood, saliva, urine, and tumoral tissues for the four biomarkers.

The second test performed for the validation of the needle 3D stochastic sensors and screening method was the recovery test. Known amounts of each of the biomarkers (CA 72-4, CA 19-9, CEA, and CA 125) were added to whole blood, urine, saliva, and tumoral tissues. The amounts of CA 72-4, CA 19-9, CEA, and CA 125 were determined before and after their addition into the whole blood, urine, saliva, and tumoral tissue samples. The difference between the final amount found into the biological sample and the initial amount (determined before the addition of known amounts of CA 72-4, CA 19-9, CEA, and CA 125 to the sample) was compared with the known amount added into the sample for each of the biomarkers. Results obtained for the recovery tests are shown in Table 2.

Table 2. Recovery tests of CA72-4, CA19-9, CA125, CEA performed using the needle 3D stochastic microsensors (N=10).

Needle 3D stochastic microsensor based on	**Biomarker**	**Whole blood**	**Saliva**	**Urine**	**Tumoral tissue**
		%, Recovery			
NBGr-2	CA72-4	98.99±0.03	99.43±0.04	99.29±0.03	97.25±0.05
	CA19-9	97.23±0.05	98.21±0.03	98.14±0.03	98.01±0.03
	CA125	98.47±0.02	99.12±0.05	98.37±0.04	97.15±0.04
	CEA	99.05±0.02	99.54±0.05	98.11±0.02	98.00±0.04
NBGr-1	CA72-4	99.09±0.08	99.01±0.01	99.12±0.02	98.29±0.08
	CA19-9	99.00±0.02	97.59±0.04	99.87±0.07	97.97±0.09

CA125	98.32±0.05	98.06±0.02	98.93±0.04	98.19±0.04
CEA	98.27±0.03	98.89±0.05	98.90±0.03	98.05±0.02

The results presented in Table 2 shown high recovery values for all biomarkers: CA 72-4, CA 19-9, CA 125, and CEA when recovered from whole blood, saliva, urine, and tumoral tissue samples. Very low %, RSD values were also reported.

Based on the first and second validation test one can conclude that the proposed needle 3D stochastic microsensors can be reliable used for the simultaneous assay of CA 72-4, CA 19-9, CA 125, and CEA in whole blood, saliva, urine, and tumoral tissue. The test may be used as mass screening test of population, for early diagnosis of gastric cancer.

Part 2- Biomedical applications for the developed stochastic sensors

In this thesis, a novel molecular method to determine the location and the main clinicopathological features with high sensitivities and high specificities based on the levels of MMR proteins and KRAS obtained using stochastic sensors in whole blood, saliva and urine samples is proposed. Due to the use of stochastic sensors, the five biomarkers' levels can be determined quickly, simultaneously and without significant costs.

1. Patient description

After the informed consents being received, there were collected the three kinds of samples from 116 colorectal cancer patients (107 whole blood samples, 79 saliva samples and 88 urine samples).

The patients were selected from the database of the project GRAPHSENSGASTROINTES, and used accordingly with the Ethics committee approval nr. 32647/2018 awarded by the County Emergency Hospital from Targu-Mures. A small description of the patients is given in Table 1.

Table 1. Characterisation of the patients

Colorectal adenocarcinoma patients' features		Number of patients	Percent
Age	≤60 years	31	26.96%
	60-69 years	42	36.52%
	70-79 years	30	26.09%
	≥80 years	12	10.43%
Gender	Male	85	73.28%
	Female	31	26.72%
Tumor location	Ascending colon	14	12.07%
	Transverse colon	7	6.03%
	Descending colon	2	1.72%
	Sigmoid colon	25	21.55%
	Rectosigmoid junction	11	9.48%
	Rectum	37	31.90%
	Rectum with radiotherapy	20	17.24%
Gross aspect	Malignant polyps	2	1.83%
	Vegetant	27	24.77%

	Vegetant and ulcerated	26	23.85%
	Infiltrative	54	49.54%
Mucus presence	Overall	36	31.86%
Stroma Type	With fibrous compound	59	65.56%
	Inflammatory	31	34.44%
Molecular subtype	Mesenchymal compound	31	38.75%
Invasions	Blood vessels	29	25.66%
	Lymph vessels	54	47.79%
	Perineural	36	31.86%
	Lymph node	50	44.25%
Survival rate	≥1 year	21	18.10%
	<2 years	47	40.52%
	≥2 years	7	6.03%
TNM grading system	pT2	19	17.12%
	pT3	55	49.55%
	pT4a	25	22.52%
	pT4b	12	10.81%
	Tumor deposits	11	9.91%
	Metastases	18	15.52%

2. Results

The levels of each biomarker have been evaluated by using stochastic method in all the three biological fluids and the values have been searched for correlations with clinicopathological features in colorectal adenocarcinoma patients. All these features have been recorded by the pathologists and the geneticist from the Pathology Department of the County Emergency Hospital from Targu-Mures. All the correlations have been optimized by using Microsoft Office Suite Software, Matlab and Mathcad.

For each feature, an algorithm based on mathematical formulas or on probability criteria has been developed and described. As all the results are mathematically based and artificial intelligence has a fast development in medicine, we propose a code in Matlab that can predict with high probability the clinicopathological features in colorectal adenocarcinoma patients. This code is given in Supplementary Material. Starting from this code, by introducing the levels of each biomarker in each biological fluid, the results are generated in a very short time.

Each feature has been separately analyzed and the best correlations have been selected and widely described. The first step was represented by the calculus of the p values for each feature and each biomarker. Some derivative formulas were also searched for the p values. These formulas are based on biochemical kinetics and they were adapted for each feature if it was necessary as a mathematical optimization.

The first feature discussed in this paper is represented by tumor location. The colorectal area has been practically divided in six areas namely ascending colon, transverse colon, descending colon, sigmoid colon, rectosigmoid junction with adjacent area and rectum. To avoid the effect of adjuvant therapy on biomarkers' levels, only the patients who did not benefit from therapy at the moment of sampling were taken into consideration for tumor location establishment.

Before introducing the derivative parameters, the p values have been calculated for each biomarker's level and for some main ratios between the concentrations of different biomarkers in the same biological fluid. The p values are given in Table 2.

Table 2. The p values calculated for each biomarker in each biological fluids and for the main ratios

Biomarker or Ratio	**Biological fluid**		
	Whole blood	Urine	Saliva
MLH1	0.143	0.928	0.256
MSH2	0.391	0.344	0.365
MSH6	0.783	0.278	0.780
PMS2	0.080	0.382	0.996
KRAS	0.921	0.367	0.013
MLH1/MSH2 (ng/pg)	0.261	0.540	0.200
PMS2/MSH6 (ng/pg)	0.204	0.942	0.015
MLH1/PMS2	0.195	0.142	0.878
MSH2/MSH6	0.085	0.814	0.386
MLH1/KRAS (ng/μg)	0.217	0.071	0.285

For the levels of biomarkers and the values of the selected ratios, some observations have been done regarding their correlations with the location:

- whole blood MLH1/PMS2 ratio values are lower in rectosigmoid junction (<5, 66.66%) and rectum (<5, 67.74%) adenocarcinoma patients;

- whole blood MSH2/MSH6 ratio values are higher in ascending colon patients (>0.85, 69.23%) and lower values in transverse and descending colon (<0.85, 100%), rectosigmoid junction (<0.85, 66.66%) and rectum (<0.85, 61.29%) adenocarcinoma patients;
- whole blood MLH1/MSH2 ratio values are lower in ascending colon (<1 ng/pg, 69.23%), transverse and descending colon (<1 ng/pg, 87.5%) and rectosigmoid junction (<1 ng/pg, 66.66%) adenocarcinoma patients;
- whole blood PMS2/MSH6 ratio values are higher in rectum patients (>0.9 ng/pg, 58.06%) and lower in ascending colon (<0.9 ng/pg, 61.54%) and sigmoid colon (<0.9 ng/pg, 75%) adenocarcinoma patients;
- whole blood MLH1/KRAS ratio values are higher in sigmoid colon (>0.009, 58.33%) and rectum adenocarcinoma patients (>0.009, 58.06%) and lower in transverse and descending colon (<0.009, 75%) and rectosigmoid junction (<0.009, 77.78%) adenocarcinoma patients;
- urinary MLH1/PMS2 ratio values are lower in ascending colon (<3, 70%), rectosigmoid junction (<3, 77.78%) and rectum (<3, 57.14%) adenocarcinoma patients;
- urinary MSH2/MSH6 ratio values are higher in ascending colon (>0.9, 70%) adenocarcinoma patients;
- urinary MLH1/MSH2 ratio values are lower in ascending colon (<1.5 ng/pg, 80%) and rectosigmoid junction (<1.5 ng/pg, 77.78%) adenocarcinoma patients;
- urinary PMS2/MSH6 ratio values are lower in transverse and descending colon (<0.25 ng/pg, 85.71%) adenocarcinoma patients;
- salivary MLH1/MSH2 ratio values are lower in ascending colon (<0.25 ng/pg, 77.78%) and transverse and descending colon (<0.25 ng/pg, 71.43%) adenocarcinoma patients;
- salivary PMS2/MSH6 ratio values are lower in ascending colon (<0.8 ng/pg, 66.66%) and rectosigmoid junction (<0.8 ng/pg, 100%) adenocarcinoma patients;
- salivary MLH1/PMS2 ratio values are higher in ascending colon (>1.55, 77.78%), sigmoid colon (>1.55, 68.42%) and rectosigmoid junction (>1.55, 77.78%) adenocarcinoma patients;
- MLH1/KRAS has higher values in sigmoid colon adenocarcinoma patients (>0.012, 73.69%) and lower values in transverse and descending colon (<0.012, 100%) and rectosigmoid junction (<0.012, 77.78%) adenocarcinoma patients.

As the main differences on biomolecules dynamics are given by gravitation force, morphology and vascularization, three derivate parameters are used for location estimation. These parameters that evaluates each biomarker's biodynamics are represented by S (the sum between twice the level of a biomarker in urine and the level of the biomarker in saliva), r_1 (the ratio between a biomarker whole

blood concentration and its concentration in urine), and r_2 (the ratio between a biomarker whole blood concentration and its concentration in saliva).

For each derivative parameter, the biological significance is widely detailed in discussions section. The p values were calculated for each derivative parameter and for each biomarker. These p values are given in Table 3.

Table 3. The p values for each derivative parameter related to biodynamics of each marker

Biomarker	Derivative parameter	p value	Derivative parameter	p value	Derivative parameter	p value
MLH1	S	0.771	r_1	0.058	r_2	0.853
MSH2	S	0.960	r_1	0.537	r_2	0.749
MSH6	S	0.364	r_1	0.702	r_2	0.806
PMS2	S	0.448	r_1	0.806	r_2	0.663
KRAS	S	0.040	r_1	0.548	r_2	0.540

By analyzing the values of the above-mentioned biodynamics parameters, some location-related observations have been done:

- ascending colon adenocarcinoma patients associate r_1(MSH2) >1.5, r_1(MSH6) <0.7 and S(MSH6) <600 pg/mL;
- transverse and descending colon adenocarcinoma patients associate r_1(MSH2) <1.5, S(MSH2) >500 pg/mL, r_2(MSH2) >0.75 and r_1(KRAS) <0.45;
- sigmoid colon adenocarcinoma patients associate r_2(PMS2) <0.6 and r_1(KRAS) <1.4;
- rectosigmoid junction adenocarcinoma patients associate r_1(MSH6) <0.5, S(MSH6) >1500 pg/mL and r_2(MSH2) <0.75;
- rectum adenocarcinoma patients associate r_2(PMS2) >0.6 and r_1(KRAS) >1.4.

All the above parameters have analyzed related to each location and some observations have been. As all the biomarkers are met in all the locations and their concentrations depend on the tumor mass and its clinicopathological features, the direct levels are not enough for differentiation and location has to be evaluated by probability. For each location, there have been established criteria and as the number of met criteria is higher, the probability for a specific location is higher too. Moreover, some locations share similar levels of a biomarker, a ratio or a derivative parameter, so even some of them which did not have small p value are used for criterial algorithm. The algorithm is widely described in discussion section.

After establishing the location with very high probability, the gross aspect has been evaluated for correlation.

Gross aspect has been described as vegetant (1), vegetant and ulcerated (2), ulcero-infiltrative and infiltrative (3) and malignant polyp (4). For these 4 possibilities, p values calculated relative to all five biomarkers' levels are given in Table 4.

Table 4. P values calculated for gross aspect and biomarkers' levels in different biological fluids

Biological fluid	Biomarker	p value
Whole blood samples	MLH1	0.4023
	MSH2	0.5867
	MSH6	0.7683
	PMS2	0.2563
	KRAS	0.1418
Urine samples	MLH1	0.2588
	MSH2	0.2874
	MSH6	0.0926
	PMS2	0.0320
	KRAS	0.0717
Saliva samples	MLH1	0.5747
	MSH2	0.1557
	MSH6	0.8343
	PMS2	0.3890
	KRAS	0.9521

Out of the 15 combinations, gross aspect seemed to be most corelated with MSH6, PMS2 and KRAS levels in urine samples. Starting from these 3 biomarkers, a criteria-based algorithm has been developed to differentiate between these 4 possibilities. For this differentiation, three variables have been introduced namely Grs_1=[MSH6] • [KRAS] (pg•μg/mL^2), Grs_2=[MSH6] • [KRAS]/[PMS2] (pg•μg/(ng•mL)) and Grs_3=[MSH6] • [KRAS]/[PMS2]^2 (ng•μg/pg^2). Starting from the biomarkers' levels and the values of the three variables, the next observations have been done:

- malignant polyps associate $[MSH6]_{urine}$ <30 pg/mL, $[PMS2]_{urine}$ <10 ng/mL and $[KRAS]_{urine}$ < 3 μg/mL;
- colorectal adenocarcinoma patients whose tumor mass presents a vegetant compound associate Grs_1 >387 ng•μg/mL^2, Grs_2 >25 ng•μg/(pg•mL) and Grs_3 >0.5 ng•μg/pg^2;

- colorectal adenocarcinoma patients whose tumor mass does not present a vegetant compound associate Grs_1 <387 ng•μg/mL^2, Grs_2 <25 ng•μg/(pg•mL) and Grs_3 <0.5 ng•μg/pg^2.

Tumor dimensions (maximum diameter and maximum depth) were individually analyzed for each tumor location. In this case, the colorectum was divided in 5 regions – ascending colon (C1), transverse and descending colon (C2 – due to their similarities, these two locations were considered together), C3 (sigmoid colon), C4 (rectosigmoid junction and adjacent area) and C5 (rectum). P values regarding correlation between each biomarker's level and maximum diameter are given in Table 5 and for maximum depth are given in Table 6.

Table 5. P values calculated for maximum diameter and biomarkers' levels in different biological fluids

Biological fluid	**Biomarker**	**Location**				
		C1	C2	C3	C4	C5
whole blood samples	MLH1	0.8669	0.0652	0.2765	0.4034	0.7378
	MSH2	0.8837	0.5392	0.1267	0.3764	0.4929
	MSH6	0.4876	0.0204	0.2405	0.7609	0.2512
	PMS2	0.1623	0.4395	0.3628	0.6253	0.1689
	KRAS	0.9259	0.7824	0.7604	0.1115	0.3707
urine samples	MLH1	0.7096	0.3948	0.6147	0.9011	0.3915
	MSH2	0.8528	0.7152	0.0881	0.6411	0.7394
	MSH6	0.7122	0.4167	0.7073	0.8052	0.1462
	PMS2	0.2391	0.7576	0.6916	0.7039	0.4293
	KRAS	0.7370	0.0010	0.8240	0.8745	0.6624
saliva samples	MLH1	0.3647	0.0071	0.1135	0.2373	0.7911
	MSH2	0.9854	0.5659	0.1220	0.3649	0.6238
	MSH6	0.5792	0.3025	0.8692	0.2347	0.1923
	PMS2	0.7048	0.4765	0.0805	0.1941	0.8686
	KRAS	0.3972	0.0046	0.1491	0.8622	0.6808

Table 6. P values calculated for maximum depth and biomarkers' levels in different biological fluids

Biological fluid	**Biomarker**	**Location**				
		C1	C2	C3	C4	C5

whole blood samples	MLH1	0.2631	0.3809	0.4755	0.0877	0.1425
	MSH2	0.2440	0.4272	0.0234	0.3441	0.3552
	MSH6	0.1770	0.5903	0.1245	0.0314	0.6932
	PMS2	0.7061	0.7830	0.3788	0.1853	0.0633
	KRAS	0.6150	0.1612	0.0528	0.7995	0.7339
urine samples	MLH1	0.5234	0.3565	0.7672	0.8110	0.0781
	MSH2	0.2131	0.4006	0.0383	0.3417	0.1168
	MSH6	0.9874	0.3758	0.3372	0.7504	0.8672
	PMS2	0.4808	0.7437	0.8236	0.9154	0.8362
	KRAS	0.6203	0.7067	0.0616	0.6317	0.4282
saliva samples	MLH1	0.5865	0.8590	0.2711	0.1487	0.0422
	MSH2	0.3892	0.8804	0.1359	0.8630	0.6078
	MSH6	0.7042	0.1386	0.6893	0.1016	0.3818
	PMS2	0.0045	0.5828	0.1415	0.0359	0.1470
	KRAS	0.1872	0.5305	0.2176	0.0309	0.7098

Starting from p values calculated for both maximum dimensions, there have been chosen most related biomarkers and for them, there have been determined equations that can calculate with little error these parameters. All the proposed equations are given in discussions section.

The next step regards correlations to the presence of a mucinous compound among the tumor mass. Due to variations in factors that influence mass transfer of biomolecules in tumor matrix and morphology of cells in different segments, colorectal area has been divided for evaluation of this feature in three main regions – ascending, transverse and descendent colon (Cm1), sigmoid colon (Cm2) and rectosigmoid junction and rectum (Cm3). Each region has been searched for correlations with the presence of mucinous compound and the results are given in Table 7.

Table 7. Correlation of each biomarker's level in each biological fluid to the presence of mucus

Location		**Cm1**	**Cm2**	**Cm3**
Biological fluid	Biomarker	p value	p value	p value
whole blood	MLH1	0.419	0.034	0.538
	MSH2	0.258	0.825	0.623

	MSH6	0.360	0.658	0.056
	PMS2	0.915	0.831	0.679
	KRAS	0.574	0.542	0.656
urine	MLH1	0.600	0.590	0.346
	MSH2	0.448	0.951	0.889
	MSH6	0.939	0.137	0.189
	PMS2	0.119	0.186	0.058
	KRAS	0.163	0.507	0.181
saliva	MLH1	0.754	0.329	0.826
	MSH2	0.046	0.683	0.721
	MSH6	0.393	0.257	0.059
	PMS2	0.487	0.166	0.610
	KRAS	0.391	0.526	0.371

Presence of a mucus compound can be predicted with a criteria-based algorithm. The next observations have been done:

- Cm1-located colorectal adenocarcinoma patients' mucus presence is associated with $[PMS2]_{urine} > 40$ ng/mL, $[KRAS]_{urine} > 5$ μg/mL and $[MSH2]_{saliva} < 180$ pg/mL;
- Cm2-located colorectal adenocarcinoma patients' mucus presence is associated with $[MLH1]_{whole\ blood} > 20$ ng/mL, $[MSH6]_{urine} < 30$ pg/mL and $[PMS2]_{urine} < 10$ ng/mL;
- Cm3-located colorectal adenocarcinoma patients' mucus presence is associated with $[MSH6]_{whole\ blood} > 220$ pg/mL, $[PMS2]_{urine} < 45$ ng/mL and $[MSH6]_{saliva} > 280$ pg/mL.

Just as important as mucus presence for biomarker's mass transfer is the stroma type. The stroma type is considered as inflammatory, fibrous and inflammatory or hyaline. The patients were evaluated for correlations with presence of a fibrous compound by using p values. For stroma type, the colorectal area is considered as a whole and is not divided. The results are given in Table 8.

Table 8. Correlation of each biomarker's level in each biological fluid to the presence of a fibrous compound

Biological fluid	Biomarker	p value
whole blood	MLH1	0.0689
	MSH2	0.0449
	MSH6	0.9916

	PMS2	0.0564
	KRAS	0.0509
urine	MLH1	0.0110
	MSH2	0.0727
	MSH6	0.0002
	PMS2	0.3525
	KRAS	0.0050
saliva	MLH1	0.0891
	MSH2	0.2519
	MSH6	0.2194
	PMS2	0.2807
	KRAS	0.9444

In the same way as for mucus presence, the presence of a fibrous compound is analyzed by using criteria which allows differentiation between inflammatory, fibrous or fibrous and inflammatory stroma. For the development of the criteria, it was observed that a fibrous compound among tumor mass associates $[PMS2]_{\text{whole blood}} > 90$ ng/mL, $[KRAS]_{\text{urine}} < 4$ μg/mL and the value of the product $[MSH2]_{\text{urine}} \bullet [MSH6]_{\text{urine}} > 23000$ $(pg/mL)^2$.

Next future which was analyzed is represented by molecular subtype. Colorectal adenocarcinomas are divided into epithelial, mixed or mesenchymal by molecular subtype. An algorithm to differentiate the tumors which present a mesenchymal compound from the ones which do not. The p values were calculated and they are given in Table 9.

Table 9. Correlation of each biomarker's level in each biological fluid to the presence of a mesenchymal compound

Biological fluid	Biomarker	p value
whole blood	MLH1	0.2219
	MSH2	0.5725
	MSH6	0.8595
	PMS2	0.5361
	KRAS	0.3569
urine	MLH1	0.7552

	MSH2	0.6020
	MSH6	0.0265
	PMS2	0.1195
	KRAS	0.5785
saliva	MLH1	0.8100
	MSH2	0.0464
	MSH6	0.9329
	PMS2	0.7139
	KRAS	0.0729

By analyzing the data, it was observed that the colorectal adenocarcinoma patients whose tumor mass associates a mesenchymal compound present $[MSH6]_{urine}$ >325 pg/mL, $[KRAS]_{saliva}$ <2.2 μg/mL and $[MLH1]_{whole\ blood}$ <25 ng/mL.

By using the results presented above, some microscopic features of the tumor mass can be predicted with high probability. Therefore, the next step consists in evaluation of the blood vessels, the lymph vessels, the perineural and the lymph node invasions. For each pair of biomarker and invasion, the p values were calculated and they are given in Table 10.

Table 10. P values calculated for each type of invasion and biomarkers' levels in different biological fluids

Biological fluid	**Biomarker**	**Invasion**				
		Blood vessels	Lymphatic vessels	Perineural	Lymph node	Percent of invaded lymph nodes
whole blood	MLH1	0.6059	0.6238	0.4997	0.0285	0.4997
	MSH2	0.3908	0.7620	0.3507	0.0231	0.3507
	MSH6	0.1164	0.5139	0.3985	0.1467	0.3985
	PMS2	0.0434	0.5751	0.0820	0.3734	0.0820
	KRAS	0.0001	0.0009	0.0262	0.0372	0.0262
urine	MLH1	0.3833	0.7276	0.5731	0.9705	0.5731
	MSH2	0.0915	0.9905	0.4122	0.7417	0.4122
	MSH6	0.0521	0.7811	0.2438	0.8311	0.2438

	PMS2	0.5606	0.5151	0.8632	0.9334	0.8632
	KRAS	0.2637	0.3388	0.6571	0.6300	0.6571
saliva	MLH1	0.1564	0.9218	0.1627	0.7492	0.1627
	MSH2	0.5902	0.8745	0.6299	0.0944	0.6299
	MSH6	0.9995	0.9855	0.4148	0.1437	0.4148
	PMS2	0.5318	0.0859	0.0629	0.3331	0.0629
	KRAS	0.0469	0.8982	0.8182	0.4013	0.8182

Starting from Table 10 data, there have been selected the most representative biomarkers for each type of invasion and by using the levels of each biomarker, there have been established algorithms for determine the presence of invasion with high probability. As the number of lymph nodes is variable, depending on the dimension of specimen, for invaded lymph nodes there is proposed an algorithm to determine the percent of invaded lymph nodes in each colorectal cancer patient.

The observations from which the criteria were developed are:

- blood vessels invasion is associated with $[KRAS]_{whole\ blood} > 13\ \mu g/mL$, urinary MSH product $Pu = [MSH2] \cdot [MSH6] > 25000\ (pg/mL)^2$ and urinary MSH ratio $Ru = [MSH2]/[MSH6] > 1$;
- lymph vessels invasion is associated with $[KRAS]_{whole\ blood} > 8.4\ \mu g/mL$, $[PMS2]_{saliva} > 38$ ng/mL and the KRAS ratio $[KRAS]_{whole\ blood} / [KRAS]_{urine} > 2$;
- perineural invasion is associated with $[PMS2]_{whole\ blood} /[PMS2]_{saliva} < 0.45$, $[PMS2]_{whole\ blood} / [KRAS]_{whole\ blood} < 0.55$ ng/μg and $[PMS2]_{saliva} > 17$ ng/mL;
- lymph node invasion is associated with $[MLH1] \cdot [KRAS]/[MSH2] > 4 ng \cdot \mu g/(pg \cdot mL)$, $[MLH1] \cdot [KRAS] > 185\ ng \cdot \mu g/mL^2$ and $[MLH1]/[MSH2] > 0.75$ ng/pg;
- for percent of invaded lymph nodes, equations have been elaborated and widely discussed in discussions section.

As that the results regarding the invasion have been presented, the next feature regards the survival of the patients. In our project, the patients were selected and followed up on a period of three years. Therefore, the proposed evaluation of survival regards the survival less or over one year and the survival over or less than two years. The p values for correlations between each biomarker's level and the survival category are given in Table 11.

Table 11. p values for evaluation of the survival rate relative to one year and two years

Biological fluid	**Biomarker**	**vs. 1 year**	**vs. 2 years**
whole blood	MLH1	0.2809	0.2265

	MSH2	0.0012	0.0467
	MSH6	0.0946	0.7323
	PMS2	0.9671	0.0642
	KRAS	0.6310	0.6429
urine	MLH1	0.1594	0.0575
	MSH2	0.6634	0.0717
	MSH6	0.7449	0.0005
	PMS2	0.8014	0.2165
	KRAS	0.2905	0.2361
saliva	MLH1	0.0380	0.0632
	MSH2	0.4368	0.0397
	MSH6	0.0786	0.4033
	PMS2	0.8034	0.8257
	KRAS	0.6438	0.3627

Analyzing the data, the next observations are given:

- patients who survived less than a year associate $[MSH2]_{whole\ blood}$ >340 pg/mL and $[MLH1]_{saliva}$ >52 ng/mL;
- patients who survived between one year and two years associate $[MSH2]_{whole\ blood}$ <340 pg/mL and $[MLH1]_{saliva}$ <52 ng/mL, but $[MSH6]_{urine}$ <260 pg/mL and $[MSH2]_{saliva}$ >140 pg/mL;
- patients who survived more than two years associate $[MSH6]_{urine}$ >260 pg/mL and $[MSH2]_{saliva}$ <140 pg/mL.

The last correlations have been done to the elements of TNM staging. There have been developed algorithms for establishing pT value and evaluation of pN and pM.

All the patients included in our project were at least pT2 as most of the colorectal patients that come at the physician. Therefore, the proposed algorithm evaluates with high probability only the patients with pT2, pT3, pT4a or pT4b and it is based on exclusion step-by-step of each value for pT. Firstly, the criteria established for pT2 are checked and if they are not verified, it involved that the pT is at least 3 and so on. For each step-by-step evaluation, the p values for differentiation of a given pT value patients from the remaining pT values patients were calculated and they are given in Table 12.

Table 12. p values for the evaluation of the pT value

Biological fluid	Biomarker	pT2 vs others	pT3 vs pT4	pT 4a vs pT 4b
whole blood	MLH1	0.6228	0.3825	0.3254
	MSH2	0.5240	0.6135	0.5830
	MSH6	0.0972	0.2645	0.8704
	PMS2	0.3195	0.1473	0.0559
	KRAS	0.4826	0.1215	0.2049
urine	MLH1	0.9645	0.2080	0.1321
	MSH2	0.9224	0.2883	0.0320
	MSH6	0.6914	0.4597	0.2988
	PMS2	0.9863	0.1849	0.2132
	KRAS	0.6178	0.0779	0.8858
saliva	MLH1	0.4619	0.1598	0.4662
	MSH2	0.2068	0.8527	0.4951
	MSH6	0.6980	0.0862	0.9500
	PMS2	0.0491	0.9013	0.1562
	KRAS	0.4797	0.5990	0.1220

The observations that allow the criteria development are:

- pT2 colorectal adenocarcinoma patients associate $[MSH6]_{saliva} \cdot [PMS2]_{saliva} > 50000$ $pg \cdot ng/(mL)^2$, $[MSH6]_{saliva} \cdot [PMS2]_{saliva} / [MSH2]_{saliva} > 45$ ng/mL and $[MSH2]_{saliva} \cdot [PMS2]_{saliva} > 50000$ $pg \cdot ng/(mL)^2$;
- pT3 colorectal adenocarcinoma patients associate $[PMS2]_{whole\ blood} / [MSH6]_{whole\ blood} < 1.2$ ng/pg, $[PMS2]_{whole\ blood} \bullet [KRAS]_{whole\ blood} / [MSH6]_{whole\ blood} < 14.5$ $ng \cdot \mu g/(pg \cdot mL)$, $[MLH1]_{saliva} < 30$ ng/mL and $[KRAS]_{urine} < 4$ μg/mL;
- pT4b colorectal adenocarcinoma patients (in comparison to pT4a colorectal adenocarcinoma patients) associate $[PMS2]_{whole\ blood} < 25$ ng/mL, $[PMS2]_{saliva} > 18$ ng/mL, $[PMS2]_{whole\ blood} /[KRAS]_{whole\ blood} < 1.5$ ng/μg and $[PMS2]_{saliva} /[KRAS]_{saliva} < 5.5$ ng/μg.

As the number of found lymph nodes is variable, pN value in this study has been evaluated through the percent of invaded lymph nodes and presence of deposits. pM value is evaluated by the presence of metastases. The exact value of pN can be evaluated if a mathematical model of lymph vessels and lymph node distribution throughout the colorectal area would be developed. Therefore, the number of lymph nodes in a curative excision specimen with the percent of invaded lymph nodes would allow approximation of the number of invaded lymph node. This is at the moment a future

perspective. The presence of tumor deposits is considered independent from lymph node invasion. Therefore, it is evaluated separately. The metastases were evaluated at the moment of diagnostic and during the follow-up period. The patients who did not present metastases at the moment of diagnostic or during the follow-up period were considered as not having metastases. The presence of metastases has been evaluated regardless of the metastasis place. The p values for the correlations of each biomarker's level in each biological fluid and the selected features are given in Table 13.

Table 13. p values for evaluation of pN and pM

Biological fluid	Biomarker	Tumor deposits	Metastases
whole blood	MLH1	0.9885	0.5626
	MSH2	0.6009	0.4230
	MSH6	0.4793	0.1739
	PMS2	0.0554	0.1835
	KRAS	0.9294	0.0024
urine	MLH1	0.4575	0.1646
	MSH2	0.9981	0.2737
	MSH6	0.5285	0.1579
	PMS2	0.3419	0.1139
	KRAS	0.0334	0.0002
saliva	MLH1	0.9423	0.0130
	MSH2	0.2486	0.9907
	MSH6	0.5150	0.7827
	PMS2	0.9199	0.4167
	KRAS	0.5323	0.6541

The observations regarding presence of tumor deposits and presence of metastases are:

- tumor deposits presence is related to $[PMS2]_{whole\ blood}$ >450 ng/mL, $[PMS2]_{urine}$ <32 ng/mL, $[KRAS]_{urine}$ <1.75 μg/mL and $[MSH2]_{saliva}$ <125 pg/mL;
- presence of metastases is related to [KRAS]/[MSH6] >0.05 μg/pg, [KRAS]/[PMS2] >0.34 μg/ng and [PMS2] <14 ng/mL.

All the developed algorithms and equations will be widely described in the discussions section. By applying them, the selectivity for each feature is given in Table 14.

Table 14. Sensitivity and specificity in predicting the clinicopathological features

Clinicopathological feature	Characteristic	Sensitivity	Specificity
Tumor location	Ascending colon	100%	93.48%
	Transverse colon	100%	91.66%
	Descending colon	100%	91.66%
	Sigmoid colon	87.50%	89.47%
	Rectosigmoid junction	100%	95.74%
	Rectum	89.47%	87.50%
Gross aspect	Malignant polyps	100%	98.60%
	Vegetant	88%	66.60%
	Vegetant and ulcerated	66.60%	76%
	Non-vegetant	73.91%	71.43%
Mucus presence	Cm1 located tumor	87.50%	100.00%
	Cm2 located tumor	100%	78.58%
	Cm3 located tumor	77.77%	88.24%
	Overall	86.96%	87.18%
Stroma Type	Fibrous compound	86.11%	80.95%
	Inflammatory compound	80.95%	86.11%
Molecular subtype	Mesenchymal compound	93.75%	72.22%
Invasions	Blood vessels	84.21%	79.37%
	Lymph vessels	74.19%	71.42%
	Perineural	84.21%	71.70%
	Lymph node	72.41%	75.76%
Survival rate	vs. 1 year	90.48%	77.78%
	vs. 2 years	100%	86.84%
TNM grading system	pT2	90%	89.09%
	pT3	89.66%	89.47%
	pT4a vs. pT4b	100%	81.25%
	Tumor deposits	80%	91.84%
	Metastases	90%	77.27%

As observed from the Table 14 given above, all the algorithms for determination of the clinicopathological features associate high sensitivities and specificities. Discovery of new biomarkers

and new algorithms to predict the clinicopathological features with higher sensibilities and specificities are future perspectives for larger studies.

Appendix 1

PARTICIPATION TO NATIONAL AND INTERNATIONAL CONFERENCES

1. Ruxandra-Maria Ilie-Mihai, Raluca-Ioana Stefan-van Staden, Alexandru Adrian Bratei, Damaris-Cristina Gheorghe, Stochastic sensors as new tools for the assay of CA72-4, CA19-9, CA12-5 and CEA in biological samples, Transnational Multiplier event of REALME project - A Mixed Reality E-Learning Platform Dedicated for Medical Engineering, 18 – 19 OCTOBER 2023, National University of Science and Technology POLITEHNICA Bucharest. (POSTER)

2. Ruxandra-Maria Ilie-Mihai, Raluca-Ioana Stefan-van Staden, Alexandru Adrian Bratei, Damaris-Cristina Gheorghe, Bianca Maria Tuchiu, OP9-5-3. DNA Mismatch Repair Assessment in Gastric and Colon Cancers Using Stochastic Microdisks, Euroanalysis XXI, Geneva, Switzerland, 27-31 August, 2023. (ORAL PRESENTATION)

3. Ruxandra-Maria Ilie-Mihai, Raluca-Ioana Stefan-van Staden, Alexandru Adrian Bratei, Damaris-Cristina Gheorghe, PS2-22. Stochastic sensors as new tools for the assay of CA72-4, CA19-9, CA12-5 and CEA in biological samples, Euroanalysis XXI, p. 254, Geneva, Switzerland, 27-31 August, 2023. (POSTER)

4. Raluca-Ioana Stefan-van Staden, Damaris Cristina Gheorghe, Alexandru A A Bratei, Ruxandra Maria Mihai, (Invited) New Challenges in Early Diagnosis of Gastric Cancer, 241st ECS Meeting, May 29 – June 2, 2022, Vancouver, Canada (ORAL PRESENTATION)

Appendix 2

ARTICLES PUBLISHED IN PEER-REVIEWED JOURNALS

Total IF = 38.5

This PhD thesis is based on the following papers:

I. Stefan-van Staden, R.-I.; **Bratei, A.A.** *et al.* Miniplatforms for Screening Biological Samples for KRAS and Four Mismatch Repair Proteins as New Tools for Fast Screening for Gastric and Colon Cancers. *J. Electrochem. Soc.* ***2023***, 170, *057510*. **DOI:** 10.1149/1945-7111/acd358. ***IF=3.9***

II. Stefan-van Staden, R.-I., **Bratei, A.A.** et al. New stochastic devices for simultaneous analysis of mismatch repair proteins and KRAS in biological samples. Journal of Pharmaceutical and Biomedical Analysis **2023**, 115630, ISSN 0731-7085. https://doi.org/10.1016/j.jpba.2023.115630. **IF= 3.4**

III. Stefan-van Staden, R.-I., **Bratei, A.A.** et al. Bioanalysis of MMR and KRAS – a key factor in diagnosis of colorectal cancer RSC Adv. **2023**, 13, 24086. DOI: 10.1039/d3ra04260j . **IF= 3.9**

IV. Stefan-van Staden, R.-I.; **Bratei, A.A.** et al. DNA Mismatch Repair Assessment in Gastric and Colon Cancers Using Stochastic Microdisks. *ChemElectroChem* **2023**, 10, e202300273. https://doi.org/10.1002/celc.202300273. **IF=4**

V. **Bratei, A.A.**; Stefan-van Staden, R.-I. *et al.* Molecular Differentiation of Cathepsins B and D, and of p53 Protein, and their Quantitative Assay in Biological Samples. *J. Electrochem. Soc.* **2023**, 170, 097503. https://doi.org/10.1149/1945-7111/acf622. **IF=3.9**

VI. **Bratei, A.A.**; Stefan-van Staden, R.-I.; Ilie-Mihai, R.-M.; Gheorghe, D.-C. Simultaneous Assay of CA 72-4, CA 19-9, CEA and CA 125 in Biological Samples Using Needle Three-Dimensional Stochastic Microsensors. *Sensors* **2023**, *23*, 8046. https://doi.org/10.3390/s23198046. **IF=3.9**

VII. **Bratei, A.A.**; Stefan-van Staden R.-I., Ilie-Mihai R.-M. Electroanalysis of maspin in whole blood. *U.P.B. Sci. Bull., Series B*, ISSN 1454-2331, **2024**. **IF=0.5**.

VIII. **Bratei, A.A.;** Stefan-van Staden, R.-I. Correlation between Maspin Levels in Different Biological Samples and Pathologic Features in Colorectal Adenocarcinomas. *Life* **2023**, *13*, 1060. https://doi.org/10.3390/life13041060. **IF=3.2**

IX. **Bratei, A.A.**; Stefan-van Staden, R.-I. Minimally Invasive and Fast Diagnosis of Gastric Cancer Based on Maspin Levels in Different Biological Samples. *Diagnostics* **2023**, *13*, 1857. https://doi.org/10.3390/diagnostics13111857. **IF=3.6**

X. **Bratei, A.A.**; Stefan-van Staden, R.-I. Differentiation between Gastric and Colorectal Adenocarcinomas Based on Maspin, MLH1, PMS2 and K-Ras Concentrations Determined Using Stochastic Sensors. *Gastrointest. Disord.* **2023**, *5*, 487-499. **IF=0.7**

XI. **Bratei, A.A.**; Stefan-van Staden, R.-I. Correlations between MSH2 and MSH6 Concentrations in Different Biological Fluids and Clinicopathological Features in Colorectal Adenocarcinoma

Patients and Their Contribution to Fast and Early Diagnosis of Colorectal Adenocarcinoma. *Biomedicines* **2023**, *11*, 3213. https://doi.org/10.3390/biomedicines11123213. **IF=4.7**

XII. **Bratei, A.A.**, & Stefan-van Staden, R.-I. (2023). The Importance of KRAS Quantification for a Clinicopathological Characterization in Colorectal Cancer Patients. Medinformatics.

XIII. **Bratei, A.A.**; Stefan-van Staden R.-I. Pathological features of colorectal adenocarcinoma patients related to MLH1. *Cellular and Molecular Bioengineering* **2024**. **IF=2.8**

ARTICLES SENT TO PUBLICATION

I. **Bratei, A.A.**; Stefan-van Staden, R.-I. Fast diagnosis and pathological features related to MLH1 and PMS2 in gastric cancer patients and to PMS2 in colorectal cancer patients.

II. **Bratei, A.A.**; Stefan-van Staden, R.-I. Evaluation of clinicopathological features in colorectal adenocarcinoma patients based on the concentrations of MMR proteins and KRAS.

Selected References

[5] Coros, M.; Pruneanu, S.; Stefan-van Staden, R.-I. Recent progress in the graphene-based electrochemical sensors and biosensors. A review. *J. Electrochem. Soc.* **2020**, *167*, 037528.

[6] Gu, L.Q.; Braha, O.; Conlon, S.; Cheley, S.; Bayley, H. Stochastic sensing of organic analytes by a pore-forming protein containing a molecular adapter. *Nature* **1999**, *398*, 686–690.

[7] Gugoasa, L.A.; Stefan-van Staden, R.I.; Dima, A.; Visan, C.A.; Streinu-Cercel, A.; Biris, A.; Calenic, B. Fast screening of biological fluids for cytokines and adipokines using stochastic sensing. *Microelectron. Eng.* **2015**, *148*, 64–69.

[8] Ilie-Mihai, R.M.; Gheorghe, D.C.; Stefan-van Staden, R.I.; Lungu-Moscalu, A.; Pruneanu, S.M.; van Staden, J.F. Fast screening method of biological samples based on needle stochastic sensors for early detection of gastric cancer. *Rev. Chim.* **2021**, *72*, 22–34.

[9] Ilie-Mihai, R.M.; Gheorghe, S.S.; Stefan-van Staden, R.-I.; Bratei, A. Electroanalysis of interleukins 1β, 6, and 12 in biological samples using a needle stochastic sensor based on nanodiamond paste. *Electroanalysis* **2021**, *33*, 6–10.

[10] Ilie-Mihai, R.M.; Stefan-van Staden, R.-I.; Lungu-Moscalu, A.; Pogacean, F.; Pruneanu, S.M. Sulphur Doped Graphenes Based 3D-Needle Stochastic Sensors as New Tools for Biomedical Analysis. *J. Electrochem. Soc.***2021**, *168*, 037509.

[15] Stefan-van Staden, R.-I.; Ilie-Mihai, R.M.; Pogacean, F.; Pruneanu, S. Graphene-based stochastic sensors for pattern recognition of gastric cancer biomarkers in biological fluids. *J. Porph. Phthal.* **2019**, *23*, 1365–1370.

[16] Stefan-van Staden, R.-I.; Negut, C.C.; Gheorghe, S.S.; Ciorîță, A. 3D stochastic microsensors for molecular recognition and determination of heregulin-α in biological samples. *Anal. Bioanal. Chem.* **2021**, *413*, 3487–3492.

[17] Stefan-van Staden, R.I.; Bogea, I.M.; Ilie-Mihai, R.M.; Gheorghe, D.C.; Coroş, M.; Pruneanu, S. Stochastic microsensors based on modified graphene for pattern recognition of maspin in biological samples. *Anal. Bioanal. Chem.* **2022**, *414*, 3667–3673.

[18] Stefan-van Staden, R.I.; Comnea-Stancu, I.R.; Surdu-Bob, C.C. Molecular Screening of Blood Samples for the Simultaneous Detection of CEA, HER-1, NSE, CYFRA 21-1 Using Stochastic Sensors. *J. Electrochem. Soc.***2017**, *164*, B267–B273.

[19] Stefan-van Staden, R.I.; Gheorghe, D.C.; Ilie-Mihai, R.M.; Barbu-Tudoran, L.; Pruneanu, S.M. Stochastic biosensors based on N and S-doped graphene for the enantioanalysis of aspartic acid in biological samples. *RSC Adv.* **2021**, *11*, 23301–23309.

[20] Stefan-van Staden, R.I.; Gheorghe, S.S.; Ilie-Mihai, R.M.; Badulescu, M. Disposable Stochastic Sensor Based on Deposition of a Nanolayer of Silver on Silk for Molecular Recognition of Specific Biomarkers. *J. Electrochem. Soc.* **2021**, *168*, 037515.

[21] Stefan-van Staden, R.I.; Ilie-Mihai, R.M.; Magerusan, L.; Coros, M.; Pruneanu, S. Enantioanalysis of glutamine—A key factor in establishing the metabolomics process in gastric cancer. *Anal. Bioanal. Chem.* **2020**, *412*, 3199–3207.

[91] Banias, L.; Gurzu, S.; Kovacs, Z.; Bara, T.; Bara, T., Jr.; Jung, I. Nuclear maspin expression: A biomarker for budding assessment in colorectal cancer specimens. *Pathol. Res. Pract.* **2017**, *213*, 1227–1230.

[92] Banias, L.; Jung, I.; Bara, T.; Fulop, Z.; Simu, P.; Simu, I.; Satala, C.; Gurzu, S. Immunohistochemical-based molecular subtyping of colorectal carcinoma using maspin and markers of epithelial-mesenchymal transition. *Oncol. Lett.* **2020**, *19*, 1487–1495.

[93] Banias, L.; Jung, I.; Gurzu, S. Subcellular expression of maspin—from normal tissue to tumor cells. *World J. Meta-Anal.* **2019**, *7*, 142–155.

[102] Gurzu, S.; Bara, T.; Molnar, C.; Bara, T., Jr.; Butiurca, V.; Beres, H.; Savoji, S.; Jung, I. The epithelial-mesenchymal transition induces aggressivity of mucinous cystic neoplasm of the pancreas with neuroendocrine component: An immunohistochemistry study. *Pathol. Res. Pract.* **2019**, *215*, 82–89.

[103] Gurzu, S.; Ciortea, D.; Ember, I.; Jung, I. The possible role of Mena protein and its splicing-derived variants in embryogenesis, carcinogenesis, and tumor invasion: A systematic review of the literature. *Biomed. Res. Int.***2013**, *2013*, 365192.

[104] Gurzu, S.; Copotoiu, C.; Tugui, A.; Kwizera, C.; Szodorai, R.; Jung, I. Primary gastric choriocarcinoma—a rare and aggressive tumor with multilineage differentiation: A case report. *World. J. Clin. Cases* **2019**, *7*, 1837–1843.

[105] Gurzu, S.; Fetyko, A.M.; Bara, T.; Banias, L.; Butiurca, V.O.; Bara, T., Jr.; Tudorache, V.; Jung, I. Gastrointestinal mixed adenoneuroendocrine carcinoma (MANEC): An immunohistochemistry study of 13 microsatellite stable cases. *Pathol. Res. Pract.* **2019**, *215*, 152697.

[106] Gurzu, S.; Kadar, Z.; Bara, T.; Bara, T., Jr.; Tamasi, A.; Azamfirei, L.; Jung, I. Mixed adenoneuroendocrine carcinoma (MANEC) of gastrointestinal tract: Report of two cases and review of the literature. *World. J. Gastroenterol.* **2015**, *21*, 1329–1333.

[107] Gurzu, S.; Szentirmay, Z.; Popa, D.; Jung, I. Practical value of the new system for Maspin assessment, in colorectal cancer. *Neoplasma* **2013**, *60*, 373–383.

[108] Gurzu, S.I.; Sugimura, H.; Stefan-van Staden, R.I.; Yamada, H.; Natsume, H.; Iwashita, Y.; Szodorai, R.; Szederjesi, J. Maspin subcellular expression of wild-type- and mutant TP53 gastric cancers. *World. J. Gastrointest. Oncol.* **2020**, *12*, 741–755.

[111] Kovacs, Z.; Jung, I.; Szalman, K.; Banias, L.; Bara, T.J.; Gurzu, S. Interaction of arylsulfatases A and B with maspin: A possible explanation for dysregulation of tumor cell metabolism and invasive potential of colorectal cancer. *World. J. Clin. Cases* **2019**, *7*, 3990–4003.

[123] Turdean, S.G.; Gurzu, S.; Jung, I.; Neagoe, R.M.; Sala, D. Unexpected maspin immunoreactivity in Merkel cell carcinoma. *Diagn. Pathol.* **2015**, *10*, 206.